Small Clusters of II-VI Materials

Small Clusters of II-VI Materials

Doctoral Dissertation

Jon M. Matxain

Director: Jesus M. Ugalde

2002ko Apirila

Esker mila!!!

Hau tesiaren atalik zailena da idazteko, gauza anitzengatik. Alde batetik jende asko eskertu behar dudalakotz. Bestetik, bildur naiz jende guztiaz gogoratuko ote naizen. Norbait ahantziz gero, barka nazala, nahita ez da izan eta. Hasteko, hastapenetik hasiko gara. Jesusek bere taldean lan egiteko aukera eman zidan, eta egia esan arras gustora egon naiz. Gauza asko ikasi ditut, eta laguntza handiak altxatu ere bai. Dudak asaldatzean, edo emaitza batzuk interpretatzen zailtasunak edukitzean, berarengana jo eta arras ideia interesgarriak eman dizkit. Bestalde, taldeko kideengan jarritako konfidantza eta ematen duen askatasuna dela eta gaur egun toki gutxitan aurkitzen ahal den lan-giroa dugu. Horrela, tesiarekin hasi nintzenean hainbat espezimen ezagutzeko aukera izan nuen. Joseph izan zen tesi honen ideia izan zuena. Joseph Estatu Batuetatik Euskal Herrira etorri zen 96an eta haruntza berriz bidali genuen txapela buruan eta eskupilota eskuan zuela. Aurreko kuadroetan iaioa zen bai, atzekoetara iristen ez ginelakotz!! Txema taldean sartu aurretik ezagutu nuen, non eta Iruñeko taberna 'zulo' batean, bera ameriketan zegoen garaian. A ze nolako txapadak sartu dizkiodan ondoren, batez ere ordenadore kontuetan. Hori bai, sustengu morala eman dit garai anitzetan, berak arras ongi dakien moduan: 'El once de Osasuna, valiente y luchador...' Zorionez aurten ez dugu behar izan, behintzat momentuz. Berarekin komunikazio handia izan dut, baita emailez ere, nahiz eta atzerrian ez egon! Willy, zu ere eskertu behar zaitut, nola ez, hasi nintzenean ordenadorea lapurtu zenidan arren. Basurdejana oraindik ez dugu egin, baina lasai, Asterix, noizpait eginen dugu. Hala ere, jakin ezazu bodegon Alejandrora joateko beti prest egonen naizela. Eskerrik asko Betz apunteengatik eta azalpenengatik. Taldeko beste inmortal bat Arantxa dugu. Eskerrak zuri ere Rociito, arras giro polita izan dugulakotz, eta lanean dudak eta askatzen lagundu zenidalakotz. Hasi nintzenean tesiarekin Iñaki ere taldean hasi zen, bera oraindik ikaslea izan arren. Lau urte hauetan gauza dexente ikasi ditut zuregandik, matematika batez ere!! Sartu nintzenean taldean jende hau guztia zegoen, baina jende gehiago pasa da, eta hasi egin da. Amerika kubatarra hiru hilabetez egon zen hemen nire tesiaren hasieran, eta aipatu gabe ezin da gelditu. Elmer ere, Venezuelatik etorri zitzaigun Colonbiarra, zure pazientziagatik eta azalpenengatik mila esker. Nelaine kubatarra hilabete batez egon zen gurekin ere, eta kubako kultura apur bat gehiago erakutsi zigun. Oso goxoa zegoen Havana Club-a!! Eta bukatzeko taldean hasi den azkenekoa, baina atal berezia merezi duena. Joni, eres el puto amo. Istorio anitz kontatzen ahal ditut berari buruz, karrera lehenengo mailan elkarrekin hasi ginelakotz eta handik aitzina dexente elkarrekin ibili garelakotz, baina ez da plana hemen trapu zikinak astintzea. Gogoratu bakarrik campus erdian bota egin zenean, parrezka. Besarkada handi bat, Joni. Eskertu nahi nituzke ere fakultateko beste irakasle batzuk, Xabi, Cecilia eta Jose Mari. Mila esker Jose Mari euskera kontuetan laguntzeagatik. Beti atsegina da zurekin aritzea. Tesian zehar Cambridgen hiru hilabetez aritzeko aukera izan nuen, Cavendish laborategian. Eskertu nahi nuke Richard eta Mike bertan emandako laguntzagatik, eta Simone italiarra. Baita bertan ezagututako jendeari ere.

Jende askorekin pisua konpartitu dut. Tesia hastean Miren eta Idoia izan ziren. Beranduago Agurtzanerekin egon nintzen, urte eta erdiz. Amarako

etxean gustora egon ginen, ezta, Agurtzane? Noizean behin Asterix etortzen zitzaigun, eta pozio majikoa hartu beharrean garbantzuak eramaten zituen... baina tira. Bertatik jende gehiago pasa zen, Juan Luis, Dani, eta gero Raul, gasteiztarra. Agurtzane joaterakoan Antxon etorri zen... a ze hirukotea bildu ginen!! El ciego, el sordo y el despistado mayor del reino. Kakauete, how are you doing Irlandan? Lehendik Lasallen egon nintzen, eta ezin utzi aipatu gabe bertan eginiko lagunak: Otsobi, Rosino, Oskar, Ivan, Iker, Aritza... ezin denak aipatu!

Tesia Donostian egin arren, kimika teorikoan Utrecht-en murgildu nintzen. Bertan bi urte pasa nituen. Frans-ekin eta Jan-ekin lan egin nuen lehenengo urtean. Baina ez dira beraiek bakarrik taldea osatzen zutenak, Jeanne, Paul, Joop, Simon, Fokke, Remco, Walter, Elly, Huub, Alekos, Arno eta Rogier. Esker mila denoi! Eta baita Herbehereetan ezaguturiko beste jenderi, batez ere Ramon eta Gert Jan (Euskal Herri independientearen Lehenengo Lehendakaria!!). Eta nola ez, Ritox-eko eta FOC-eko jendea. Euskaldunak ere ezagutu nituen bertan, eta batzuk oso lagun onak dira gaur egun: Jota, Elsa, Bertanis, Aizpeia, Ñi-Ñi, Estela, Martino, Eñaut eta Iban. Eta Amsterdam-en ezaguturiko jendea... Castellonen ezaguturiko jendea ere agurtu nahi nuke.

Kimikako karreran zehar ezagutu dudan jendea ere ezin dut ahantzi, lagun arras onak egin baititut. Batez ere Jetas, Kasper, Kalbo, Aitor, Fernando eta berriz Joni. Joni, telepatia ote dugu? Leire, Rakel... mugimendu subersibotan ibilitako jendea!! Barañaingo lagunak, Cesar, David, Joseba, Ines, Josean, Samu, Arapa, Ainhoa, Iñaki, Nerea (ez naizela ezkontzen!!!), Aitor eta Marta (oraingoan bai, je je je) Iparraldeko denak, Victor, Loli, Edurne, Mirentxu, Ixone eta bertan biltzen den txusma, Paco barne! Victor, musean ez diguzu berriz irabaziko!!! Kartak markatzen dituzula konturatu gara!!!!

Eta aipamen berezia familiarendako. Gurasoek beti prest laguntzeko, kanpora joan nedin esfortzua egin eta beti suporta. Betidanik konfidantza eman didazue eta edozertarako prest egon zarete. Ez da gauza makala, gurasoek seme-alaben bidea errespetatzea eta onartzea ez baita orokorrean gertatzen. Mila esker! Eta anaiei ere, Iker eta Ibai, lasai Ibai, ez baitut Julianek deitzen dizkizun izenik paratuko eta!! Bestela berak ere ikusi beharko lituzkeenak! Eta Erasoko familia ere, denoi, osaba-izeba, lehengusu-lehengusin, eta nola ez, amona. Denen izena ez dut idatziko, bakarrik esan bertan denak biltzen garenean ia 40 pertsona garela, eta bakarrik amaren partetik. Mila esker denoi! Eta ez bakarrik pertsonei, bordari ere eskerrak. Gizarte industrializatu honetatik ihesbide ezinhobea ematen didalakotz.

Aknowledgements

This is one of the most difficult things to be done in a thesis. Basically because there are many people to be acknowledged, and I am afraid that I will forget some of you. If so, please forgive me!! Let us start from the begining. Jesus gave me the opportunity to work in his lab, which has been a real pleasure for me. I have learned a lot while working with you, Jesus, and I have found help whenever I needed, in order to overcome the arising problems. Moreover, I would like to point out the freedom and confidance you have given me, and everybody in the lab, to carry out my research project. Due to this fact there is an unbeatable atmosphere in the lab. When I started with my Ph.D. four years ago I had the chance to meet very nice people. Joseph the american had the idea of this project. He came from the states in 96 and went back with a txapela (basque-hat) in his head and eskupilota (basque-ball) is his hands. In the front-squares he was very smart, because we couldn't achieve the back ones!!! I met Txema before joining the group, in a 'hole' in Iruñea. Since then I have asked too many questions to him, basically concerning computers and linux! But he also gave me moral support, as he knows: 'El once de Osasuna, valiente y luchador...' Fortunatelly, at the moment we don't need it! I have very good communication with him, even via email without being abroad!! Willy, I have to thak you as well, although you stole my computer when I started. We still haven't done the wild-pig eating, but don't be afraid, Asterix, we will do so! However, I have no problem to go to bodegon Alejandro again!! Thank you Betz for trying to teach me the few you knew (he he)!! Arantxa is as old as Willy, that is, very very old. Thank you Rociito, we had a fantastic atmosphere and you helped a lot. Gora dultzaina!! When I started the Ph.D. Iñaki started in the group as well, although as undergraduate student. In these four years I learnt a lot from you, specially mathematics. Moreover, you have the quality of asking questions nobody thinks on. These people were in the group when I started, but some others have come to us. Amerika came from Cuba for three months, a very funny 'lady'. Elmer, a colombian coming from Venezuela, thank you very much for your patiente! Nelaine, from Cuba as well, spent one month with us, and thaught a bit about cuban culture. Finally, to end with, Joni, the last signing up. Joni Mujika is the best! I can tell a lot of istories about him, we started chemistry together almost nine years ago, but this is not the best place to do so. Only remember the day he stayed in the ground laughing in front of the Chemistry Department. I would like to thank other people from the group, Xabi, Cecilia and Jose Mari. Jose Mari is always ready to help even he is busy with other things. He has helped me a lot with the basque new rules. Thank you! During my research I spent three months in Cambridge, in the Cavendish laboratory. I would like to thank Richard, he gave me the chance to visit Cambrigde, and Mike and Simone as well. And I would like to remember all the people I met in Castellon!

I would like to remember my housemates. I have had a lot during these years. Idoia and Miren in Antigua. Then I went to Amara, with an unofficial member of our group, Agurtzane. We spent one year and a half there, until she went with Betz. Later, in the same hause, I spent six months with Antton and Raul. We had a great time, eh, guys? Kakauete, how are you doing in Ireland? I

also want to remember Otsobi, Rosino, Oskar, Ivan and the other people of Lasalle!!

I have carried out my Ph. D. in Donostia, but I was born in this world of Quantum Chemistry in Utrecht, in the Netherlands. I spent two unforgetable years there, working with Frans, Jeanne, Joop, Paul, Walter, Jan, Fokke, Simon, Remco, Huub, Alekos, Arno, Rogier and Elly. Dank julli well, mijn nederland is goed niet, maar ik kun een beetje schrijven! I met more dutch and foreign people there, Ramon and Gert Jan (The first president of an independent Basque Country), people from Ritox and FOC. But I met basque people as well, and some of them are very good friends actually: Jota, Elsa, Bertanis, Aizpeia, Ñi-Ñi, Estela, Martino, Eñaut and Iban. And more people I met in Amsterdam, and in... and in.... Unforgetable.

I have met very nice people during my studies, Jetas, Casper, Kalbo, Aitor, Fernando, Igor and Joni. I would like to remember my friends Cesar, David, Joseba, Ines, Ainhoa, Josean, Samu, Arapa, Nerea and all the people we meet in the Iparralde. Victor, Loli, Edurne, Mirentxu, Ixone... and Paco! Victor, you won't win us playing mus any more!

Special words for the family. My parent always helping me, although they do understand nothing of my work, and my brothers Iker and Ibai. And all my family from Eraso, I'm not going to write all the names 'cause we are almost forty people. But not only people, I would like to thank a lot to the borda, the hause in the mountains, because it has given me the chance to escape from our ugly civilization.

Thank you all!!

Contents

Sarrera Orokorra

Gizakiaren aurrerapen nabarmenetako bat historiaurrean gertatu zen, gure arbasoek sua egiten eta erabiltzen ikasi zutenean. Aurrerakuntza horrek energi iturri naturalen erabilpena ekarri zuen, derrigorrezkoa geroago gertatuko zen zibilizazioaren garapenerako. Gaur egun gure zibilizazioak energi kantitate izugarria behar du. Industriaren garapena, eta noski mendebaldeko bizimodu erosoak kontsumitzeko energia anitz behar du. Energia hor da, naturan, eta gizakiak egin duen gauza 'bakarra' energia hori nola erabili eta eraldatu ikastea izan da, termodinamikaren lehenengo printzipioak erraten duenarekin bat etorriaz, alegia. Urteen poderioz anitz energi iturri aurkitu eta garatu dira, gaur egun ezagutzen dugun garapen teknologiko izugarria suertatzeko garrantzitsuenak XIX. mendearen bukaeran eta XX. mendearen hasieran garatu zirelarik. Petrolioa zein energia nuklearra ditugu honen adierazgarri. Edisonek bonbila asmatu izanak ere bere garrantzia izan zuen. Bonbilak aurretik ezagutzen zen energi mota bat erabiltzen du: elektrizitatea. Elektrizitatea elektronikaren oinarria da, gure teknologiaren oinarrietariko bat izanik. Energi iturrien erabilpenak mendebaldeko zibilizazioaren bizimodua zeharo aldatu du, baina ez beti era egoki batean. 1 Irudian zorigaiztoko eragin hauetako batzuk irudikatzen dira.

Energia nuklearraren erabilera ezegokiaren eragin kaltegarriak ezagunak dira, berotegi efektuaren eragin kaltegarriak ere, marea beltzek eraginiko kalteak, eta abar. Zoritxarrez, zerrenda luzea da.

Figure 1: a) Urre beltzaren sukarraren garaiko irudia b) Bonba atomikoaren ziza. c) Marea beltzak harrapaturiko pinguinoak.

a) b) c)

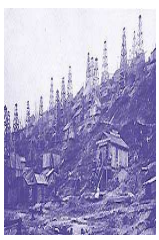

Figure 2: a) Errota zahar bat b) Elektrizitatea sortzeko errota modernoak c) Estazio Espazial Internazionalaren irudi bat, bertan estaziorako elektrizitatea sortzen duten eguzki-zelulak erabiltzen direlarik.

a) b) c)

Erabilienak diren energi iturrien eragin kaltegarriak direla eta, ingurugiroa gutxiago kutsatzen edo kutsatzen ez duten energi iturri berriak beharrezkoak dira. Hauek dira, alegia, energi iturri berriztagarriak, hauen adierazgarri eguzki-energia edota energia eolikoa direlarik, besteak beste. Energi berriztagarriak aspaldi ezagunak dira, errotak garia txikitzeko denbora luzez erabiliak izan dira, ogia egiteko beharrezkoa den irina lortzeko. Gaur egun errota modernoak erabiltzen dira elektrizitatea sortzeko. Euskal Herriko mendietan hauetako anitz ikusten ahal dira. Arbasoek ere eguzki-energia erabiltzen zuten, ura berotzeko, adibidez. 2 Irudian energi iturri berriztagarri hauetako batzuk irudikatzen dira.

Lan honetan eguzki-zelula fotovoltaikoetan erabiltzen diren material batzuei buruz arituko gara. Eguzki-zelulek eguzki-energia elektrizitate bihurtzen dute. Eguzki-zeluletan erabiltzen diren materialak solido ioniko zein metalikoak dira, ioiak zelulan zehar homogeneoki banatuta direlarik. Dena dela, larogeita hamargarren hamarkadan clusterretan oinarrituriko solidoak garatu dira, aplikazio fotovoltaikoa dutela ikusi delarik. Aurrerapen hau nanoteknologiak ezagutu duen aurrerakada izugarriaren baitan kokatzen da. Hurrengo ataletan zelula fotovoltaikoak eta nanoteknologia sakonago aztertuko dira.

Eguzki-zelula fotovoltaikoak

Anitz motatako materialak erabiltzen dira eguzki-zeluletan, baina hauek guztiak propietate bat dute komunean: erdieroaleak dira. Erdieroaleen ezaugarri

Figure 3: Eguzki-zelula tipikoa

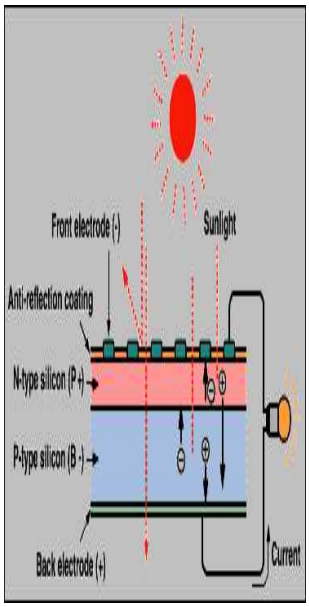

nagusiena okupaturiko azkeneko banda eta okupaturik gabeko lehengo bandaren artean dagoen energi langa ingurunetik energia bereganatuz erlatiboki errez gainditzen ahal dela da. Eguzki-zelulen kasuan bereganatzen den energia hau eguzkitik heltzen den energia da. Eguzki-energia zelulara heltzerakoan elektroiek absorbatzen dute, okupaturiko bandatik okupatu gabeko bandara pasatzen direlarik, modu honetan korronte elektrikoa sortuz. Material desberdin anitz erabiltzen dira eguzki-zeluletan. Historikoki lehenbizikoa silizioa izan zen. Silizioaren propietate eroaleak eta produkzio koste txikiak eguzki-zeluletan erabiltzeko material egokia egiten zuten silizioa. Hala ere, beste material anitz eraginkorragoak direla ikusi da, garestiagoak izanagatik. GaAs bezalako III-V materialak [1, 2, 3] edo CdTe bezalako II-VI materialak [4-22] silizioaren ordez erabiltzeko material egokiak dira eraginkortasun handiko eguzki-zelulak garatzeko. Eguzkitik Lurrera heltzen den energia gehiena eremu ikuskorrean da, eta gainerakoa honen inguruan, eremu ultramorean zein infragorrian. Eremu ikuskorra 1.75 - 3 eV tartean dago. Hortaz, eguzki-zeluletan erabilgarria izateko material batek energi langa inguru honetan izan behar luke, ahalik eta energia gehien absorbatzeko. II-VI konposatuak material hauetako batzuk dira, beren energi langak 1.45 eV (CdTe) eta 3.66 eV (ZnS) tartean daudelarik.

Ondoren eguzki-zelula fotovoltaiko baten funtzionamendua 3 irudian adierazten da [23].

Bi erdieroale mota beharrezkoak dira zelula osatzeko. Alde batetik negatiboki kargaturiko elektroiak garraiatzen dituen n-motako erdieroale bat eta beste

aldetik positiboki kargaturiko zuloak garraiatzen dituen p-motako erdieroalea. Azken honi absorbatzailea deritzo, eta lehenengoari leihoa. Leihoaren energi langa handiagoa da, eta energiaren absortzioa gehienbat absorbatzailean gertatzen da, izenak adierazten duen bezala. Behin eguzki-energia zelulara helduta, elektroiek energi langa gainditzeko eta okupatu gabeko bandara pasatzeko behar duten energia absorbatzen dute. Orduan elektroiak n-motako erdieroalera igaro eta aurreko elektrodoan biltzen dira. Era berean, sorturiko zulo positiboak atzeko elektrodoan pilatzen dira. Honen ondorioz bi gainazalen artean potentzial diferentzia bat sortzen da, eta biak elkartzean korronte elektrikoa agertzen da. Irudian bonbila piztuta ikusten ahal da honen adierazgarri.

Energi langa egokiez gain, eguzki-zeluletan erabilgarriak izateko materialek goian aipaturiko ezaugarriak izan behar dituzte, n-motako zein p-motako erdieroankortasuna ukan behar dute. II-VI materialek propietate hauek dituzte, eta eraginkortasun handiko eguzki-zelulen garapenerako aproposak izaten ahal dira.

Clusterrak, nanoegiturak eta nanoteknologia

Joan den mendeko lehenengo erdialdean nanoteknologia, teorikoen ustetan, ez zen aurrera aterako. Erwing Schrödinger-ek 'atomoak ezin direla gehiago indibidualki kontsideratu' ondorioztatu zuen [24], eta ziurgabetasun printzipioa proposatu zuen Werner Heisenberg-ek 'atomoek probabilitate eta posibilitateen munduan daudela, gauzen edo gertakizunen munduan beharrean' pentsatzen zuen [25]. Hau da, atomoak izaera indibidualik gabeko enteak zirela pentsatzen zuten. Dena dela, gaur egun badakigu atomoak indibidualki tratatzen ahal direla [26]. Richard Feinmann Nobel Saridunak esan zuen bezala [27] 'There is plenty of room at the bottom'. Gai honetan aintzidariak ziren Arthur von Hippel-ek [28] edota K. Erik Drexler-ek [29, 30] iragarri zutenarekin bat dator gaur egun nanoteknologiak ezagutu duen bultzada ikaragarria.

Gaur egun nanoteknologian zenbait bide zabaldu dira, nanoelektronikaren inguruan, nanokableak, nanomekanika, eta abar, eta teknika berri eta iraultzaileak garatu dira, hala nola indar atomikozko mikroskopioa (AFM), edota tunel efektozko mikroskopioa (STM). Nanokableek eta nanoelektronikak txip txiki eta azkarragoen garapenean posibilitate zabal berriak ireki dituzte [31, 32, 33, 34]. 30nm-ko transistoreak garatu dira, eta NewScientist aldizkarian projektuan parte hartu duen batek erraten duen bezala [35] 'Gure ikerketak transistore txiki hauek gaur egungo aparatuak bezala funtzionatzen dutela probatzen du, eta bolumen handi batean produzitzeko oinarrizko mugarik ez dagoela erakusten du'. 20nm-ko beste transistore bat ere aurkeztu dute [36] Grenoblen, French Atomic Energy Commission's Electronic, Technological and Instrumentation Laboratory-n (LETI).

Atomo indibidualekin elkarrekintza izateko posibilitatea material eta sistema berriak garatzeko lehengo pausoa da. Konposatu berdineko sistema kristalinoak baino aplikazio gehiago izaten ahal duten materialak eratzen ahal dira. Esparru honetan artikulo garrantzitsuak agertu dira [37, 38, 39, 40, 41]. Hobekien ezagutzen diren cluster edo nanoegitura 'berriak' 1985. urtean aurkituriko

[42] karbono hutsezko esferoideak dira, fulerenoak alegia. Literaturan fulerenoei buruzko [43, 44, 45, 46] eta beren solidoei buruzko [47, 48] hainbat lan agertu dira. Clusterretan oinarrituriko solido hauek besteak beste propietate supereroaleak [49, 50, 51] izaten ahal dituzte, eta horretaz gain zelula fotovoltaikoetan ere erabilgarriak direla [52, 53] ikusi da.

Karbono-clusterren antzera, balentzi isoelektronikoak diren III-V edo eta II-VI materialen clusterren gaineko interesa agudo hazten ari da. III-V materialen clusterren lan teoriko [54, 55, 56, 57, 58, 59] zein esperimentalak [60, 61] aurkitzen ahal dira literaturan. Bestalde, dopaturiko II-VI nanopartikula fotoluminiszenteak [62, 63], fotosentikorrak [64], eta beste batzuk, dopatuak [65, 66, 67, 68] zein dopatugabeak [69], argitaratu dira.

Lan honen helburuak

Aurreko ataletan ikusitakoarekin arrunt interesgarria bihurtzen zaigu bi eremu hauen fusioa, clusterrak alde batetik eta II-VI materialak bestetik, alegia. Lan honen helburua II-VI materialen clusterren azterketa teorikoa egitea da. Lehenbizi minimo global eta lokalak karakterizatu behar dira, behin hau egina dagoela eszitazio energiak kalkulatu ahal izateko. Modu honetan cluster hauen absortzio propietateak aztertuko ditugu, eta horrela eguzki-zelula eraginkorragoen eraketan material aproposak direnentz behatzerik izanen dugu. Clusterretan oinarrituriko solidoak errealitate dira gaur egun. Fulerenoetan oinarrituriko solidoak eraiki dira, eta propietate interesgarriak dituzte, lehen ikusi bezala. C_{60} deribatuen solidoak eguzki-zelula eraginkorragoak osatzeko baliogarriak izaten ahal dira. M_3C_{60} konposatuak supereroaleak dira, eta C_{28}-oinarria duten solidoak tenperatura altuko supereroaleak izaten ahal dira.

Posible izanen litzateke beraz II-VI materialak optimizatzea eragin handiko eguzki-zelulak osatzeko, sistema kristalinoak baino eraginkorrago diren materialak sortuz. Tesi honen lehenengo atalean (2., 3., 4. eta 5. kapituluak) Zn_iX_i, $i = 1 - 9, 12, 15$, X=O, S, Se, Te, -ren minimo orokorrak zein lokalen egiturak karakterizatu ditugu. Bigarren atalean (6., 7., 8. eta 9. kapituluak) minimo orokorren eszitazio energiak kalkulatu ditugu. Bukatzeko, ondorio orokorrak eta gerorako lana aurkezten da. Lan hau guztia burutzeko gaur egun boteretsuak diren kimika kuantikoaren metodo eta programak erabili ditugu. Hurrengo atalean kimika kuantikoa laburki gogoratuko dugu.

Kimika kuantikoa

Joan den mendearen hasieran garaturiko teoria kuantikoak [70, 71, 72, 73] zeharo aldatu zuen mundu mikroskopikoaren inguruan fisikariek zuten ikuspuntua. Teoria hau baino lehenago garaturiko teoria guztiek ezin zuten atomoen egonkortasuna azaldu. Bohr-ek atomo sinpleenaren egonkortasuna elektroiak nukleoaren inguruan orbita estazionarioetan bueltaka ibiltzen direla esanez azaldu zuen. Elektroi batek orbita batetik bestera mugitzeko energi kuantu

bat askatu edo absorbatu egin behar du. beste hitzetan esanda, energia kuantizaturik dago, ez da jarraia. Teoria kuantikoan hau teoriaren ondorioa da, ez da aldez aurretik finkaturiko gauza. Hasiera batean teoria fisikarien munduan garatu zen, baina berehala kimikan izaten ahal zituen aplikazioak behatu ziren, kimika kuantikoa sortuz. Urteen poderioz kimika kuantikoa kimikariendako arrunt erabilgarria bihurtu da, molekulen propietateak kalkulatu, ulertu eta iragartzeko.

Printzipioz sistema bati buruzko informazio guztia bere uhin funtzioak ematen digu. Uhin funtzioa zein den jakiteko 'bakarrik' Schrödinger-en ekuazioa askatu behar dugu:

$$\widehat{H}\Psi = E\Psi \qquad (1)$$

$\widehat{H}$ hamiltondarrak nukleo eta elektroien energia kinetikoa, elektroi-elektroi, elektroi-nukleo eta nukleo-nukleo elkarrekintzak kontuan hartzen ditu. Born-Oppenheimer [74] hurbilketa kontuan hartuta, elektroien eta nukleoen higidura banatzen dira, eta hortaz $\widehat{H}$-an nukleoen koordenatuak parametro konstanteak dira. Zoritxarrez, ekuazio hau elektroi bat baino ez duten sistemen kasuan bakarrik askatzen ahal da, hidrogeno atomoa, adibidez. Hau dela eta metodo hurbilduak garatu behar izan dira:

1. Uhin-funtzioan oinarritzen diren metodoak: bariazionalak (konfigurazioen elkarrekintza) edo gorputz-anitzezko perturbazio teoria.
2. Dentsitate-funtzionalaren teoria (DFT).
3. Quantum Monte Carlo (QMC).

Ez da atal honen helburua metodo hauen guztien deskribapen osoa egitea. Beraz, interesaturik dauden irakurleak gai hauek lantzen dituzten literaturara zuzentzen ditugu. Ikusi adibidez [75, 76, 77, 78, 79].

Uhin-funtzioan oinarrituriko metodoak garatu ziren lehenengoak izan ziren. Urteetan zehar erabilienak izan diren bi metodoak Balentzi Lotura (BL) metodoa eta Molekula-Orbitalen (MO) metodoa izan dira. BL metodoa 1927. urtean Heitler eta London-ek formulatu zuten [80]. MO metodoa beranduago garatu zen, Hund [81], Mulliken [82] eta beste batzuen eskutik. Metodo hau erabiliena bilakatu zen bere botere kuantitatiboaren ondorioz. MO-k orbital ortogonalak erabiltzen ditu, kalkulua anitz errazten delarik. Ez ordea VB metodoak, orbital ez-ortogonalak erabiltzearen ondorioz kalkulua luzeagoa eta korapilotsuagoa, hortaz garestiagoa, delarik.

Hastapenetan garatu zen lehendabizietako molekula-orbital metodoa Hartree-Fock metodoa [83, 84] izan zen. Bertan uhin-funtzioa elektroi-bakarreko orbitalen antisimetrizaturiko biderkadura da. Elektroiak nukleoaren eta beste elektroien eraginez sorturiko batezbesteko eremuaren eraginpean higitzen direla suposatzen da. Metodo honen arazorik handiena da kontrako spina duten elektroien arteko korrelazioa kontuan hartzen ez duela. Korrelazio mota hau kontuan hartzeko hainbat bide dago. Møller-Plesset [85] teoria (MPn, n perturbazio-ordena izanik) bezalako perturbazio-metodoetan elektroi-korrelazioa HF

arazoaren perturbazioa bezala kontsideratzen da. Konfigurazioen Elkarrekintza (KE) [86, 87] metodoan uhin-funtzioa konfigurazio desberdinen konbinazio lineala bezala adierazten da, elektroi-anitzezko uhin-funtzio zehatzaren emaitza bariazional hobeagoa lortzeko asmoz. Beste metodo sofistikatuagoak egon badaude, Coupled Cluster (CC) [88, 89, 90], Erreferentzia-Anitzezko Konfigurazioen Elkarrekintza (EAKE) edo Espazio Eraginkor Osoa (EEO) [91, 92] metodoak, oinarrizko egoera zein egoera eszitatuen propietate elektronikoak aztertzeko tresna arras erabilgarriak direlarik.

Quantum Monte Carlo metodoak sistema anitzen oinarrizko egoeren [93, 94, 95, 43] zein egoera eszitatuen [96, 97] propietate elektronikoak kalkulatzeko orduan oso boteretsuak direla ikusi da. Lan honetan ez dira erabili, eta interesaturik dagoena ondorengo lanetara bidaltzen ditugu [79, 98].

Tesi honetan aurkezten dugun lanaren gehiena dentsitate-funtzionalean oinarrituriko metodoak erabilita burutu da. Ondorengo azpiatalean metodo hauek sakonago deskribatuko ditugu.

Dentsitate-Funtzionalaren Teoria

Denborarekiko askea den Dentsitate-Funtzionalaren Teoria

Dentsitate-Funtzionalaren Teoriaren formalismoak N elektroiren uhin-funtzioa eta dagokion Schrödinger-en ekuazioaren ordez askoz ere sinpleagoa den $\rho(\vec{r})$ elektroi-dentsitatea jartzen du. Hau hiru aldagai espazialen funtzioa da. Egoera elektronikoa, energia eta edozein sistemaren propietate elektroniko guztiak $\rho(\vec{r})$ honen funtzioan deskribatzen ahal dira [77, 78].

Hohenberg eta Kohn-ek [99] degeneratua ez den oinarrizko egoera duen sistema baten propietate elektronikoak $\rho(\vec{r})$ elektroi-dentsitateak determinatzen dituela demostratu zuten. Hortaz, E_0 oinarrizko egoeraren energia $\rho(\vec{r})$-ren funtzionala da. Orokortuz, oinarrizko egoearen elektroi-dentsitatea jakinez gero, oinarrizko egoeraren propietate elektroniko guztiak kalkulatzea posible da, behin funtzional-dependentziak finkatu ondoren. Energi funtzionala aurkitzeko energiaren bariazio-printzipio bat finkatu zuten, uhin-funtzioaren bariazio-printzipioaren antzerakoa. Horrela, $E[\rho]$ funtzionalaren forma zehatza jakinik oinarrizko egoeraren dentsitatea bilatzen ahal dugu (uhin-funtzioaren kasuaren antzera). Tamalez, funtzioanalaren forma esaktoa ezezaguna denez, Kohn eta Sham-ek [100] funtzional honen hurbilketa ez-zuzen bat garatu zuten, Kohn-Sham metodoa, alegia. Ondorioz DFT kalkulu zehatzak egiteko tresna erabilgarria bihurtu zen. Haiek N elektroiz osaturiko eta ρ oinarrizko egoeraren elektroi-dentsitate duen molekula baten E_0 oinarrizko egoeraren energia elektronikoa ondorengoa dela erakutsi zuten:

$$E_0 = -\frac{1}{2}\sum_{i=1}^{N} < \psi_i(1)|\nabla_1^2|\psi_i(1) > + \int \upsilon(r)\rho(1)d\vec{r}_1 \\ +\frac{1}{2}\int\int \frac{\rho(1)\rho(2)}{r_{12}} d\vec{r}_1 d\vec{r}_2 + E_{xc}[\rho] \qquad (2)$$

$\upsilon(r) = -\sum_\alpha \frac{Z_\alpha}{r_{1\alpha}}$ nukleoen eraginez dagoen kanpo-potentziala da, ψ_i Kohn-Sham orbitalak dira, eta $E_{xc}[\rho]$ truke-korrelazio energia da.

Kohn-Sham prozeduran oinarrizko egoeraren ρ esaktoa Kohn-Sham orbitaletatik lortzen ahal da,

$$\rho = \sum_{i=1}^{N} |\psi_i|^2 \qquad (3)$$

eta Kohn-Sham orbitalak

$$\hat{F}_{KS}(1)\psi_i(1) = \varepsilon_i\psi_i(1) \qquad (4)$$

elektroi bakarreko ekuazioak ebatziz lortzen dira, $\hat{F}_{KS}$ Kohn-Sham operadorea

$$\hat{F}_{KS} = -\frac{1}{2}\nabla_1^2 + \upsilon(1) + \sum_{j=1}^{n} \hat{J}_j(1) + V_{xc}(1) \qquad (5)$$

delarik. $\hat{J}$ Coulomb operadorea da, eta V_{xc} truke-korrelazio potentziala. $\hat{F}_{KS}$ HF ekuazioetan agertzen den Fock operadorea bezalakoa da, gauza batean izan ezik. Truke operadorearen ordez, truke eta korrelazioa kontuan hartzen dituen V_{xc} jartzen da.

Ekuazio hauek iteratiboki ebazten dira. Hasierako dentsitate batetik hasita $\hat{F}_{KS}$ eraikitzen da, eta (3) ekuazio-taldea ebazten da. Emaitza $\hat{F}_{KS}$ berri bat eratzeko erabiltzen da. Prozedura hau konbergentzia lortu arte errepikatzen da.

Kohn-Sahm orbitalen esanahi fisikoa eztabaidan dago oraindik. Autore batzuen arabera ez dute inolako esanahirik, bakarrik ρ zehatzaren kalkuluan erabilgarriak dira. Era berean, Kohn-Sham orbitalen energiak molekula-orbitalen energiekin ez lirateke nahastu behar. Beste batzuk, ordea, HOMO-ren Kohn-Sham energia ionizazio potentzialaren negatiboa dela kontuan harturik [101, 102], eta honetaz gain Kohn-Sham ekuazioak, HF kasuaren antzera, partikula askeen eredua gogora ekartzen duela kontuan harturik, Kohn-Sham orbitalei HF orbital kanonikoek duten antzeko esanahi fisikoa egokitzen diete.

Azken aldiko argitalpenetan DFT-aren bidez lorturiko molekula-orbitalak eta estandar MO-LCAO metodoen bidez lorturikoak arras antzekoak direla ikusi da. Hortaz, molekulei buruzko informazio erabilgarri anitz beraien MO-ak aztertuz lortzen ahal da, hauek DFT-aren bidez lortuak izan arren [101, 103].

Dena dela, beste arazo bat dago: $E_{xc}[\rho]$ truke-korrelazio funtzionala eta beraz $v_{xc}[\rho; \overrightarrow{r}]$ truke-korrelazio potentziala elektroi-gas uniformearen kasurako baino ez da ezagutzen. Zorionez, funtzional hurbilduak garatu dira. Hurbilketa sinple bat dentsitate lokalaren hurbilketa (DLH) da. Honen ideia $\rho(\overrightarrow{r})$ dentsitate lokala duen bolumen elementu bakoitza elektroi-gas homogeneoa bezala kontsideratzea da. Ikuspuntu honetatik hurbilketa hau dentsitatea espazioan zehar mantso aldatzekotan zehatza izanen da. $E_{xc}[(\rho)]$ ondorengo espresioak ematen du:

$$E_{xc}^{LDA}[(\rho)] = \int \rho(\vec{r})\varepsilon_{xc}(\rho)d\vec{r} \qquad (6)$$

$\varepsilon_{xc}(\rho)$ ρ elektroi-dentsitate duen elektroi-gas homogeneoaren truke plus korrelazio-energia elektroi bakoitzeko da. $\varepsilon_{xc}(\rho)$-rendako espresio zehatz bat Vosko, Wilk eta Nusair-ek [104] aurkitu zuten. Espresio hau aplikatuta dentsitate lokalaren hurbilketa (DLH) edo spin dentsitate lokalaren hurbilketa (SDLH) [105] lortzen dira. Azken honen kasuan spin desberdina duten eleketroiendako orbital eta ρ^{α} eta ρ^{β} dentsitate desberdinak erabiltzen dira. Noski, molekulen kasuan hauek benetako funtzionalaren hurbilketak besterik ez dira, ρ homogeneoa ez delakotz. Hurbilketa dentsitate-gradientearen araberako espansio bat eginez hobetzen ahal da. Metodo hauek generalizaturiko gradientearen hurbilketa (GGA) dira, eta molekulen azterketan garrantzi handia dute, elektroi-dentsitatea homogeneoa dela ezin baita kontsideratu.

DFT metodoek sistema kimiko gehienetan emaitza bikainak ematen dituztela demostratu da [106], CPU intentsiboak diren elektroi-korrelazio metodoekin konparagarriak izanik. Hala ere, anitzetan loturen disoziazio energiak gainestimatzen dituzte [107]. HF eta DFT-ren arteko hibridoak disoziazio energiaren zehaztasuna handitzen dute, Johnson-ek et. al. erakutsi bezala [108]. Becke 3 [109] hibridoa Lee-Yang-Parr (B3LYP) [99, 110, 111] korrelazio funtzionalarekin konbinatuta, erabilienetako bat bihurtu da, ondorengo forma duelarik:

$$(1-a_0)E_x^{LSDA}+a_0E_x^{HF}+a_xE_x^{B88}+a_cE_c^{LYP}+(1-a_c)E_c^{VWN} \qquad (7)$$

Parametroen baloreak a_0=0.20, a_x=0.72 eta a_c=0.81 dira, hurrenez hurren. Funtzional honi Becke-ren 3 parametrodun funtzionala esaten zaio, B3LYP.

DFT kalkuluek E_{xc} zehatza erabiltzen ez dutenez, ez dira, zehazki mintzatuz, ab-initio kalkuluak. Dena dela, datu esperimentalak doitzeko parametrorik erabiltzen ez dutenez, espiritualki ab-initio kalkuluetatik erdienpirikoetatik baino gertuago daude. Metodo hauen abantaila handienetako bat HF metodoaren koste konputazional antzekoa izanik elektroi-korrelazioa kontuan hartzen dutela da. Dena dela, korrelazio efektu hauek ezin dira zehazki sailkatu, hastapenetik ez-korrelaturiko emaitzarekin nahasturik daudelakotz. Honetaz gain, sofistikazio gehiago aplikatuz, kalkuluak hobetzeko bide sistematikorik ez dago, eta honen ondorioz emaitzak diren bezala onartu behar dira. Arazo hauek izan arren, DFT-k sistema kimiko batzuen oinarrizko egoeraren propietateendako emaitza onak eman ditu, MP2-rekin alderagarria den kalitatearekin [112] batzuetan, eta hobeagoa beste kasu batzuetan. Koste konputazional baxua dela eta, sistema handien kasurako DFT aukeratzen den metodoa da, elektroi-korrelazioa MP edo CI metodoen bidez kontsideratzea biziki garestia delakotz.

Denboraren menpekoa den Densitsate-Funtzionalaren Teoria

Denborarekiko askea den bertsioan DFT-k oinarrizko egoerendako kalkulu zehatzak burutzen ditu. Tamalez, eszitazio energiak ez ditu zehazki kalkulatzen. DFT-ren denboraren menpekoa den formalismoak (ikusi [113, 114, 115]) kargadentsitatearen erantzun dinamikoaren kalkuluarendako bide zehatza ematen du. Honek, erantzun linealaren teoriarekin konbinatuta, eszitazio elektroniko bertikalaren espektroa kalkulatzeko aukera ematen digu [114, 116, 117, 118, 119]. TDDFT arrunt sistema desberdinetan erabili da, konposatu metalikoetan

[120, 121, 122], organiko [123, 124, 125] zein ezorganikoetan [126, 127], edo eta sistema zabalduetan [128]. Hortaz, sistema errealen eszitazio energiak kalkulatzeko tresna hagitz sendoa da. Dena dela, Rydberg egoerak ez ditu zehazki kalkulatzen [129, 130].

Hohenberg-Kohn teoriaren energi minimoaren printzipioaren antzekoa den ekintza-geldikorraren printzipio bat garatzen ahal da. Hau, v-errepresentagarritasunari buruzko onarpen egokiekin batera, denboraren menpekoa den Kohn-Sham ekuazioa garatzeko erabiltzen ahal da:

$$\left[-\frac{1}{2}\nabla^2 + v\left(r,t\right) + \int \frac{\rho\left(r',t\right)}{|r-r'|}dr' + v_{xc}^{\sigma}\left(r,t\right)\right]\psi_{j\sigma}\left(r,t\right) = i\frac{\partial}{\partial t}\psi_{j\sigma}\left(r,t\right) \tag{8}$$

$v_{xc}^{\sigma}\left(r,t\right)$ formalki truke-korrelazio ekintzaren, A_{xc}-ren, deribatu-funtzionala da, baina hurbilketa gehienek hurbilketa adiabatikoa erabiltzen dute,

$$v_{xc}^{\sigma}\left(r,t\right) = \frac{\delta A_{xc}\left[\rho_{\uparrow},\rho_{\downarrow}\right]}{\delta\rho_{\sigma}\left(r,t\right)} \cong \frac{\delta E_{xc}\left[\rho_{\uparrow}^{t},\rho_{\downarrow}^{t}\right]}{\delta\rho_{\sigma}^{t}\left(r\right)} \tag{9}$$

$\rho_{\sigma}^{t}\left(r\right)$ t denbora jakin batean kalkulaturiko $\rho_{\sigma}\left(r,t\right)$ funtzioa eta E_{xc} denborarekiko askea den Kohn-Sham teoriaren truke-korrelazio funtzionala direlarik.

$\overline{\alpha}\left(\omega\right)$ polarizabilitate dinamikoak denboraren menpekoa den eremu elektrikoari dipolo-momentuak emaniko erantzuna deskribatzen du. Honen ondorioz, denboraren menpekoa den dentsitate-funtzionalaren teoriatik lorturiko karga-dentsitatearen erantzunetik kalkulatzen ahal da, denboraren menpekoa den dentsitate-funtzionalaren erantzun teoria erabiliz. Honek eszitazio elektronikoaren espektroa normalean erabiltzen den dipolo hurbilketaren bidez kalkulatzeko aukera ematen du. Egoeren gaineko batura-erlazioaren arabera,

$$\overline{\alpha}\left(\omega\right) = \sum_{l}\frac{f_l}{\omega_l^2 - \omega^2} \tag{10}$$

polarizazio dinamikoaren poloek eszitazio energiak determinatzen dute, ω_l, eta f_l erresiduoek dagokien osziladore-indarrak [114]. Oinarri-talde finito formalismo bat erabiltzen da polarizabilitate dinamikoa (10) egoeren gaineko baturaren espresioa era tentsionalean paratzeko. Polo egituraren azterketak

$$\Omega\overrightarrow{F_l} = \omega_l^2\overrightarrow{F_l} \tag{11}$$

balore propio problema ebatziz eszitazio energiak lortzen ahal direla esaten digu. Ω [114, 115, 116] erreferentzietan definitzen da, eta f_l osziladore-indarrak $\overrightarrow{F_l}$ bektore propioetatik lortzen dira. Informazio gehiagorako ikusi lehen aipaturiko review-ak eta [131, 132].

Oinarri-taldeak

Uhin-funtzioan zein dentsitate-funtzionalean oinarrituriko metodoek uhin-funtzioa espanditzeko funtzio-talde bat beharrezkoa dute. Funtzio-talde hauei oinarri-taldeak deritze. Oinarri-talde egokiaren aukeraketa arras garrantzitsua da kalkuluaren arrakastarako. Dena dela, oinarri-taldearen zehaztasuna eta bere tamaina kontuan hartu behar ditugu, oinarriaren tamaina handitzean kalkuluaren kostea garestiago egiten baita. Kimika kuantikoan egiten diren kalkuluetan gehien erabiltzen diren funtzioak Kontraituriko Funtzio Gaussiarrak (KFG) dira. Hauek funtzio Gaussiarren (hasierakoak) konbinazio linealez (kontrakzioak) osaturik daude.

$$\varphi_{\mu}^{CGF}(|\vec{r}-\vec{R}_A|) = \sum_{p=1}^{L} d_{p\mu} g(\alpha_{p\mu}, |\vec{r}-\vec{R}_P|) \qquad (12)$$

$\alpha_{p\mu}$ aintzindarien berretzaileak eta $d_{p\mu}$ kontrakzioen koefizienteak elementu desberdinendako optimizatzen dira.

Normalean all-electron oinarri-taldeak erabiltzen dira. Honek oinarri-taldeak elektroi guztiak kontsideratzen dituela esan nahi du. Hala eta guztiz ere, kasu batzuetan elektroi kopuru izugarria dugu eta kalkulua arrunt garestia da. Honen ondorioz elektroi batzuk, barne-elektroiak, kalkulutik kentzen dira eta bakarrik balentzi elektroiak kontsideratzen dira. Kasu honetan kanpo-elektroiak nukleo eta barne-elektroiek eraginiko batezbesteko potentzialean higitzen dira. Tesi honetan Stevens eta kideek [133] garaturiko pseudopotentzialak erabili ditugu. Pseudopotentzial hauek, konfigurazio atomiko egokien kasuan [134], Dirac-Fock ekuazioaren emaitza numerikoetatik lorturiko balentzi elektroien orbital energiak eta dentsitateak erreproduzitzeko eraiki dira.

Pseudopotentzial hauek zink atomoen d elektroiak balentzian sartzen dituzte, $1s^2\,2s^2\,2p^6$ barne-elektroi gisa kontsideratuz. Balentzizko oinarri-taldea energi optimizaturiko oinarri-taldea da. *sp* kasurako zeta-bikoitza da eta zeta-hirukoitza *d*-rako (8sp6d/4sp3d). VIB zutabeko elementuendako $ns^2\,np^4$ elektroiak dira balentziazkoak, eta zeta-bikoitza den (5sp/2sp) oinarri-taldea erabili da.

Chapter 1

General Introduction

The apprenticeship of the use of fire by humans in the stone age was one of the most important leaps forward taken by the human race. Qualitatively it supposed the beginning of the control of the natural energy sources, indispensable for future development of civilization. Nowadays our civilization makes use of a huge amount of energy. Industrial development, and of course the comfortability of the occidental way of life needs energy to be consumed. This energy is there, in the nature, and the "only" thing humans have done is to learn how to manage and transform that energy, in concordance with the first principle of thermodynamics. Many energy sources have been discovered along the years, but the most important for the paramount technological development known in our days were discovered and developed at the end of the XIXth and the beginning of the XXth centuries. Petroleum and nuclear energy are some clear examples. Another important discovery was the bulb by Edison, since it made use of an already known kind of energy: electricity. Electricity is the basis of all electronics, and very important for the confortableness of our society. This management of natural energy sources has changed the way of life of occidental civilization, but not only in a desiderable way. In Figure 1.1 some of these negative consequences are depicted.

It is not necessary to point out the dramatic consequences of nuclear energy misuse, or the unforeesable effects of carbon dioxide emissions due to the use of petroleum derivatives, or the oil slicks... Unfortunately, there are many other ors as well.

Due to these negative impacts of the mostly used energy sources, new energy sources, with less or no negative impact in the environment are necessary. These are the so called alternative energies, i.e. solar energy, eolic energy, etc, which have been known for a long time. Windmills and watermills have been used for a long time to mill the grain, obtaining flour for bread. Nowadays modern windmills are used to generate electricity. Solar energy has also been historically used, for example, to warm water. In Figure 1.2 some of these alternative energy sources are shown.

The materials studied in this work are semiconductor materials, which are ideal for their use in photovoltaic solar cells, which make use of solar energy to ob-

Figure 1.1: a) A picture of the pioneers of black gold. b) The mushroom of the atomic bomb. c) Penguins on an oil slick.

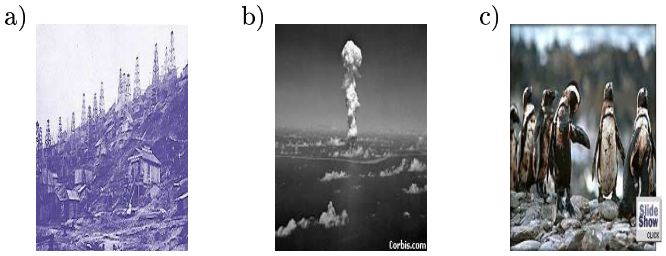

Figure 1.2: a) An old windmill. b) Modern windmills to generate electricity. c) A picture of the International Space Station, where there can be seen the photovoltaic solar cells used to generate electricity for the Station.

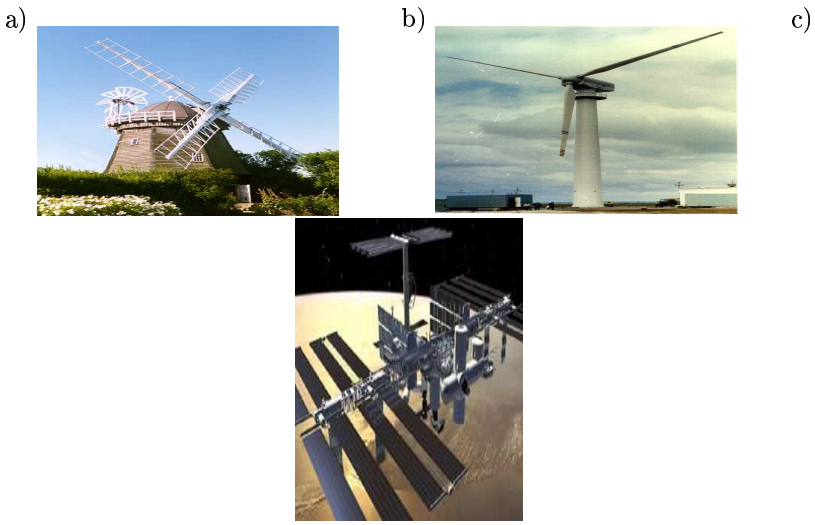

tain electricity. Materials in solar cells have been bulk solids, ionic or metallic crystals where ions are homogeneously distributed around the cell. However, in the nineties cluster based solids have been developed, and have been seen to have photovoltaic applications. This development can be associated to the huge increase of the nanotechnology, the technology of small. In the following subsections photovoltaic devices and nanotechnology are discussed in more detail.

1.1 Photovoltaic solar cells

There are many different materials which are used in photovoltaic solar cells, but all of them share an important property: they are semiconductor materials. The main characteristic of semiconductors is that they have energy gaps between the last occupied and the first unoccupied bands that may be easily gained achieving a certain amount of energy from the environment. In the case of solar cells the energy absorbed is the one that arrives from the sun. The solar energy reach the solar cell and it is absorbed by the electrons, which may be excited from the occupied band to the unoccupied one, producing current within the cell. Many different materials are used in solar cells. Historically the first one was silicon. The semiconductor properties of silicon along with the relatively cheap cost of production made it one of the most popular materials for solar cells. Nevertheless, many other materials have been seen to be more reliable, but are much more expensive. III-V compounds such as GaAs [1, 2, 3], or II-VI materials [4-22], such as CdS and CdTe are promising alternatives to substitute silicon in the production of high efficient solar cells. Most of the energy reaching the earth from the sun lies within the visible spectrum, and the rest is mainly in its nearby surroundings, ultraviolet (UV) and infrared (IR). Visible spectrum spans between 1.75-3 eV. Therefore an appropriate material for solar cells should have band gaps within this range, or below. II-VI compounds are some of these materials. Their band gaps range from 1.45 eV in the case of CdTe to 3.66 eV for ZnS.

The functioning of a solar cell is outlined in Figure 1.3 [23].

Two semiconductor types are needed to build the cell. On one hand an n-type semiconductor, which conducts the negatively charged electrons, and on the other a p-type semiconductor, which conducts the positively charged holes. The p-type semiconductor is called absorber, and the n-type one window. The window material's band gap is larger than the absorber's one, and as the name says, the absorption in the cell mainly occurs in there, although a small part of the absorption also may happen in the window. Once the sun light reaches the cell, the photons with the necessary energy to excite electrons to the unoccupied band are absorbed. The electrons then move to the n-type semiconductor and are stored in the front electrode. Similarly, positive holes are stored in the back electrode. In this way a potential difference between both surfaces is achieved, and connecting them electric current is obtained. In the picture this is represented by the swichted bulb.

Beside the importance of appropriate band gaps, materials in solar cells must

Figure 1.3: A typical solar cell

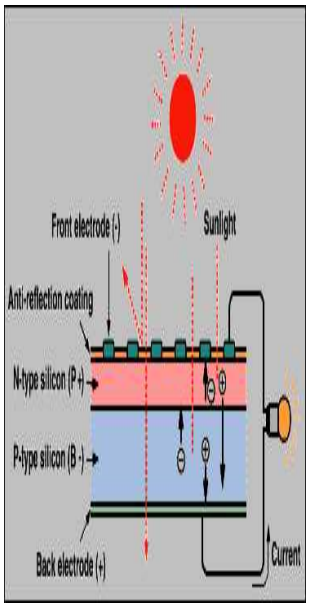

present the above explained characteristics, i.e., they must combine n- and p-semiconductors. II-VI materials do have these properties, and are promising materials for the development of high efficient solar cells.

1.2 Clusters, nanostructures and nanotechnology

Nanotechnology was claimed to be a not viable proposition by the theoreticians in the first half of the last century. Schrodinger concluded that "atoms must no longer be regarded as identifiable individuals" [24], and Werner Heisenberg, who stated the indetermination principle, thought that "atoms form a world of potentialities of possibilities rather than one of things or facts" [25]. That is, it was thought that atoms were not entities with individual nature. However, nowadays we know that atoms may be managed individually [26]. As it was pointed out by the Nobel Prize winer Richard Feinmann [27], "There is plenty of room at the bottom". Indeed, recent expectacular growth of nanotechnology agrees with the predictions of some of the pioneers in the field, such as Arthur von Hippel [28] and K. Eric Drexler [29, 30].

Nowadays there are many important developments in nanotechnology, concerning nanoelectronics, nanowires, nanomechanics, and new and revolutionary techniques have been developed, such as the atomic force microscope (AFM), the scanning tunneling microscope (STM), and others. Nanoelectronics and nanowires have provided new broad possibilities in the development of smaller

and faster chips and other machines. Recent works in this field are in references [31, 32, 33, 34]. Transistors as small as 30nm have been developed, and as one of the developers of them says in the NewScientist [35] 'Our research proves that these smaller transistors behave in the same way as today's devices and shows there are no fundamental barriers to producing these devices in high volume in the future'. A small chip, around 20nm has been reported as well [36] at the French Atomic Energy Commission's Electronic, Technological and Instrumentation Laboratory (LETI) in Grenoble.

The possibility of interact with individual atoms is the first step for developing new materials and systems. New compounds that may be useful in a broader way that their bulk counterparts might be created. In this field important articles and reviews have appeared [37, 38, 39, 40, 41]. One of the best known 'new' clusters or nanostructures are the so called fullerenes, carbon spheroid structures discovered in 1985 [42]. Many works have been published in the literature concerning fullerenes [43, 44, 45, 46], and their solids [47, 48], which have superconductive properties [49, 50, 51] and photovoltaic applications [52, 53], among many other remarkable properties.

As carbon clusters, interest in the valence isoelectronic clusters such as III-V or II-VI materials clusters is rapidly growing. Recent theoretical [54, 55, 56, 57, 58, 59] or experimental [60, 61] works concerning several III-V material clusters or nanostructures may be found in the literature. Photoluminiscent doped II-VI nanoparticles have been reported [62, 63], along with other photosensitive structures [64], and doped [65, 66, 67, 68] or undoped II-VI [69] nanostructures.

1.3 Scope of this work

In view of the comment of the previous section, it appears interesting and promising the fusion of both fields, namely, clusters and II-VI materials. Our aim is to study the clusters of II-VI materials theoretically. First the global and local minima structures have to be characterized, and once this is done the excitation energies are calculated. In this way the absorption properties of these clusters are calculated, and then it may be seen if they are feasible for their use in the development of higher efficient solar cells. Cluster-based solids are a reality nowadays. Fullerene-based solids have been characterized and have very promising properties. C_{60} derivative-based solids may lead to higher efficient solar cells. M_3C_{60} compounds are superconductor, and also C_{28}-based solids appear to have superconductivity at high temperatures.

It could be possible to optimize the II-VI materials in order to construct higher efficient solar cells, more efficient than their bulk counterparts. In Part 1 of this thesis (Chapters 2, 3, 4 and 5) the structures of global and local minima of Zn_iX_i, $i = 1 - 9, 12, 15$, X=O, S, Se, and Te, respectively, are characterized. In Part 2 (Chapters 6, 7, 8 and 9) the excitation energies of the global minima structures characterized in Part 1 are calculated. In Part 3 general conclusions and further work are presented and discussed. In order to perform all this work we make use of the nowadays powerful quantum chemistry methods and programs. Let us remind briefly a bit of quantum chemistry.

1.4 Quantum chemistry

The theory of quantum mechanics, developed in the twenties of the last century [70, 71, 72, 73], changed the viewpoint of physicist over the microscopic world. Before it, all attempts that tried to explain the stability of atoms failed. Bohr explained the stability of the simplest atom, hydrogen, by fixing that electrons were in stationary orbits around the nucleus. An electron needs a quantum of energy in order to move from one stationary orbit to another. In other words, the energy is quantized, and not continuous. In quantum mechanics this statement arises from the theory. At the beginning the theory was mainly the playground of physicists, but it soon found applications in chemistry, creating what is called quantum chemistry. Over the years quantum chemistry has become a very important tool for chemists in order to calculate, understand and predict molecular properties.

In principle, all the information of a system, a molecule, for instance, may be obtained from its wave function. In order to know it, we 'only' have to solve the Schrodinger equation (here in its time independent form):

$$\widehat{H}\Psi = E\Psi \qquad (1)$$

where the Hamiltonian $\widehat{H}$ contains the kinetic energy terms of the electrons and the nuclei, the interactions between the nuclei, the electrons, and the nuclei-electrons. Within the Born-Oppenheimer [74] approximation the motion of the nuclei are separated from that of the electrons, and therefore the coordinates of the nuclei become fixed parameters in $\widehat{H}$. Unfortunately, equation (1) can only be solved for one electron systems, i.e. the hydrogen atom. Therefore approximate methods have been developed:

1. Wave-function based methods: variational (configuration interaction, direct expansion of Ψ in some suitable basis), and many-body perturbation theory.
2. Density functional theory (DFT).
3. Quantum Monte-Carlo.

It is beyond the scope of this section to develop a full description of these methods, so refer the interested reader to the literature devoted to these topics. See for example [75, 76, 77, 78, 79].

Wave-function based methods were the earliest developed ones. Two of these methods have been widely used throughout the years, the Valence Bond (VB) method and the Molecular Orbital (MO) method. The VB method was formulated in 1927 by Heitler and London [80]. The MO method was developed a bit later in by Hund [81], Mulliken [82] and others. This theory became the most popular due to its quantitative power, which come from the use of orthogonal orbitals, in opposition to the VB theory which plays with non-orthogonal orbitals.

One of the first developed molecular orbital method was the Hartree-Fock method [83, 84], where the wave function is an antisymmetrized product of one-electron orbitals. The electrons are treated as moving in a mean field due to the nucleus and the remaining electrons. The main drawback of this method is that correlation of electrons with opposite spins is neglected. There are different ways in which this correlation can be taken into account. One of them are the perturbational methods such as Møller-Plesset [85] theory (denoted as MPn, where n is the order of the perturbation). In these methods the electron correlation is treated as a perturbation of the HF problem. In the Configuration-Interaction (CI) method [86, 87] the wave function is expressed as a linear conbination of configurations to provide a better variational solution to the exact many-electron wave function. There are other more sophisticated methods such as Coupled Cluster [88, 89, 90], Multi-Reference Configuration Interaction (MR-CI) or Complete-Active-Space (CAS) methods [91, 92], which are very useful tools to study electronic properties of both ground and excited states.

Quantum Monte Carlo methods have been shown to be very powerfull in the calculation of the electronic properties of ground states [93, 94, 95, 43] or excited states [96, 97] of many systems. They have not been used in this work, and we refer the reader to more detailed papers [79, 98].

Mainly all the work presented in this thesis has been carried out within the density-functional framework. In the following subsection these methods are described in more detail.

1.4.1 Density Functional methods

Time independent Density Functional Theory

The Density Functional Theory formalism replaces the N-electron wave function and the associated Schrödinger equation by a much simpler electron density $\rho(\vec{r})$ which is a function of the three spatial variables. Then, the electronic state, the energy and all the electronic properties of a system can be described in terms of this $\rho(\vec{r})$ [77, 78].

Hohenberg and Kohn [99] proved that the electronic properties of a system with a nondegenerate ground state are uniquely determined by the electron density $\rho(\vec{r})$. Hence, the ground-state energy E_0 is a functional of $\rho(\vec{r})$, and therefore, if we know the ground-state electron density it is possible to calculate all the ground-state electronic properties from ρ once we have been able to set all the appropriate functional dependencies. In order to find these functionals, they also established an energy variational principle for the energy functional, analogous to the variational principle for wave functions. Thus, knowing the exact form of the $E[\rho]$ functional, we can search for the ground state density (as it is the case for the wave function). However, since the exact form of the functional is unknown, Kohn and Sham [100] developed an indirect approach to this functional, the Kohn-Sham method, and DFT turned into a practical tool for rigorous calculations. They showed that the exact ground-state purely

electronic energy E_0 of an N-electron molecule with ground-state electron probability density ρ is given by

$$E_0 = -\frac{1}{2}\sum_{i=1}^{N} < \psi_i(1)|\nabla_1^2|\psi_i(1) > + \int \upsilon(r)\rho(1)d\vec{r}_1 + \\ + \frac{1}{2}\int\int \frac{\rho(1)\rho(2)}{r_{12}} d\vec{r}_1 d\vec{r}_2 + E_{xc}[\rho] \qquad (2)$$

where $\upsilon(r) = -\sum_\alpha \frac{Z_\alpha}{r_{1\alpha}}$ is the external potential due to the nuclei, ψ_i are the Kohn-Sham orbitals, and the $E_{xc}[\rho]$ is the exchange-correlation energy.

In the Kohn-Sham procedure, the exact ground state ρ can be found from the Kohn-Sham orbitals according to,

$$\rho = \sum_{i=1}^{N} |\psi_i|^2 \qquad (3)$$

and the Kohn-Sham orbitals are found by solving the one-electron equations

$$\hat{F}_{KS}(1)\psi_i(1) = \varepsilon_i\psi_i(1) \qquad (4)$$

being the Kohn-Sham operator $\hat{F}_{KS}$

$$\hat{F}_{KS} = -\frac{1}{2}\nabla_1^2 + \upsilon(1) + \sum_{j=1}^{n} \hat{J}_j(1) + V_{xc}(1) \qquad (5)$$

where $\hat{J}$ is the Coulomb operator, and V_{xc} is called the exchange-correlation potential. $\hat{F}_{KS}$ is like the Fock operator in HF equations, except that the exchange operators are replaced by V_{xc}, which handles the effects of both the exchange and electron correlation.

These equations are iteratively solved. Starting from a guess density, $\hat{F}_{KS}$ is build and the set of equations (3) solved. The solution then is transfered to $\hat{F}_{KS}$, in order to build a new $\hat{F}_{KS}$. This process is repeated until convergence is achieved.

The physical significance of the Kohn-Sham orbitals is still under debate. Some authors claim that they do not have any significance other than in allowing the exact ρ to be calculated from (2). Likewise, the Kohn-Sham orbital energies should not be confused with molecular orbital energies. However, others based on the fact that the exact Kohn-Sham orbital energy for the HOMO is just the negative of ionization potential [101, 102], and due to the fact that the set of Kohn-Sham equations remind us, as in the HF case, the independent particle model, they associate to the Kohn-Sham orbitals a similar physical significance and legitimacy than to the HF canonical orbitals. In recent publications it is shown the results obtained from molecular orbitals obtained from DFT are quite similar to the molecular orbitals from standard MO-LCAO methods, and that one can extract a lot of useful information about molecular systems from analysis of their MOs even if the density functional methods are used [101, 103].

However, there is one more problem: the exchange-correlation functional $E_{xc}[\rho]$ and hence the exchange-correlation potential $v_{xc}[\rho; \vec{r}]$ is not known except for the case of the uniform electron gas. Fortunately, approximate functionals have been developed. One simple approximation is the so called local density approximation (LDA). The idea is to consider each volume element with local density $\rho(\vec{r})$ to be a homogeneous electron gas. From this point of view the approximation would be expected to be accurate if the density varies slowly in space. Then, $E_{xc}[(\rho)]$ is given by

$$E_{xc}^{LDA}[(\rho)] = \int \rho(\vec{r})\varepsilon_{xc}(\rho)d\vec{r} \qquad (6)$$

where $\varepsilon_{xc}(\rho)$ is the exchange plus correlation energy per electron in a homogeneous electron gas with electron density ρ. An accurate expression for $\varepsilon_{xc}(\rho)$ was found by Vosko, Wilk and Nusair [104]. Application of this expression leads to the local density approximation (LDA), or local spin density approximation (LSDA) [105], if one uses different orbitals and densities ρ^{α} and ρ^{β} for electrons with different spins. Of course, in the case of molecules these are only approximations to the true functionals, since ρ is far from being homogeneous. One might hope to improve the approximation by introducing an expansion in terms of gradients of the density. These methods are called generalized gradient approximations (GGA), and are of great importance in the study of molecules, where the electron density can not be considered as homogeneous.

Density functional methods have proved to give excellent results in most chemical systems [106], with results comparable to those given by CPU intensive electron-correlation methods. However they frequently overestimate bond dissociation energies [107]. The hybrids of HF and DFT theories increment the accuracy of the dissociation energy as was validated by Johnson *et al.* [108]. The hybrid [109] Becke 3 combined with the correlation functional Lee-Yang-Parr (B3LYP) [99, 110, 111] has become one of the most popular one, having the following form:

$$(1 - a_0)E_x^{LSDA} + a_0E_x^{HF} + a_xE_x^{B88} + a_cE_c^{LYP} + (1 - a_c)E_c^{VWN} \qquad (7)$$

being the values of the parameters a_0=0.20, a_x=0.72 and a_c=0.81. This functional is known as the Becke's 3 parameter functional, B3LYP.

Since density-functional calculations do not use the exact E_{xc} they are not, strictly speaking, ab-initio calculations. However, they do not use parameters fitted to experimental data, hence they lie closer in spirit to ab-initio calculations than to semiempirical ones. One of the main advantages of these methods is that with a similar computational cost to HF methods, they include some kind of electron correlation, being the major drawback that the correlation effects cannot be sorted out precisely. They are already mixed from the beginning with the uncorrelated solution. Besides, there is not any systematic way to improve the calculations by applying more and more sophistication, so the results must be accepted as they stand. In spite of these facts, DFT have been found to yield good results for ground state properties of various chemical systems, with a quality comparable to MP2 results [112], or even better in

some cases. Due to their relative low computational cost, DFT is the method of choice for large systems, for which the inclusion of electron correlation by MP or CI methods is prohibitive.

Time-Dependent Density Functional Theory

In the time independent version DFT provides accurate calculations for ground states. However, excitation energies are not accurately calculated. The Time-Dependent generalization of the density-functional theory formalism (see [113, 114, 115] for reviews) offers a rigorous route to the calculation of the dynamic response of the charge density. Combining this with linear response theory allows the calculation of vertical electronic excitation spectra [114, 116, 117, 118, 119]. TDDFT has been applied to very different systems, i.e. metal compounds [120, 121, 122], organic [123, 124, 125] or inorganic compounds [126, 127], extended systems [128], becoming a very powerfull tool to calculate excitation energies of real systems. However, it has been seen that Rydberg states are not calculated accurately [129, 130].

A stationary action principle may be derived, analogous to the minimum energy principle of Hohenberg-Kohn theory, and this can be used, together with appropriate assumptions concerning v-representability to derive the time-dependent Kohn-Sham equation:

$$\left[-\frac{1}{2}\nabla^2 + v\left(r,t\right) + \int \frac{\rho\left(r',t\right)}{|r-r'|}dr' + v_{xc}^{\sigma}\left(r,t\right)\right]\psi_{j\sigma}\left(r,t\right) = i\frac{\partial}{\partial t}\psi_{j\sigma}\left(r,t\right) \qquad (8)$$

$v_{xc}^{\sigma}\left(r,t\right)$ is formally the functional derivative of the exchange-correlation action, A_{xc}, but most calculations make use of the adiabatic approximation,

$$v_{xc}^{\sigma}\left(r,t\right) = \frac{\delta A_{xc}\left[\rho_{\uparrow},\rho_{\downarrow}\right]}{\delta\rho_{\sigma}\left(r,t\right)} \cong \frac{\delta E_{xc}\left[\rho_{\uparrow}^{t},\rho_{\downarrow}^{t}\right]}{\delta\rho_{\sigma}^{t}\left(r\right)} \qquad (9)$$

where $\rho_{\sigma}^{t}\left(r\right)$ is the $\rho_{\sigma}\left(r,t\right)$ function evaluated at a fixed time, t, and E_{xc} is the exchange-correlation functional of time-independent Kohn-Sham theory.

Since the dynamic polarizability, $\overline{\alpha}\left(\omega\right)$, describes the response of the dipole moment to a time-dependent electric field, it may be calculated from the response of the charge density obtained from time-dependent density-functional theory, hence using time dependent density functional response theory. This allows the determination of the electronic excitation spectrum in the usual dipole approximation, because according to the sum-over-states relation,

$$\overline{\alpha}\left(\omega\right) = \sum_{l}\frac{f_l}{\omega_l^2 - \omega^2} \qquad (10)$$

the poles of the dynamic polarizability determine the excitation energies, ω_l, while the residues, f_l, determine the corresponding oscillator strengths [114]. A finite basis set formalism is used to cast the dynamic polarizability in the

tensorial form of the sum-over-states expresion (10). Examination of the pole structure then shows that the transition energies may be obtained by solving a matrix eigenvalue problem,

$$\Omega\overrightarrow{F_l} = \omega_l^2\overrightarrow{F_l} \qquad (11)$$

where Ω is defined in references [114, 115, 116] and the oscillator strengths f_l are obtained from the eigenvectors $\overrightarrow{F_l}$. For more information see the above mentioned reviews and i references [131, 132].

1.4.2 Basis Sets

In both wave function based methods and density functional theory a set of functions to span the wave function are needed. These sets of function are the so called basis sets. The choice of an appropriate basis set is an essential requirement for the success of the calculation. However, we have to balance the precision of the basis set and its size, since increasing the size of the basis set the calculation cost becomes more expensive. The Contracted Gaussian Functions (CGF) are the most used in quantum chemistry calculations. They consist of linear combinations (contractions) of Gaussian functions (primitives),

$$\varphi_\mu^{CGF}(|\vec{r} - \vec{R}_A|) = \sum_{p=1}^{L} d_{p\mu} g(\alpha_{p\mu}, |\vec{r} - \vec{R}_P|) \qquad (12)$$

where the exponent of the primitives $\alpha_{p\mu}$ and the contraction coefficients $d_{p\mu}$ are optimized for the different elements.

Usually all-electron basis sets are used, which means that all electrons are considered in the basis set. However, in some cases due to the huge number of electrons and consequently the prohibitive cost of the calculation, some electrons, the core electrons, are removed from the calculation and only the outer electrons are considered. In this case the outer electrons move in an averaged potential due to the core electrons and the nuclei. In this thesis the relativistic compact effective potentials and shared exponent basis sets developed by Stevens et. al. [133] have been used. These effective potentials are constructed to reproduce the valence electron orbital energies and densities obtained from numerical solutions of the Dirac-Fock equations for an appropriate atomic configuration [134].

This RCEP includes the Zn d electrons in the valence, being the $1s^2\,2s^2\,2p^6$ electrons considered as the core. The Contracted Gaussian valence basis set is an energy-optimized, double zeta quality sp and triple zeta quality d basis set (8sp6d/4sp3d). For the VIB column elements the $ns^2\,np^4$ electrons are considered as the valence. A double-zeta quality (5sp/2sp) basis set is used.

Part I

Cluster structures

Chapter 2

Small Clusters of II-VI Materials: Zn_iS_i, $i = 1 - 9$

Abstract

The improvements in the characterization of II-VI compounds based solar cells and the recent experimental characterization of small clusters and nanoparticles make the study of small II-VI clusters very interesting. In this work, the ground states of small Zn_iS_i clusters are studied, $i = 1 - 9$. Ring-like structures have been found to be the global minima in the case of the smaller studied clusters, i.e. $i = 1 - 5$, and three dimensional spheroid structures for larger ones, $i = 6 - 9$. This is due to the stability of obtuse S-Zn-S angles in the first case, and to the stability gained from higher coordination in the second case. The three dimensional structures may be envisioned as being built from Zn_2S_2 and Zn_3S_3 rings. Cohesive energy and atomic charges show a unequivocal trend to bulk-like properties even in such small systems.

2.1 Introduction

Interest in II-VI compound semiconductors has grown spectacularly in recent years due to their paramount technological potential. In addition to the importance of experimental research, theoretical studies are of great importance not only because of their ability to expand our understanding, but also because of their predictive power. Some theoretical studies of zinc sulfide have appeared in the literature [139, 140]. Remarkable works are those of Muilu and Pakkanen [141, 142], and Pollman and coworkers [143, 144, 145, 146, 147, 148].

In studying bulk and surface properties of crystals, cluster models are and have been widely used. Cluster properties change from molecular to bulk properties as size increases. Large enough clusters have bulk-like properties, and may be used to simulate infinite systems. Nevertheless, the fact that cluster and nanoparticle characterization is becoming technologically possible have made clusters specially interesting in themselves. Therefore, the literature in the field is growing rapidly. Many experimental [149, 150, 151, 152, 153, 154] and theoretical [155, 156, 157, 158, 159, 160] studies have been reported concerning clusters of various compositions, which have important and interesting applications. For example, Fe_2O_3 nanoparticles can be precipitated in a gel, forming the so-called ferro-gels. These compounds have electromagnetic properties, making them suitable for applications in human mobile prothesis that are able to answer mental electrical messages.

Due to the interest in both II-VI compounds and clusters it occurred to us that it would be interesting to perform a theoretical study of II-VI compound clusters, fusing in this way both fields, as it is done in the case of carbon clusters such as fullerenes, which have photovoltaic applications [52, 53]. In this paper, calculated structure and properties of the Zn_iS_i, $i = 1 - 9$, clusters are reported, All the calculations have been performed at the B3LYP level of theory, combined with the SKBJ relativistic pseudopotentials.

2.2 Method

All geometries were fully optimized using the Becke3 exchange potential and Lee-Yang-Parr correlation potential (B3LYP) gradient-corrected density-functional method [99, 109, 110, 111] analytic gradients. Harmonic vibrational frequencies were determined by analytical differentiation of gradients.

The relativistic compact effective core potentials and shared-exponent basis set [133] of Stevens, Krauss, Basch and Jasien (SKBJ) was used as the basic basis set in this study. The d electrons of Zn were included in the valence, and an extra d function was added on both Zn (α=0.3264) and S (α=0.7) atoms, due to their importance in the formation of bonds. We denote the final basis set used as SKBJ(d).

Because there are so many possible structures for these clusters, several starting points for these complete B3LYP/SKBJ(d) optimizations were generated using a simulated annealing approach at the PM3 [161] level of theory. Of course, additional starting points were derived from simple chemical intuition.

Table 2.1: Relative energies (kJ/mol) between two minima of the same cluster size, calculated with the three described basis sets.

	SKBJ(d)	SKBJ(expan)	TZ2P
ΔE ($E_{Zn_4S_4^{GM}}$-$E_{Zn_4S_4^{LM}}$)	117.27	130.62	118.32
ΔE ($E_{Zn_6S_6^{GM}}$-$E_{Zn_6S_6^{LM_1}}$)	38.40	35.22	42.25
ΔE ($E_{Zn_6S_6^{GM}}$-$E_{Zn_6S_6^{LM_2}}$)	75.15	56.52	70.29

All the geometry optimizations and frequency calculations were carried out with the GAUSSIAN94 [162] and GAUSSIAN98 [163] package. For the PM3 simulated annealing technique the HYPERCHEM [164] program was used.

2.2.1 Basis set selection

In the previous section it was mentioned that the basis set used during these calculations was SKBJ(d). Although a larger basis set is not expected to change significantly the geometry of the obtained structures, the relative energies between them may be affected. In order to check the reliability of our SKBJ(d) basis set, single point energy calculations using larger basis sets were performed on several structures which will be detailed later. Two other basis sets were examined. The first was a simple expansion of the previously described SKBJ(d) basis. Two s and p functions (with α=1.335122, 1.120129), one d (α=2.561376), and one f (α=3.115413) were added the Zn basis. The SKBJ(d) basis was expanded for S as well with the two new s and p functions having exponents α=1.231541,0.373393, and the f function, α=0.593345. All of these added functions were energy optimized at the MP2 level of theory using the GAMESS US [165] package. As the SKBJ(d) basis set only has one d function on S, it was decided that upon the addition of another, the exponents of both should be energy optimized. The exponents for the two d functions in this expanded basis were 0.896605 and 0.288732. This expanded basis set will be referred to as SKBJ(expan). The second examined basis set was an all electron triple-ζ double polarization (TZ2P) basis (14s11p6d2f/10s8p3d2f) for Zn [166, 167, 168] and (13s10p2d1f/6s5p2d1f) for S [169, 170]. The relative energies between two minima of each cluster size chosen is shown in Table 2.1.

These results demonstrate the reliability of the used SKBJ(d) basis set. The relative energies calculated using the various basis sets vary little, and the difference in CPU ussage is great. Thus, we have chosen the SKBJ(d) basis to be used throughout this work.

Figure 2.1: Calculated global minima of Zn_iS_i, $i = 2-5$, labeled, from left to right, $Zn_2S_2^{GM}$, $Zn_3S_3^{GM}$, $Zn_4S_4^{GM}$ and $Zn_5S_5^{GM}$, respectively. Dark, larger atoms are those of Zn.

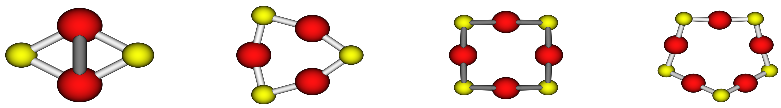

2.3 Results and discussion

2.3.1 Structure of the calculated minima of Zn_iS_i clusters. $i = 1-9$.

In this section the calculated minima are presented. Although our interest is mainly centred on global minima, structures and properties of higher-lying local minima are presented as well.

In order to show the calculated structures in a more understandable way, we have arbitrarily divided these clusters into two groups, according to the structure of the global minimum. In the first group, Group 1, structures of the clusters Zn_iS_i, $i = 1-5$, are included which global minima are planar or near planar ring-like structures, and in the second group, Group 2, the rest, $i = 6-9$, for which the global minima are three dimensional spheroids. Bader analysis [171] of all these structures have been performed as well. For that purpose the all electron 6-311G [166, 167] basis for Zn and 6-31G [172, 173, 174, 152, 176] basis for S were used.

The presented structures are labeled according to the following scheme: $Zn_iS_i^a$, where i denotes the number of ZnS units, and the superscript a may be GM (global minimum) or LM (local minimum).

Group 1

As we have mentioned above, in this section we will describe the calculated structures of Zn_iS_i, $i = 1-5$. The principal characteristic of the calculated global minima is that all are planar, except in the case of $Zn_5S_5^{GM}$, which is quasiplanar. The planar Zn_5S_5 ring is a stationary point of Hessian order two, and lies 6.95 kJ/mol above the minimum. In Figure 2.1, the calculated global minima of the different cluster sizes are presented, and the structures of the characterized local minima are shown in Figure 2.2.

A quick glance at this shows that while the calculated local minima of the smallest clusters, namely $Zn_2S_2^{LM}$ and $Zn_3S_3^{LM}$, are planar, the local minima of Zn_4S_4 and Zn_5S_5 are not. In Table 2.2 important values such as molecular

Figure 2.2: Calculated local minima of Zn_iS_i, $i = 2 - 5$, labeled, from left to right, $Zn_2S_2^{LM}$, $Zn_3S_3^{LM}$, $Zn_4S_4^{LM}$ and $Zn_5S_5^{LM}$, respectively.

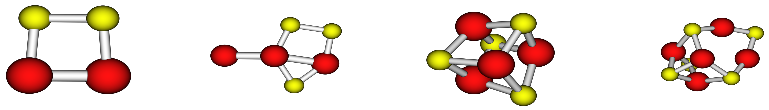

Table 2.2: Zn-S bond lengths, S-Zn-S angles and symmetry groups of the structures of Fig. 2.1 and Fig. 2.2. For the local minima, energies relative to the corresponding global minimum are in kJ/mol.

	R(Zn-S) Å	α(S-Zn-S)^o	Point Group	Rel. E. (kJ/mol)
$Zn_1S_1^{GM}$	2.09	-	$C_{\infty v}$	-
$Zn_2S_2^{GM}$	2.27	114.5	D_{2h}	-
$Zn_2S_2^{LM}$	2.34	-	C_{2v}	+ 117.10
$Zn_3S_3^{GM}$	2.21	157.8	D_{3h}	-
$Zn_3S_3^{LM}$	2.20 -2.26	131.1-141.4	C_s	+ 233.75
$Zn_4S_4^{GM}$	2.19	177.4	D_{4h}	-
$Zn_4S_4^{LM}$	2.38	105.4	T_d	+ 117.27
$Zn_5S_5^{GM}$	2.18	178.9	C_s	-
$Zn_5S_5^{LM}$	2.21-2.41	102.4 - 159.3	C_1	+ 68.19

geometries, energies, and the symmetry of the presented structures are shown.

$Zn_1S_1^{GM}$ is obviously a linear structure which belongs to the $C_{\infty v}$ point group. However, while the molecular structure is trivial, the short Zn-S bond length should be pointed out.

Both the global minimum, $Zn_2S_2^{GM}$, shown in Figure 2.1 and the next lower-lying local minimum, $Zn_2S_2^{LM}$, in Figure 2.2, have been found to be planar. $Zn_2S_2^{LM}$ lies 117.10 kJ/mol above the global minimum. It seems logical that $Zn_2S_2^{GM}$ is the most energetically stable structure, since it contains the favorable cross-ring Zn-Zn interaction as well as four Zn-S bonds. Noticeable as well is the shorter Zn-S bond length of $Zn_2S_2^{GM}$, while the Zn-Zn bond-length is similar to that of $Zn_2S_2^{LM}$. Nevertheless, Zn-S bond lengths are 0.18 Å longer than in $Zn_1S_1^{GM}$. $Zn_2S_2^{GM}$ belongs to the D_{2h} point group, and $Zn_2S_2^{LM}$ to the C_{2v} point group.

$Zn_3S_3^{GM}$ is depicted in Figure 2.1 and $Zn_3S_3^{LM}$ in Figure 2.2. As in the case of Zn_2S_2, only planar structures have been found. This, of course, does not

mean that the existence of nonplanar structures may be ruled out. However, all attempts to locate non-planar local minima eventually led to planar structures.

The Bader analysis of this molecule shows a planar ring-like structure where each atom has a coordination number two; there are no Zn-Zn interactions as in $Zn_2S_2^{GM}$. Nevertheless, as it may be viewed in Table 2.2, the Zn-S bond-length is 0.06 Å shorter than in $Zn_2S_2^{GM}$, and the S-Zn-S angle is much more open, as allowed by the larger ring. This structure has D_{3h} symmetry. $Zn_3S_3^{GM}$ is a very important structure, which will become more obvious later. Note that the two known crystal structures for zinc sulfide, both zincblende and wurtzite, are built of Zn_3S_3 rings. $Zn_3S_3^{LM}$ belongs to the C_s point group.

The two characterized minima are shown in Figure 2.1, $Zn_4S_4^{GM}$, and Figure 2.2, $Zn_4S_4^{LM}$. This latter structure is specially interesting for two reasons. the first is that it is the first nonplanar minimum found. The second, very interesting as well, is that it can be viewed as being built from six equivalent units of an earlier presented structure: Zn_2S_2 rings as occurring in $Zn_2S_2^{GM}$. The resulting structure has T_d symmetry. However, in these faces Zn-Zn bonds are not reported by the Bader analysis. The Zn-S bond is enlongered by 0.11 Å, and the S-Zn-S angle bent by 10 $^\circ$ in comparison to $Zn_2S_2^{GM}$. In this structure all the atoms have coordination number three, compared to $Zn_4S_4^{GM}$, where each atom has coordination number two. Thus, one might think that the cage structure would be more stable. However, it is the planar structure which lies 117.27 kJ/mol lower in energy. This D_{4h} planar structure, compared to the already shown $Zn_2S_2^{GM}$ and $Zn_3S_3^{GM}$ rings, presents shorter Zn-S bond-lengths, and the S-Zn-S angle is close to 180°. This tendency to form near-linear S-Zn-S angles is strong, and the geometrical constraints of the three dimensional $Zn_4S_4^{LM}$ result in a strained S-Zn-S angle of 105.4°, and therefore the planar ring is more stable.

The two Zn_5S_5 minima characterized in this work are presented in Figure 2.1, $Zn_5S_5^{GM}$, and Figure 2.2, $Zn_5S_5^{LM}$. At this size, the strictly planar structure is not the global minimum. The structure when constricted to planarity yields a stationary point of hessian order two, that is, it has two negative vibrational frequencies. Departing from that structure, a quasiplanar structure has been found to be the global minimum, $Zn_5S_5^{GM}$, which lies 6.95 kJ/mol below the planar stationary point. Four Zn atoms are contained in the same plane, and the other, along with the two sulfur atoms bonded to it lie to one side of that plane. The remaining sulfur atoms alternate up and down around the ring. This structure allows Zn to form near linear S-Zn-S bonds, as occurring in $Zn_4S_4^{GM}$.

As in the case of $Zn_4S_4^{LM}$, $Zn_5S_5^{LM}$ is three dimensional, and can be seen as being built from units of $Zn_2S_2^{GM}$, squares, and $Zn_3S_3^{GM}$, hexagons. Examining Figure 2.2 one may picture $Zn_5S_5^{LM}$ as a structure of two joined rings of Zn_2S_2 and Zn_3S_3. In one side a Zn_2S_2 ring is contained, and in the other a bent Zn_3S_3 ring. These two structures are bonded on one extreme,where new Zn_2S_2 rings appear, and on the opposite extreme the Zn_3S_3 ring is bent. It is interesting to note that the Zn-S bond lengths are significantly longer than those of the planar structure. Various lengths are found in a wide range from 2.21 Å to

Figure 2.3: Calculated global minima of Zn_iS_i, $i = 6 - 9$, labeled, from left to right, $Zn_6S_6^{GM}$, $Zn_7S_7^{GM}$, $Zn_8S_8^{GM}$ and $Zn_9S_9^{GM}$, respectively.

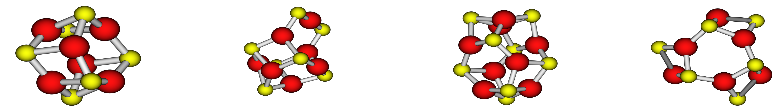

.

Figure 2.4: Calculated local minima of Zn_iS_i, $i = 6 - 9$, labeled, from left to right, $Zn_6S_6^{LM_1}$, $Zn_6S_6^{LM_2}$, $Zn_7S_7^{LM}$ and in the second row $Zn_8S_8^{LM_1}$, $Zn_8S_8^{LM_2}$ and $Zn_9S_9^{LM}$, respectively.

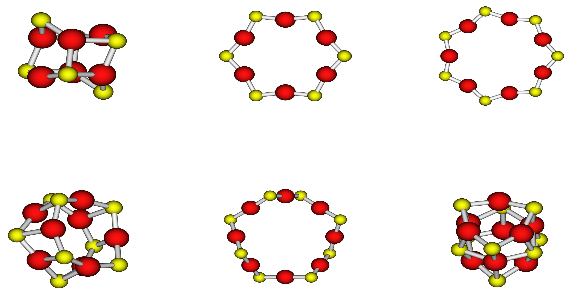

2.41 Å.

The global minima of the clusters in Group 1 have been found to be planar rings, $Zn_2S_2^{GM}$, $Zn_3S_3^{GM}$ and $Zn_4S_4^{GM}$ or a near-planar ring, $Zn_5S_5^{GM}$. In these structures a strong tendency of Zn to form linear S-Zn-S bonds is seen. Nonplanar local minima have been found only for Zn_4S_4 and Zn_5S_5, and these can be pictured as being built from squares, $Zn_2S_2^{GM}$, and hexagons, $Zn_3S_3^{GM}$. Nevertheless, the internal geometry of these rings change significantly. In the three dimensional structures Zn-S bond lengths are longer and S-Zn-S angles are more bent than in the planar and near-planar global minima.

Group 2

This group contains the clusters of which the global minima are nonplanar, Zn_iS_i, $i = 6 - 9$. In Figure 2.3 the global minima are shown, and in Figure 2.4 the local minima.

In Table 2.3 the Zn-S bond lengths, S-Zn-S angles, and symmetry points of the presented structures are given.

Table 2.3: Zn-S bond lengths, S-Zn-S angles and point groups of the structures of Fig. 2.3 and Fig. 2.4. For the local minima, energies relative to the corresponding global minimum are in kJ/mol.

	R(Zn-S) Å	α(S-Zn-S)^{o}	Point Group	Rel. E (kJ/mol)
$Zn_6S_6^{GM}$	2.31-2.47	140.55	D_{3d}	-
$Zn_6S_6^{LM_1}$	2.40	96.7 - 155.2	D_{2d}	+ 38.40
$Zn_6S_6^{LM_2}$	2.18	194.05	D_{6h}	+ 75.15
$Zn_7S_7^{GM}$	2.20 - 2.58	97.4 - 175.0	C_s	-
$Zn_7S_7^{LM}$	2.18	198.30	D_{7h}	+ 107.52
$Zn_8S_8^{GM}$	2.28 - 2.42	100.3 - 137.1	S_4	-
$Zn_8S_8^{LM_1}$	2.28 - 2.50	100.7 - 154.4	D_{4d}	+ 78.94
$Zn_8S_8^{LM_2}$	2.18	177.79	D_{4d}	+ 166.33
$Zn_9S_9^{GM}$	2.28 - 2.33	103.8 - 138.0	C_{3h}	-
$Zn_9S_9^{LM_1}$	2.29 - 2.45	92.5 - 147.2	D_{3d}	+ 146.41

As it has been mentioned already, the main difference at first sight between $Zn_6S_6^{GM}$ and the previously seen global minima is that $Zn_6S_6^{GM}$ is nonplanar. There has been a transition, from a situation in which the planar ring structures were favoured, to a situation where three-dimensional structures are favoured. Examining the trend in relative energies between the ring and three-dimensional structures for $i = 4, 5, 6$ we find that the ring structure was more stable for $i = 4$ by 117.27 kJ/mol. That difference was reduced to 68.19 kJ/mol for $i = 5$, and here with $i = 6$ the tree-dimensional structure is finally more stable than the ring by 75.17 kJ/mol.

As in the case of the smaller three-dimensional structures, $Zn_6S_6^{GM}$ can be envisioned as being built up from smaller building blocks: squares and hexagons. In the case of $Zn_6S_6^{GM}$, it is formed by two bent hexagons, stacked one on top of the other, which are linked together by six squares. The resulting structure has D_{3d} symmetry. Bader analysis of this molecule shows that there are no Zn-Zn interactions in this structure.

The six zinc atoms of $Zn_6S_6^{LM_1}$ form a octahedron. The sulfur atoms are placed as follows: two of them are found on opposite edges, and the rest are placed above the octahedral faces, two in the upper half, and two in the lower half. This atomic placement leads to the formation of Zn_2S_2 and Zn_3S_3 rings as in previous three dimensional structures. The resulting structure has D_{2d} symmetry.

Of course, an important question arises at this point: why is the ring structure, $Zn_6S_6^{LM_2}$, not the global minimum? In Table 2.3 it may be seen that the S-Zn-S angles in $Zn_6S_6^{LM_2}$ are far from linearity. Hence, this planar structure is not as stable as $Zn_4S_4^{GM}$ and $Zn_5S_5^{GM}$. Besides, the coordination number of $Zn_6S_6^{GM}$ is three for all atoms, while it is two for $Zn_6S_6^{LM_2}$. The combination of these factors makes the three-dimensional $Zn_6S_6^{GM}$ more stable. In the case of $Zn_6S_6^{LM_1}$, all atoms have coordination number three, except the two sulfurs

placed on the equatorial plane formed by the zincs of the octahedron. This structure is also more stable than the planar one.

As in Zn_6S_6, nonplanar structures built from small cluster structures are found to be more stable than a ring structure for Zn_7S_7. The S-Zn-S angles found in this ring structure are even further from linearity than those of Zn_6S_6, and one may think that therefore the energy difference between $Zn_7S_7^{GM}$ and $Zn_7S_7^{LM}$ will be larger. Indeed, it is. The energy difference between $Zn_7S_7^{GM}$ and $Zn_7S_7^{LM}$ is 107.52 kJ7mol, as compared to 75.17 kJ/mol in the case of Zn_6S_6.

$Zn_7S_7^{GM}$ can be seen as a structure of two joined ring structures: a Zn_3S_3 and a bent Zn_4S_4 ring. Half of the Zn_4S_4 ring is linked to the Zn_3S_3 ring, forming in this way new Zn_2S_2 rings as in $Zn_6S_6^{GM}$, and a second bent Zn_4S_4 ring.

$Zn_7S_7^{LM}$ is a planar ring, which belongs to the D_{7h} point group.

Three calculated structures of Zn_8S_8 are presented, $Zn_8S_8^{GM}$ in Figure 2.3, and $Zn_8S_8^{LM_1}$ and $Zn_8S_8^{LM_2}$ in Figure 2.4. These structures are interesting, not only because of the reappearance of the building blocks, but also for the manner in which these blocks are used. $Zn_8S_8^{GM}$ may be viewed as a polyhedron formed by four long faces composed of one Zn_2S_2 and one Zn_3S_3 unit that are inverted on the next face. The polyhedron is closed on the top and the bottom by a Zn_2S_2 unit. The resulting global minimum has S_4 symmetry.

$Zn_8S_8^{LM_1}$ is composed by two "parallel" Zn_4S_4 units bonded together by Zn_2S_2 units, as occurs in the previous structures. The resulting structure is of D_{4d} symmetry. $Zn_8S_8^{LM_2}$ is a ring structure with coplanar zinc atoms, where the sulfur atoms alternate up and down around the ring. This break in planarity can be understood looking at the S-Zn-S angles, which are close to 180, while if the molecule were planar, they will be far from linearity. Thus, bond-lengths similar to other ring structures are found. However, the energy difference between $Zn_8S_8^{GM}$ and $Zn_8S_8^{LM_2}$ is even larger than in smaller cases, 166.33 kJ/mol, and this is due to the stability gained by the coordination number three, in a largely stable geometrical configuration.

The global minimum, $Zn_9S_9^{GM}$, is given in Figure 2.3, and one local minimum, namely, $Zn_9S_9^{LM}$ in Figure 2.4. As in the previous cases, these structures can be envisioned as being built with the same basic Zn_2S_2 and Zn_3S_3 blocks. In the case of $Zn_9S_9^{GM}$, Zn_3S_3 units may be viewed as caps to a polyhedron joined by a ring formed of Zn_2S_2 and Zn_3S_3 units. The ring is formed by alternating one Zn_3S_3 and two joined Zn_2S_2 units. The resulting structure has C_{3h} symmetry.

$Zn_9S_9^{LM}$ is formed by three "parallel" Zn_3S_3 rings, bonded together by Zn_2S_2 units. It may be constructed by the addition of an extra Zn_3S_3 unit to $Zn_6S_6^{GM}$. The resulting structure has D_{3d} symmetry.

It is interesting to notice that in all of these structures the coordination number of some atoms has increased from three to four.

Two main reasons have been given to explain the transition from ring global minima in Group 1 to three dimensional spheroid global minima in Group

Table 2.4: Natural charges (e) of the shown global minima.

	Zn	S
$Zn_1S_1^{GM}$	0.900	-0.900
$Zn_2S_2^{GM}$	1.159	-1.159
$Zn_3S_3^{GM}$	1.183 - 1.184	-1.183 - -1.184
$Zn_4S_4^{GM}$	1.200	-1.200
$Zn_5S_5^{GM}$	1.182 - 1.216	-1.174 - -1.224
$Zn_6S_6^{GM}$	1.270	-1.270
$Zn_7S_7^{GM}$	1.194 - 1.269	-1.217 - -1.285
$Zn_8S_8^{GM}$	1.276 - 1.291	-1.279 - -1.288
$Zn_9S_9^{GM}$	1.285 - 1.293	-1.287 - -1.297

2. On one hand, the tendency to form linear S-Zn-S angles, and on the other hand the achievement of higher coordination number. We have seen that higher coordination is preferred when achieving that goal does not present too much of a strain on the bond angle. Three dimensional spheroid structures have been found as well in other related compounds, i.e. zinc oxide molecules [177].

2.3.2 Natural charges

At this point we analyze the natural orbital charges, obtained by Natural Bonding Analysis [178] at the B3LYP/SKBJ(d) level of theory, which are given in Table 2.4.

The cationic nature of zinc and the anionic nature of sulfur can be observed in all the structures. The atomic charges are larger as cluster size increases, and a trend towards the charge separation in the bulk ($|1.43e|$) is seen.

2.3.3 Cohesive energy

The cohesive energy per zinc sulfide unit is calculated as $E_f = (iE_{Zn} + iE_S - E_{Zn_iS_i})/i$, where i is the number of ZnS units. The cohesive energy may be depicted versus the inverse of the cubic root of i, and then a line can be fit to the obtained points. Extrapolating it to $i^{-1/3}$=0, that is, to i =∞, or the bulk, a theoretical value which can be compared to the experimental one is obtained[17–18]. We have taken that same approach. Nine points representing the cohesive energy of the studied global minima, given in Table 2.5, are plotted in Figure 2.5.

In fitting a line to the data, not all the points are representative, and only the points belonging to three dimensional structures, i.e. $Zn_6S_6^{GM}$ to $Zn_9S_9^{GM}$ have been taken into account. A line was fit to the cohesive energy of $Zn_6S_6^{GM}$ to $Zn_9S_9^{GM}$ versus $i^{-1/3}$, and it was found to have the equation y=563.358-291.893×x. The correlation of this line is 0.99858, which is some indication

Table 2.5: Cohesive energy, E_f, (kJ/mol) of characterized global minima.

E_f (kJ/mol)	
$Zn_1S_1^{GM}$	99.99
$Zn_2S_2^{GM}$	285.94
$Zn_3S_3^{GM}$	375.21
$Zn_4S_4^{GM}$	392.73
$Zn_5S_5^{GM}$	394.85
$Zn_6S_6^{GM}$	403.12
$Zn_7S_7^{GM}$	410.21
$Zn_8S_8^{GM}$	417.18
$Zn_9S_9^{GM}$	423.43

Figure 2.5: Cohesive energy (kJ/mol) vs the inverse of the cubic root of ZnS units $\left(i^{1/3}\right)$.

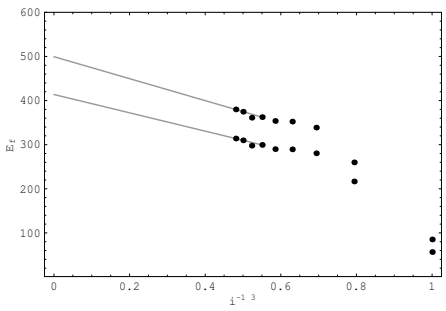

that we have properly located the global minima of such clusters. The extrapolated value, as is obvious from the linear equation, is 563.358 kJ/mol, which represents 92.73% of the experimental value 607.51 kJ/mol.

These results may be compared to those obtained by Muilu and Pakkanen [141, 142]. As it has been mentioned earlier, they used a HF-MO method to study ZnS clusters. They performed calculations for clusters of different size, the largest one being of size $Zn_{240}S_{240}$. Their best extrapolated value was 520.72 kJ/mol, 85.7% of the experimental. The fact that electron correlation is taken into account in our calculations explains why we obtain results closer to the experimental value, even with smaller clusters.

2.4 Conclusions

There are two main factors determining whether a ring or three-dimensional structure will be the global minimum for the small zinc sulfide clusters: the stability of very obtuse S-Zn-S bond angles, and the stability gained from higher coordination. For Zn_iS_i, $i = 2-5$, the first term outweighs the second and ring structures are predicted to be the global minima. For $i \geq 6$, however, the size of the cluster allows for both obtuse S-Zn-S bond angles and higher coordination in the three dimensional spheroid structures, making these the most stable.

These three dimensional clusters can be envisioned as being built of smaller building blocks, basically Zn_2S_2 and Zn_3S_3 rings, as carbon fullerenes are. The most stable carbon fullerenes are built of pentagons and hexagons, but less stable ones are found to be built of squares and hexagons.

Cohesive energy and atomic charges show a unequivocal trend to bulk-like properties even in such small systems. Moreover, the fact that the cohesive energies of these clusters fit a line indicates that we are dealing with the real global minima, otherwise the cohesive energy a local minimum will be clearly below the line.

Chapter 3

Small Clusters of II-VI Materials: Zn_iO_i, $i = 1 - 9$.

Abstract

The improvements in the characterization of II-VI compounds based solar cells and the recent experimental characterization of small clusters and nanoparticles make the study of small II-VI clusters very interesting. In this work, the ground states of small Zn_iO_i clusters are studied, $i = 1 - 9$. Ring-like structures have been found to be the global minima for clusters as large as $i = 7$, and three dimensional spheroid structures for larger ones, $i = 8, 9$. This is due to the stability of obtuse O-Zn-O angles in the first case, and to the stability gained from higher coordination in the second case. The three dimensional structures may be envisioned as being built from Zn_2O_2 and Zn_3O_3 rings, as was the case for ZnS three dimensional global minima, and other ZnO calculations. Calculated natural orbital charges are larger as cluster size increases, showing a tendency towards bulk charges.

3.1 Introduction

During the last decade interest in II-VI compounds has increased notably due to their paramount technological potential. To understand the occurring phenomena it is essential to study the structure and electronic properties of these compounds, thereby providing more information for the optimization of these materials in order to enhance their applicability.

Nevertheless, there are some properties related to these compounds that have been seen to be local phenomena, that is, when they happen, they happen at a certain point on the surface. A property of this type is the adsorption. Thus, it is important to study small clusters of these compounds, whose electronic and structural properties could give insight into understanding these local properties. In addition to this reason, the fact that cluster and nanoparticle characterization is becoming technologically possible is remarkable.

Due to the interest in both II-VI compounds and clusters it occurred to us that it would be interesting to perform a theoretical study of II-VI compound clusters, fusing in this way both fields. In this work we focus on zinc oxide clusters, Zn_iO_i, $i = 1-9$. Previous molecular dynamic calculations predict that spheroid ZnO clusters are stable for $i \geq 11$, which may be related to fullerene-type structures [177]. These spheroid structures are built from hexagons and rombi, in other words, rings of Zn_2O_2 squares, or Zn_3O_3 hexagons. In the previous chapter we found for Zn_iS_i, $i = 1 - 9$ similar building blocks used in order to form related spheroid structures.

3.2 Method

All geometries were fully optimized using the hybrid [109] B3LYP approximate gradient-corrected density functional procedure [99, 110, 111]. Harmonic vibrational frequencies were determined by analytical differentiation of gradients.

The relativistic compact effective core potentials and shared-exponent basis set [133] of Stevens, Krauss, Basch and Jasien (SKBJ) was used as the basic basis set in this study. The d electrons of Zn were included in the valence, and an extra d function was added on both Zn (α=0.3264) and O (α=0.85) atoms, due to their importance in the formation of bonds. Note that pure angular momentum functions were used throughout this study. We denote the final basis set used as SKBJ(d).

Because there are so many possible structures for these clusters, several starting points for these complete B3LYP/SKBJ(d) optimizations were generated using a simulated annealing approach at the Stewart semiempirical model parameterization (PM3) [161] level of theory. Of course, additional starting points were derived from simple chemical intuition.

All the geometry optimizations and frequency calculations were carried out with the GAUSSIAN98 [163] package. For the PM3 simulated annealing technique the HYPERCHEM [164] program was used.

Table 3.1: Relative energies (kJ/mol) between two minima of the same cluster size, calculated with the three described basis sets.

	SKBJ(d)	SKBJ(expan)	TZ2P
ΔE ($E_{Zn_4O_4^{GM}}$-$E_{Zn_4O_4^{LM}}$)	+ 245.15	+ 254.73	+ 208.83
ΔE ($E_{Zn_8O_8^{GM}}$-$E_{Zn_8O_8^{LM_1}}$)	+ 13.54	+ 19.55	+ 2.18
ΔE ($E_{Zn_8O_8^{GM}}$-$E_{Zn_8O_8^{LM_2}}$)	+ 46.70	+ 26.64	+ 92.19

3.2.1 Basis set selection

In the previous section it was mentioned that the basis set used during these calculations was SKBJ(d). Although a larger basis set is not expected to change significantly the geometry of the obtained structures, the relative energies between them may be affected. In order to check the reliability of our SKBJ(d) basis set, single point energy calculations using larger basis sets were performed on several structures which will be detailed later. Two other basis sets were examined. The first was a simple expansion of the previously described SKBJ(d) basis.

Two s and p functions (with α=1.335122, 1.120129), one d (α=2.561376), and one f (α=3.115413) were added the Zn basis. The SKBJ(d) basis was expanded for O as well with the two new s and p functions having exponents α=1.206642,0.561051, and the f function, α=1.666029.

All of these added functions were energy optimized at the MP2 level of theory using the GAMESS US [165] package. As the SKBJ(d) basis set only has one d function on O, it was decided that upon the addition of another, the exponents of both should be energy optimized. The exponents for the two d functions in this expanded basis were 2.179302 and 0.628849. This expanded basis set will be referred to as SKBJ(expan). The second examined basis set was an all electron triple-ζ double polarization (TZ2P) basis (14s11p6d2f/10s8p3d2f) for Zn [166, 167, 168] and (11s5p2d1f/4s3p2d1f) for O [169, 170]. The relative energies between two minima of each cluster size chosen is shown below in Table 3.1.

All basis sets predict both the same global minima and the sequential positioning of the local minima. Nevertheless, for Zn_8O_8 the relative energies are quite small, and therefore we have decided to perform single point calculations with both SKBJ(expan) and TZ2P for the cases where the relative energies are smaller than 100 kJ/mol. In this way the validity of the SKBJ(d) relative energies is checked,

3.2.2 Reliability of B3LYP results

In order to check the feasibility of the B3LYP calculations, Coupled Cluster [88, 89] with Single, Double [179, 180, 181, 182] and a correction term for the

Table 3.2: CCSD(T) relative energies (kJ/mol) for Zn_iO_i, $i = 2, 3$.

	CCSD(T)/TZ2P	CCSD(T)/SKBJ(d)	B3LYP/SKBJ(d)
ΔE $(i = 2)$	+ 188.06	+ 183.04	+ 120.17
ΔE $(i = 3)$	-	+ 368.06	+ 328.19

Triple [183] substitutions, CCSD(T), calculations were carried out for Zn_iO_i, $i = 2, 3$. For the smallest cluster, the TZ2P basis set was chosen, but the computational effort increased dramatically from $i = 2$ to $i = 3$. Thus, only the relative energy corresponding to $i = 2$ was calculated with this TZ2P basis set. Nevertheless we performed CCSD(T) calculations for $i = 2, 3$, with a smaller basis set, *i.e.* SKBJ(d). The obtained results for the relative energy of the first local minimum with respect to the ground state are shown in Table 3.2.

Notice that for $i = 2$, the CCSD(T)/TZ2P and CCSD(T)/SKBJ(d) relative energies are very similar: 188.06 kJ/mol and 183.04 kJ/mol, respectively. Notice that part of the difference should be ascribed to relativistic effects that, although they are known [184] to be smaller for the first-row transition metals, one should recall that Zn is the heaviest of them. This reinforces our statement of section 3.2.1 on the reliability of the SKBJ(d) basis set and validates the use of CCSD(T)/SKBJ(d) relative energies as reference values instead of the computationally more demanding CCSD(T)/TZ2P ones for further checks.

Both CCSD(T) and B3LYP predict the same sequence of global and local minima. The relative energies are found to be larger at the CCSD(T)/SKBJ(d) level of theory. For $i = 2$ the difference between both methods is 62.87 kJ/mol, but it is lowered to 39.87 for $i = 3$. These results illustrates the agreement between both methods and therefore B3LYP will be used hereafter.

3.3 Results and discussion

3.3.1 Structure of the calculated minima of Zn_iO_i clusters. $i = 1 - 9$.

In this section the calculated minima are presented. Although our interest is mainly centered on global minima, structures and properties of higher-lying local minima are presented as well.

The presented structures are labeled according to the following scheme: $Zn_iO_i^a$, where i denotes the number of ZnO units, and the superscript a may be GM (global minimum) or LM (local minimum).

In order to make the presentation of the results easier to the reader, we have divided this section into small parts where structures of the same size are presented, starting from the smallest and moving on to the largest ones. In Table

Table 3.3: Zn-O bond lengths, O-Zn-O angles and symmetry groups of the calculated structures. For the local minima, energies relative to the corresponding global minimum are in kJ/mol.

	R(Zn-O) Å	α(O-Zn-O)$^\circ$	Point Group	Rel. E. (kJ/mol)
$Zn_1O_1^{GM}$	1.713	-	$C_{\infty v}$	-
$Zn_2O_2^{GM}$	1.892	103.7	D_{2h}	-
$Zn_2O_2^{LM}$	1.976	106.2	C_{2v}	+ 120.17
$Zn_3O_3^{GM}$	1.826	146.3	D_{3h}	-
$Zn_3O_3^{LM}$	1.817 - 2.097	136.15	C_s	+ 328.19
$Zn_4O_4^{GM}$	1.794	165.5	D_{4h}	-
$Zn_4O_4^{LM}$	1.996	97	T_d	+ 245.15
$Zn_5O_5^{GM}$	1.780	174.9	C_s	-
$Zn_5O_5^{LM}$	1.853 - 2.135	98.4 - 148.2	C_1	+ 236.28
$Zn_6O_6^{GM}$	1.772	179.8	D_{6h}	-
$Zn_6O_6^{LM_1}$	1.907 - 2.102	134.0	D_{3d}	+ 95.90
$Zn_6O_6^{LM_2}$	1.793 - 2.156	143.7 - 157.8	C_2	+ 99.90
$Zn_7O_7^{GM}$	1.767	176.6	D_{7h}	-
$Zn_7O_7^{LM_1}$	1.766 - 1.882	143.6 - 172.6	C_s	+ 43.91
$Zn_7O_7^{LM_2}$	1.783 - 2.180	92.93 - 165.2	C_s	+74.86
$Zn_8O_8^{GM}$	1.86 - 2.185	92.6 - 152.5	D_{4d}	-
$Zn_8O_8^{LM_1}$	1.879 - 2.063	92.7 - 131.6	S_4	+ 13.54
$Zn_8O_8^{LM_2}$	1.766	175.91	D_{4d}	+ 46.70
$Zn_9O_9^{GM}$	1.89 - 1.99	93.1 - 130.7	C_{3h}	-
$Zn_9O_9^{LM_1}$	1.918 - 2.037	92.2 - 136.0	D_{3d}	+ 29.79
$Zn_9O_9^{LM_2}$	1.766	175.1 - 177.7	C_1	+ 127.91

3.3 geometrical values such as bond-lengths and bond angles, point groups and relative energies of all the calculated structures are given. These energies have been calculated with the SKBJ(d) basis set.

It can be seen that for larger clusters, i.e. Zn_iO_i, $i \geq 6$ the relative energies are smaller than 100 kJ/mol, except for $Zn_9O_9^{LM_2}$. Hence single point calculations for these structures have been performed using the previously described SKBJ(expan) and TZ2P basis sets. The obtained results are shown in Table 3.4.

SKBJ(expan) raises all relative energies except for $E_{Zn_8O_8^{GM}}$-$E_{Zn_8O_8^{LM_2}}$. TZ2P has exactly the opposite effect and the effect is significantly larger. Note that all cases in which the TZ2P basis makes a large difference, comparison is being made between 3D and ring structures. The TZ2P basis set stabilizes the 3D structures in every case. All basis sets predict both the same global minima and the sequential positioning of the local minima, except the case of $Zn_6O_6^{LM_1}$ and $Zn_6O_6^{LM_2}$, where SKBJ(d) and TZ2P predict the same sequential positioning, but SKBJ(expan) does not. Nevertheless the difference is very small, and all basis sets predict clearly the same global minimum. These results suggest

Table 3.4: Relative energies (kJ/mol) of the calculated structures of Zn_iO_i, $i = 6 - 9$, using the SKBJ(d), SKBJ(expan) and TZ2P basis sets.

	SKBJ(d)	SKBJ(expan)	TZ2P
ΔE ($E_{Zn_6O_6^{GM}}$-$E_{Zn_6O_6^{LM_1}}$)	95.90	110.50	51.07
ΔE ($E_{Zn_6O_6^{GM}}$-$E_{Zn_6O_6^{LM_2}}$)	99.90	102.51	88.27
ΔE ($E_{Zn_7O_7^{GM}}$-$E_{Zn_7O_7^{LM_1}}$)	43.91	47.97	34.51
ΔE ($E_{Zn_7O_7^{GM}}$-$E_{Zn_7O_7^{LM_2}}$)	74.86	88.04	41.74
ΔE ($E_{Zn_8O_8^{GM}}$-$E_{Zn_8O_8^{LM_1}}$)	13.54	19.55	2.18
ΔE ($E_{Zn_8O_8^{GM}}$-$E_{Zn_8O_8^{LM_2}}$)	46.70	26.64	92.19
ΔE ($E_{Zn_9O_9^{GM}}$-$E_{Zn_9O_9^{LM_1}}$)	29.79	32.24	25.54

Figure 3.1: $Zn_2O_2^{GM}$ and $Zn_2O_2^{LM}$. Small atoms are those of O.

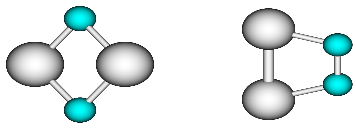

that the SKBJ(d) energies given in Table 3.3 describe correctly the sequential positioning of the global and local minima, and that the calculated relative energies are correct. Therefore, throughout this paper results from Table 3.3 will be considered.

A linear structure of $C_{\infty v}$ symmetry is found for $Zn_1O_1^{GM}$. It is interesting to note the shortness of the bond length compared to the other larger structures, as can be appreciated in Table 3.3. This length is lengthened to 1.893 Å in the triplet state, which is 22.22 kJ/mol more stable than the singlet reported in the table.

$Zn_2O_2^{GM}$, which belongs to the D_{2h} point group, and $Zn_2O_2^{LM}$, of C_{2v} symmetry, are depicted in Figure 3.1.

Both structures are planar, and $Zn_2O_2^{LM}$ lies 120 kJ/mol above the global minimum. The Zn-O bond length in both cases is longer than that of Zn_1O_1, but in the case of $Zn_2O_2^{LM}$ these bonds are remarkably long, 1.976 Å compared to 1.892 Å of $Zn_2O_2^{GM}$.

Zn_2S_2 structures are similar to these ones. In this case, the D_{2h} structure is the global minimum as well, and the relative energy between the minima is very similar: 117.10 kJ/mol for zinc sulfide and 120.17 for zinc oxide.

In Figure 3.2 $Zn_3O_3^{GM}$ and $Zn_3O_3^{LM}$ are depicted.

Figure 3.2: $Zn_3O_3^{GM}$ and $Zn_3O_3^{LM}$

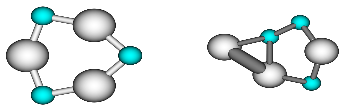

Figure 3.3: $Zn_4O_4^{GM}$ and $Zn_4O_4^{LM}$

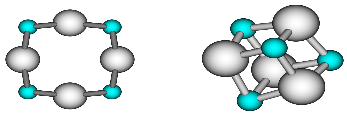

The global minimum belongs to the D_{3h} point group, and the local minimum has only C_s symmetry. Both structures are planar, as was the case for Zn_2O_2, but the energy difference between them is much larger, 328.19 kJ/mol compared to 120.17 kJ/mol of the smaller one. The Zn-O bond length in $Zn_3O_3^{GM}$ is 1.826 Å, shorter than that in $Zn_2O_2^{GM}$ by 0.07 Å. The O-Zn-O angles are larger here, of course, due to geometrical reasons.

Zn_3S_3 structures are similar to these ones, but it must be mentioned that the energy difference between the global and local minima is much larger in the case of zinc oxide (328.19 kJ/mol) than that difference for zinc sulfide (233.75 kJ/mol).

In Figure 3.3 $Zn_4O_4^{GM}$, D_{4h}, and $Zn_4O_4^{LM}$, T_d, are given.

It may be observed that the global minimum is a planar ring, like Zn_2O_2 and Zn_3O_3, but the characterized local minimum is the first three dimensional structure. It is constructed from six Zn_2O_2 units, forming a sort of deformed cube. It lies 245.15 kJ/mol higher in energy than the global minimum. The planar global minimum has Zn-O bonds that are shorter than those found in $Zn_3O_3^{GM}$ and, again, O-Zn-O angles which are larger. The Zn-O bond lengths in $Zn_4O_4^{LM}$, on the other hand, are almost 0.2 Å larger than those in $Zn_4O_4^{GM}$. This, of course, is a result of both the higher coordination number and the strained O-Zn-O bond angles (97°). In addition to this, O-Zn-O angles tend to linearity in the ring structures, and in $Zn_4O_4^{GM}$ are already 165.5°.

Characterized Zn_4S_4 structures are similar to these ones. However, again the energy difference between global and local minima is much larger in the case of Zn_4O_4: 245.15 kJ/mol compared to 117.27 kJ/mol for Zn_4S_4.

The calculated $Zn_5O_5^{GM}$ of D_{5h} symmetry and $Zn_5O_5^{LM}$ of C_1 symmetry are

Figure 3.4: $Zn_5O_5^{GM}$ and $Zn_5O_5^{LM}$

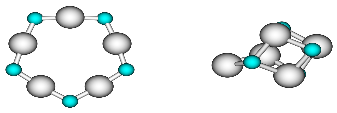

Figure 3.5: $Zn_6O_6^{GM}$, $Zn_6O_6^{LM_1}$ and $Zn_6O_6^{LM_2}$

shown in Figure 3.4.

As was the case for Zn_4O_4, a planar ring structure is found to be the global minimum and a three dimensional structure to be a local minimum. This $Zn_5O_5^{LM}$ has two different building blocks: four squares and two hexagons. The relative energy between these two structures is less than that found between the two Zn_4O_4 structures by only 9 kJ/mol, being 236.28 kJ/mol. In the planar ring the Zn-O bond lengths are 1.780 Å, similar to those of Zn_4O_4, and the O-Zn-O bond angles are very close to linearity, 174.9^o.

Similar structures, with a smaller energy difference, were found for Zn_5S_5. The ring structure of Zn_5S_5 broke planarity somewhat and was only 68.19 kJ/mol more stable than the three-dimensional local minimum.

The calculated structures $Zn_6O_6^{GM}$, $Zn_6O_6^{LM_1}$ and $Zn_6O_6^{LM_2}$ are represented in Figure 3.5.

$Zn_6O_6^{GM}$ belongs to the D_{6h} point group, $Zn_6O_6^{LM_1}$ to the D_{3d} group, and $Zn_6O_6^{LM_2}$ to the C_2 point group. $Zn_6O_6^{LM_1}$ is built from two "parallel" Zn_3O_3 units joined together by six Zn_2O_2 units. The same building blocks are found in the two other cases. $Zn_6O_6^{LM_2}$ is a planar structure with two Zn_3O_3 rings linked together by a Zn_2O_2 ring. As in the smaller cases of planar rings, one may appreciate in $Zn_6O_6^{GM}$ the tendency to form linear O-Zn-O bond angles and short bond lengths. Thus, we find angles of 179.8 ^{o}and bonds of 1.772 Å, similar to the previous cases. In the three dimensional structure we find larger bond lengths, in a wide range from 1.907 Å to 2.102 Å, and bond angles of 134.0 ^{o}. It should be pointed out that the relative energy between $Zn_6O_6^{GM}$ and $Zn_6O_6^{LM_1}$ is drastically reduced compared to those seen for the isomers of Zn_4O_4 and Zn_5O_5. For Zn_6O_6, the relative energy between planar and three dimensional structures is 95.90 kJ/mol. We see that there is a tendency to

Figure 3.6: $Zn_7O_7^{GM}$, $Zn_7O_7^{LM_1}$ and $Zn_7O_7^{LM_2}$

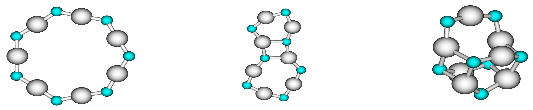

form more stable three dimensional structures as cluster size increases.

Related clusters were characterized for Zn_6S_6 (though no analog of $Zn_6O_6^{LM_2}$ was found). For smaller clusters we have seen that the planar ring-like structures were more stable for zinc oxide. Here that trend continues and while this ring is the global minimum for the zinc oxide cluster, it is not for zinc sulfide, where the D_{3d} structure is the global minimum. This stability of planar zinc oxide structures may explain the relative stability of $Zn_6O_6^{LM_2}$, while a related structure was not observed for Zn_6S_6.

The global minimum of D_{7h} symmetry $Zn_7O_7^{GM}$ and the calculated local minima are depicted in Figure 3.6.

$Zn_7O_7^{LM_1}$ and $Zn_7O_7^{LM_2}$ belong to the C_s point group. It is interesting to point out that again two planar structures are found to be the most stable ones. $Zn_7O_7^{GM}$ is a onering structure and $Zn_7O_7^{LM_1}$ a threering structure. $Zn_7O_7^{LM_1}$ lies 43.91 kJ/mol above the global minimum. In both cases the bond lengths are very similar, but bond angles differ considerably for geometrical reasons. $Zn_7O_7^{LM_2}$ is the lowest lying three dimensional structure, related to $Zn_7S_7^{GM}$. This structure lies 74.86 kJ/mol above the global minimum. This difference is smaller than in the smaller clusters, and therefore one would expect that in larger clusters the threedimensional structures will become the global minimum.

A structure related to $Zn_7O_7^{LM_2}$ was found to be the global minimum for Zn_7S_7, the ring structure lying 107.52 kJ/mol higher in energy.

As it has been mentioned already, the main difference at first sight between $Zn_8O_8^{GM}$ and the previously seen global minima is that $Zn_8O_8^{GM}$ is nonplanar. There has been a transition, from a situation in which the planar ring structures were favored, to a situation where three-dimensional structures are favoured. Examining the trend in relative energies between the ring and three-dimensional structures for $i = 4-8$ we find that the ring structure was more stable for $i = 4$ by 245.15 kJ/mol. That difference was reduced to 236.28 kJ/mol for $i = 5$, but still is large. For $i = 6$ the threedimensional structure is closer to the ring, 95.9 kJ/mol higher in energy, and this difference is reduced to 43.91 kJ/mol for $i = 7$. Finally, the threedimensional $Zn_8O_8^{GM}$ is more stable than the ring by 46.7 kJ/mol, and $Zn_9O_9^{GM}$ by 127.91 kJ/mol. It is clear that as the size of the cluster increases, the 3D structures become more stable than the rings.

Figure 3.7: $Zn_8O_8^{GM}$, $Zn_8O_8^{LM_1}$ and $Zn_8O_8^{LM_2}$

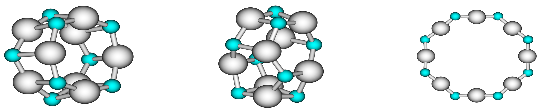

Figure 3.8: $Zn_9O_9^{GM}$, $Zn_9O_9^{LM_1}$ and $Zn_9O_9^{LM_2}$.

In Figure 3.7 the calculated structures are shown. $Zn_8O_8^{GM}$ has D_{4d} symmetry, $Zn_8O_8^{LM_1}$ S_4 and $Zn_8O_8^{LM_2}$ D_{4d} as well.

Therefore, these three calculated structures are very symmetric. $Zn_8O_8^{GM}$ may be viewed as being built by two "parallel" Zn_4O_4 rings linked together by Zn_2O_2 rings, as was $Zn_8S_8^{LM_1}$. The $Zn_8O_8^{LM_1}$ is also a three dimensional structure built by six Zn_2O_2 and four Zn_3O_3 rings, related to $Zn_8S_8^{GM}$. $Zn_8O_8^{GM}$ and $Zn_8O_8^{LM_1}$ are energetically very close, they are separated by only 13.54 kJ/mol. The bond lengths and bond angles are similar to other three dimensional structures, as may be observed in Table 3.3. No completely planar ring is found; $Zn_8O_8^{LM_2}$ has all zincs in the same plane, but the oxygen atoms alternate up and down along the ring. In this way the bond angles are close to linearity, 175.9 in this case. In a completely planar ring these angles could not be so obtuse and have the structure maintain favorable angles about the oxygen atoms, which would make the molecule less stable. Nevertheless, this ring structure is only 43.70 kJ/mol above the global minimum in energy.

For Zn_8S_8 similar structures were found, but the S_4 structure was the global minimum, 78.94 kJ/mol more stable.

In Figure 3.8 the calculated structures $Zn_9O_9^{GM}$ and $Zn_9O_9^{LM_1}$ are depicted.

$Zn_9O_9^{GM}$ is a three dimensional spheroid structure of C_{3h} symmetry composed by six Zn_2O_2 and five Zn_3O_3 rings, as was $Zn_9S_9^{GM}$. $Zn_9O_9^{LM_1}$ is formed by three stacked Zn_3O_3 rings, linked together by Zn_2O_2 units. It may be constructed by adding an extra Zn_3O_3 ring to $Zn_6O_6^{LM_1}$. This structure lies 29.79 kJ/mol above the global minimum. As in the previous case, the ring structure is no longer planar, with the oxygen atoms above and below the plane formed by the Zn atoms. This structure is labeled $Zn_9O_9^{LM_2}$ and belongs to the C_s point group. This structure is predicted to be 127.91 kJ/mol less

Table 3.5: Natural Orbital charges (e) of the shown global minima.

	Zn	O
$Zn_1O_1^{GM}$	0.973	- 0.973
$Zn_2O_2^{GM}$	1.335	- 1.335
$Zn_3O_3^{GM}$	1.412	- 1.412
$Zn_4O_4^{GM}$	1.432	-1.432
$Zn_5O_5^{GM}$	1.451	- 1.451
$Zn_6O_6^{GM}$	1.465	- 1.465
$Zn_7O_7^{GM}$	1.477	- 1.477
$Zn_8O_8^{GM}$	1.532	- 1.532
$Zn_9O_9^{GM}$	1.559	- 1.559

stable than $Zn_9O_9^{GM}$.

3.3.2 Natural Orbital charges

At this point we analyze the natural orbital charges, obtained by Natural Bonding Analysis [178] at the B3LYP/SKBJ(d) level of theory, which are given in Table 3.5.

The cationic nature of zinc and the anionic nature of oxygen can be observed in all the structures. The atomic charges are larger as cluster size increases, and a trend towards the charge separation of the bulk ($|1.91e|$) is clearly observed.

3.3.3 Cohesive energy

The cohesive energy per zinc oxide unit is calculated as $E_f = (iE_{Zn} + iE_O - E_{Zn_iO_i})/i$, where i is the number of ZnO units. The cohesive energy may be plotted versus the inverse of the cubic root of i, and then a line can be fit to the obtained points. Extrapolating it to $i^{-1/3}$=0, that is, to i =∞, or the bulk, a theoretical value which can be compared to the experimental one may be obtained.

In the previous chapter ([185]) the same approach was used for Zn_iS_i. The representative points were seen to be those corresponding to three dimensional structures. In the case of Zn_iO_i only two points belong to three dimensional structures, those corresponding to $Zn_8O_8^{GM}$ and $Zn_9O_9^{GM}$. Therefore, in order to obtain a meaningful extrapolation the cohesive energy of larger three-dimensional clusters should be taken into account, and for that purpose further calculations must be done.

The cohesive energies of the calculated global minima are given in Table 3.6.

Table 3.6: Cohesive energy, E_f, (kJ/mol) of characterized global minima.

	E_f (kJ/mol)
$Zn_1O_1^{GM}$	84.06
$Zn_2O_2^{GM}$	275.09
$Zn_3O_3^{GM}$	403.26
$Zn_4O_4^{GM}$	447.72
$Zn_5O_5^{GM}$	462.92
$Zn_6O_6^{GM}$	468.55
$Zn_7O_7^{GM}$	470.47
$Zn_8O_8^{GM}$	476.52
$Zn_9O_9^{GM}$	484.95

3.4 Conclusions

It has been seen that planar ring structures are the global minima for Zn_iO_i, $i = 1-7$, and three-dimensional structures for $i = 8, 9$. These three-dimensional global minima, along with the other calculated three dimensional local minima may be viewed as being built from Zn_2O_2 rombi and Zn_3O_3 hexagons (and an occasional Zn_4O_4 unit), as they were for zinc sulfide. However, for zinc sulfide ring structures were the global minima for $i = 2-5$, and threedimensional structures the global minima for $i = 6-9$. This different behaviour is mainly attributable to two factors. The rigidity of angles about the oxygen atom (as opposed to sulfur's more flexible bonding) plays a part, but the major difference is that sulfur atoms benefit much more from additional valence than do oxygen atoms. These clusters containing oxygen atoms are not highly stabilized by the additional bonds found in the threedimensional structures, making the ring structures the global minima for clusters with $i < 8$.

In [177] the authors predicted stable spheroid structures for Zn_iO_i, $i > 11$. We have seen, however, that these spheroid structures are stable for smaller cases, such as $i = 8, 9$. Therefore, the onset of the stability for spheroid structures is $i = 8$, according to our calculations.

In summary, there are two main factors determining whether a ring or three-dimensional structure will be the global minimum for the small zinc oxide clusters: the stability of very obtuse O-Zn-O bond angles, and the stability gained from higher coordination. For Zn_iO_i, $i = 2-7$, the first term outweighs the second and ring structures are predicted to be the global minima. For $i = 8$ and greater however, the size of the cluster allows for both obtuse O-Zn-O bond angles and higher coordination in the three dimensional spheroid structures, making these the most stable.

These three dimensional clusters can be envisioned as being built of smaller building blocks, basically Zn_2O_2 (squares) and Zn_3O_3 (hexagons) rings. Basically, the number of squares remains constant and the number of hexagons increases by one when adding an extra ZnO unit.

Chapter 4

Small Clusters of II-VI Materials: Zn_iX_i, X=Se,Te, $i = 1 - 9$

Abstract

The improvements in the characterization of II-VI compound-based solar cells and the recent experimental characterization of small clusters and nanoparticles make the study of small II-VI clusters very interesting. In this work, the ground states of small Zn_iX_i clusters are studied, X=Se,Te, $i = 1 - 9$. Ring-like structures have been found to be the global minima for clusters as large as $i = 5$, and three dimensional spheroid structures for larger ones, $i = 6 - 9$. This trend has been adscribed to the stability of obtuse X-Zn-X angles in the first case, and to the stability gained from higher coordination in the second case. The three dimensional structures may be envisioned as being built from Zn_2X_2 and Zn_3X_3 rings, as it was the case for Zn_iS_i and Zn_iO_i three dimensional structures. Calculated natural charges are larger as cluster size increases, showing a tendency towards bulk charges.

4.1 Introduction

Semiconductors are materials of great importance in the development of technology. Computer revolution and other technological devices have been and are in rapid development basically due to improved semiconductor materials. Some of these materials are the II-VI compounds, which interest has increased notably due to their paramount technological potential.

It is important to study small clusters of these compounds, whose electronic and structural properties could give insight into understanding local properties. In addition to this reason, the fact that cluster and nanoparticle characterization is becoming technologically feasible is remarkable. This makes cluster science more interesting, since in addition to the capability of understanding some surface-related properties, the improvement of applications by the use of nanotechnology could be possible. A neat example of this are the fullerenes, carbon spheroids discovered by R.F. Curl, R.E. Smalley and H.W. Kroto, which have also photovoltaic applications [52, 53].

The study of small II-VI clusters appears promising, therefore. Global and local minima of Zn_iS_i, $i = 1 - 9$ ([185]), and Zn_iO_i, $i = 1 - 9$ ([187]), clusters have been presented above in Chapter 2 and 3, respectively. Spheroid fullerene-type structures were found to be the global minima for $i \geq 6$ for Zn_iS_i, and $i \geq 8$ for Zn_iO_i, which is in accordance with previous molecular dynamics calculations [177]. In this work we focus on zinc selenide and zinc teluride clusters, Zn_iSe_i and Zn_iTe_i, $i = 1 - 9$.

4.2 Method

All geometries were fully optimized using the hybrid [109] Becke 3 Lee-Yang-Parr (B3LYP) gradient-corrected approximate density-functional procedure [99, 110, 111]. Harmonic vibrational frequencies were determined by analytical differentiation of gradients.

The relativistic compact effective core potentials and shared-exponent basis set [133] of Stevens, Krauss, Basch and Jasien (SKBJ) was used as the basic basis set in this study. The d electrons of Zn were included in the valence. An extra d function was added on Zn (α=0.3264) and two extra d and one f on both Se (α=0.537830, α=0.208111 and α=0.396026, respectively) and Te (α=0.349496, α=0.155852 and α=0.306353, respectively), due to their importance for the proper description of the high coordination of the atoms in the three-dimensional cluster structures. The exponents of all of these added functions were energy optimized using the GAMESS [165] package. Note that pure angular momentum functions were used throughout this study. We denote the final basis set used as SKBJ(d/2df).

Because there are so many possible structures for these clusters, several starting points for these complete B3LYP/SKBJ(d/2df) optimizations were generated using a simulated annealing approach at the PM3 [161] level of theory. Of course, additional starting points were derived from simple chemical intuition.

Table 4.1: SKBJ(expan) basis set for Zn, Se and Te atoms.

	Zn			Se			Te		
	α	d	d	α	d	d	α	d	d
sp	1.335122	1.0	1.0	0.750763	1.0	1.0	0.535452	1.0	1.0
sp	1.120129	1.0	1.0	0.375285	1.0	1.0	0.180824	1.0	1.0
d	2.561376	1.0		0.691855	1.0		0.408953	1.0	
d	0.326400	1.0		0.463247	1.0		0.237585	1.0	
d				0.177490	1.0		0.084947	1.0	
f	3.115413	1.0		1.048712	1.0		0.594100	1.0	
f				0.366780	1.0		0.228881	1.0	

It has to be mentioned that the large amount of structures that appears as the cluster size increases makes impossible the study of all of them. In this study only the lowest lying structures of each size have been considered.

All the geometry optimizations and frequency calculations were carried out with the GAUSSIAN98 [163] package. For the PM3 simulated annealing technique the HYPERCHEM [164] program was used.

4.2.1 Basis set selection

It was mentioned in the previous section that the basis set used during these calculations was SKBJ(d/2df). Although a larger basis set is not expected to change significantly the geometry of the obtained structures, relative energies might be affected. In order to check the reliability of our SKBJ(d/2df) basis set, single point energy calculations using larger basis sets were performed on Zn_4X_4 and Zn_6X_6 structures, which will be detailed later.

The effect of two more basis sets was examined in the case of ZnSe. The former was a simple expansion of the previously described SKBJ(d/2df) basis. Two s and p functions, one d and one f were added to the Zn SKBJ(d) basis, resulting in a final SKBJ(2sp2d1f) basis. The exponents are given in Table 4.1. The SKBJ(2df) basis was expanded for Se adding two new s and p functions, and an extra d and f functions. In addition to this, the previous two d and f functions included in SKBJ(2df) basis were reoptimized, resulting in a final SKBJ(2sp3d2f). The exponents may be seen in Table 4.1. This expanded basis set will be referred to as SKBJ(expan). The latter basis set for ZnSe was an all electron triple-ζ double polarization (TZ2P) basis (14s11p6d2f/10s8p3d2f) for Zn [166, 167, 168] and (15s13p6d1f/8s7p2d1f) for Se [188, 189, 190].

In the case of ZnTe only the effect of one larger basis was examined. Namely, the SKBJ(d/2df) basis was expanded in a similar manner as for ZnSe, with the same SKBJ(2sp2d1f) for Zn, and a final SBKJ(2sp3d2f) for Te. This expanded basis set will be denoted hereafter as SKBJ(expan). The exponents are shown in Table 4.1.

Table 4.2: Relative energies (kJ/mol) between the lowest-lying structures of the same cluster size of Zn_iX_i, with three basis sets.

	SKBJ(d/2df)	SKBJ(expan)	TZ2P
ΔE ($E_{Zn_4Se_4^{GM}}$-$E_{Zn_4Se_4^{LM}}$)	+ 97.79	+ 102.42	+ 91.16
ΔE ($E_{Zn_6Se_6^{GM}}$-$E_{Zn_6Se_6^{LM_1}}$)	+ 36.84	+ 35.70	+ 44.01
ΔE ($E_{Zn_6Se_6^{GM}}$-$E_{Zn_6Se_6^{LM_2}}$)	+ 44.71	+ 38.53	+ 52.01
ΔE ($E_{Zn_4Te_4^{GM}}$-$E_{Zn_4Te_4^{LM}}$)	+ 69.13	+ 71.10	-
ΔE ($E_{Zn_6Te_6^{GM}}$-$E_{Zn_6Te_6^{LM_1}}$)	+ 37.34	+ 37.51	-
ΔE ($E_{Zn_6Te_6^{GM}}$-$E_{Zn_6Te_6^{LM_2}}$)	+ 49.91	+ 47.74	-

Table 4.3: CCSD(T) relative energies (kJ/mol) for Zn_iSe_i and Zn_iTe_i, $i = 2-3$.

	CCSD(T)/TZ2P	CCSD(T)/SKBJ(d/2df)	B3LYP/SKBJ(d/2df)
ΔE ($i = 2$)	+ 158.95	+ 141.82	+ 96.31
ΔE ($i = 3$)	-	+ 249.70	+ 191.58
	CCSD(T)/SKBJ(expan)	CCSD(T)/SKBJ(d/2df)	B3LYP/SKBJ(d/2df)
ΔE ($i = 2$)	+ 103.92	+ 114.40	+ 74.68
ΔE ($i = 3$)	-	+ 177.99	+ 141.06

The relative energies between the two lowest-lying structures of the clusters selected are shown below in Table 4.2. Note that the full electron TZ2P basis set do not include relativistic effects.

All basis sets predict both the same global minima and the same sequential positioning of the local minima. The differences in the relative energies are small in all the cases, showing the reliability of our SKBJ(d/2df) basis set.

4.2.2 Method selection

In order to check the feasibility of the B3LYP results, Coupled Cluster [88, 89] with Single, Double [179, 180, 181, 182] and a correction term for the Triple [183] substitutions, CCSD(T), calculations were carried out for Zn_iX_i, X=Se,Te, $i = 2 - 3$.

The TZ2P basis set was chosen for Zn_2Se_2 and SKBJ(expan) for Zn_2Te_2. Since the computational effort increased dramatically from $i = 2$ to $i = 3$, we performed CCSD(T) calculations for $i = 3$ with a smaller basis set, *i.e.* SKBJ(d/2df). The relative energies of the first local minimum with respect to the ground state are shown in Table 4.3.

In Table 4.3 one may see that for $i = 2$, the CCSD(T)/TZ2P and CCSD(T)/ SKBJ(d/2df) relative energies are very similar: 158.95 kJ/mol and 141.82

kJ/mol, respectively. Similar behavior is observed for Zn_iTe_i, where for $i = 2$, the CCSD(T)/ SKBJ(expan) and CCSD(T)/SKBJ(d/2df) relative energies are 103.92 kJ/mol and 114.40 kJ/mol. Note that part of the difference should be ascribed to relativistic effects that, although they are known [184] to be small for the first-row transition metals, are largest for Zn within the row. This reinforces our statement of section 4.2.1 on the reliability of the SKBJ(d/2df) basis set and validates the use of CCSD(T)/SKBJ(d/2df) relative energies as reference values instead of the computationally more demanding CCSD(T)/TZ2P and CCSD(T)/SKBJ(expan) ones for further checks.

Both CCSD(T) and B3LYP predict the same sequence of global and local minima. The relative energies are found to be larger at the CCSD(T)/SKBJ(d/2df) level of theory. In the case of Zn_iSe_i, for $i = 2$ the difference between both methods is 45.51 kJ/mol, and 58.12 for $i = 3$. For Zn_iTe_i, these differences are similar: 39.72 kJ/mol for $i = 2$, and 36.93 for $i = 3$. These results illustrates the agreement between both methods and therefore B3LYP will be used hereafter.

4.3 Results

4.3.1 Structures of characterized minima of Zn_iX_i, X=Se,Te, $i = 1 - 9$

In this section the calculated minima are presented. Although our interest focuses on global minima, structures and properties of higher-lying local minima are presented as well.

In order to show the calculated structures in a more understandable way, we have arbitrarily divided these clusters into two groups, according to the geometrical structure of the global minimum. In Group 1, Zn_iX_i, X=Se,Te, $i = 1 - 5$, clusters are included which global minima are planar or near planar ring-like structures. In the second group, Group 2, the rest, for which the global minima are three dimensional spheroids.

The presented structures are labeled according to the following scheme: $Zn_iX_i^a$, where i denotes the number of ZnX units, and the superscript a may be GM (global minimum) or LM (local minimum), and X may be Se or Te. Hereafter, when using Zn_iX_i both Zn_iSe_i and Zn_iTe_i will be referred.

Group 1

In this section the calculated structures of Zn_iX_i, $i = 1 - 5$ will be described.

In Figure 4.1 the predicted global minima of Zn_iX_i are shown, and in Figure 4.2 their corresponding local minima. It should be pointed out that equivalent structures have been found for both Zn_iSe_i and Zn_iTe_i. In Table 4.4 properties such as molecular geometries, energies, and the symmetry of the studied structures are given.

Figure 4.1: Calculated global minima of Zn_iX_i, X=Se,Te, $i = 2-5$, labeled from left to right $Zn_2X_2^{GM}$, $Zn_3X_3^{GM}$ and in the second row $Zn_4X_4^{GM}$ and $Zn_5X_5^{GM}$, respectively. The dark larger atoms are those of selenium or telurium.

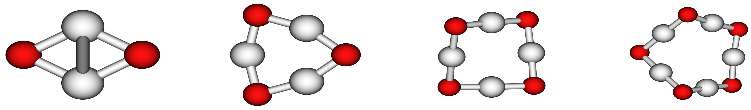

Figure 4.2: Calculated local minima of Zn_iX_i, X=Se,Te, $i = 2-5$, labeled from left to right $Zn_2X_2^{LM}$, $Zn_3X_3^{LM}$ and in the second row $Zn_4X_4^{LM}$ and $Zn_5X_5^{LM}$, respectively.

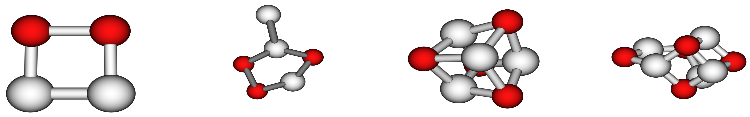

The global minima of the clusters in group 1 have been seen to be planar rings ($i = 2-3$) or near planar rings ($i = 4-5$). The main reason to break the planarity in these ring structures is the observed strong tendency to form linear X-Zn-X angles. Thus, there are found angles in a range of 170-180 degrees for $Zn_iX_i^{GM}$, $i = 4-5$. The bond lengths are shorted as the size of the ring increases. In the case of $Zn_iSe_i^{GM}$ they decrease from 2.38 Å to 2.30 Å, and in the case of $Zn_iTe_i^{GM}$ from 2.58 Å to 2.51 Å. Local minima have been found to be planar for $i = 2-3$, and 3D local minima were only found for $i = 4-5$. These structures can be pictured as being built from (squares) $Zn_2X_2^{GM}$ and (hexagons) $Zn_3X_3^{GM}$-like structures. $Zn_4X_4^{LM}$ consists of six square-like Zn_2X_2 units, which share atoms with each other, forming a sort of deformed cube. $Zn_5X_5^{LM}$ is built by four Zn_2X_2 and two Zn_3X_3 units. In these 3D structures the bond lengths are larger than the ring ones, and angles are far from linearity due to geometrical constraints.

It has to be mentioned that related structures were found for Zn_iO_i and Zn_iS_i clusters, as seen in Chapters 2 and 3. All global minima were planar rings in the case of Zn_iO_i, and all except $i = 5$ in the case of Zn_iS_i. This structural difference may be explained by the fact that linear X-Zn-X angles are preferred in the ring structures, and due to the larger size of the atoms as one goes down in the periodic table, the break of the planarity is impossed.

Having a look to the relative energies given in Table 4.4, there is observed that these values are larger in the case of Zn_iSe_i. Additionally, in both cases the largest relative energy occurs in Zn_3X_3, and when the size increases the energy

Table 4.4: Zn-X bond lengths, X-Zn-X angles, and symmetry groups of the structures of Figs. 4.1 and 4.2. For the local minima, energies relative to the corresponding minimum are in kJ/mol.

	R (Zn-X) (Å)	α (X-Zn-X) (deg)	Point Group	Rel. E.
$Zn_1Se_1^{GM}$	2.20	-	$C_{\infty v}$	-
$Zn_2Se_2^{GM}$	2.38	116.8	D_{2h}	-
$Zn_2Se_2^{LM}$	2.44	-	C_{2v}	+96.31
$Zn_3Se_3^{GM}$	2.321	160.4	D_{3h}	-
$Zn_3Se_3^{LM}$	2.32-2.36	135.2-145.4	C_s	+191.58
$Zn_4Se_4^{GM}$	2.30	177.9	C_{2v}	-
$Zn_4Se_4^{LM}$	2.50	107.0	T_d	+97.79
$Zn_5Se_5^{GM}$	2.30	172.2-178.5	C_s	-
$Zn_5Se_5^{LM}$	2.27-2.54	99.2-156.1	C_1	+49.64
$Zn_1Te_1^{GM}$	2.41	-	$C_{\infty v}$	-
$Zn_2Te_2^{GM}$	2.58	120.5	D_{2h}	-
$Zn_2Te_2^{LM}$	2.64	-	C_{2v}	+74.68
$Zn_3Te_3^{GM}$	2.53	163.6	D_{3h}	-
$Zn_3Te_3^{LM}$	2.53-2.56	140.2-150.3	C_s	+141.06
$Zn_4Te_4^{GM}$	2.52	177.7	C_{2v}	-
$Zn_4Te_4^{LM}$	2.70	109.1	T_d	+69.13
$Zn_5Te_5^{GM}$	2.51	171.1-178.4	C_s	-
$Zn_5Te_5^{LM}$	2.48-2.74	101.0-158.6	C_1	+24.09

difference between the ring structure and the 3D structure decreases. Focusing on the Zn_iSe_i case, this variation occurs as follows: 96.31, 191.58, 97.79 and 49.64 kJ/mol for $i = 2 - 5$, respectively.

Similar behavior of the relative energy was observed for Zn_iO_i and Zn_iS_i clusters. If one compares the four combinations, it is seen that the largest energies happen in Zn_iO_i and that they decrease as one goes down in the periodic table. As an example, the relative energies of Zn_5X_5 are 236.28 kJ/mol, 68.19 kJ/mol, 49.64 kJ/mol and 24.09 kJ/mol, for X= O, S, Se, Te, respectively.

Group 2

This group contains the clusters whose global minima are three dimensional spheroids, Zn_iSe_i and Zn_iTe_i, $i = 6 - 9$.

In Figure 4.3 the global minima of Zn_iX_i are shown, and in Figure 4.4 the local minima. In Table 4.5 the Zn-X bond lengths, X-Zn-X angles, electronic energies, and symmetry points of the calculated structures are given.

The structures of the characterized clusters are related to the previously seen Zn_iX_i, X=O,S, $i \geq 6$ structures. Three structures have been characterized for Zn_6X_6. $Zn_6X_6^{GM}$ is built from two "parallel" Zn_3X_3 units joined together by six Zn_2X_2 units. The same building blocks are found in the lower lying local

Figure 4.3: Calculated global minima of Zn_iX_i, X=Se,Te, $i = 6-9$, labeled from left to right $Zn_6X_6^{GM}$, $Zn_7Se_7^{GM}$ ($Zn_7Te_7^{LM_1}$) and in the second row $Zn_8X_8^{GM}$ and $Zn_9X_9^{GM}$, respectively.

Figure 4.4: Calculated local minima of Zn_iX_i, X=Se,Te, $i = 6-9$, labeled from left to right $Zn_6X_6^{LM_1}$, $Zn_6X_6^{LM_2}$, $Zn_7Se_7^{LM_1}$ ($Zn_7Te_7^{GM}$), $Zn_7X_7^{LM_2}$, and in the second row $Zn_8X_8^{LM_1}$, $Zn_8X_8^{LM_2}$ and $Zn_9X_9^{LM}$, respectively.

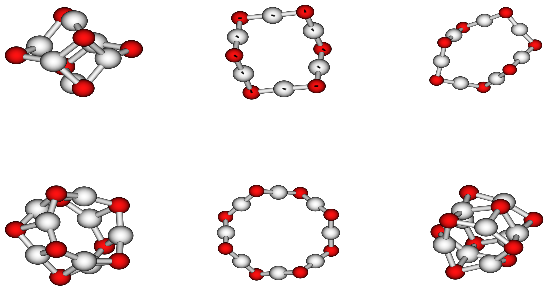

Table 4.5: Zn-X bond lengths, X-Zn-X angles, and symmetry groups of the structures of Figs. 4.3 and 4.4. For the local minima, energies relative to the corresponding minimum are in kJ/mol.

	R (Zn-X) (Å)	α (X-Zn-X) (deg)	Point Group	Rel. E.
$Zn_6Se_6^{GM}$	2.43-2.59	103.4-141.1	D_{3d}	-
$Zn_6Se_6^{LM_1}$	2.33-2.55	97.6-158.4	D_{2d}	+36.84
$Zn_6Se_6^{LM_2}$	2.30	178.1	C_{2h}	+44.71
$Zn_7Se_7^{GM}$	2.29-2.70	102.2-176.9	C_s	-
$Zn_7Se_7^{LM_1}$	2.29-2.66	95.3-160.0	C_2	+2.66
$Zn_7Se_7^{LM_2}$	2.30	173.4-179.4	D_{3d}	+45.85
$Zn_8Se_8^{GM}$	2.41-2.51	102.0-138.2	S_4	-
$Zn_8Se_8^{LM_1}$	2.41-2.60	102.6-152.3	C_{4v}	+78.92
$Zn_8Se_8^{LM_2}$	2.30	177.3	D_{4d}	+156.82
$Zn_9Se_9^{GM}$	2.40-2.51	101.7-128.9	C_{3h}	-
$Zn_9Se_9^{LM}$	2.40-2.71	100.6-149.5	D_{3d}	+162.75
$Zn_6Te_6^{GM}$	2.64-2.77	105.9-134.5	D_{3d}	-
$Zn_6Te_6^{LM_1}$	2.53-2.76	98.8-161.6	D_{2d}	+37.34
$Zn_6Te_6^{LM_2}$	2.51	178.4	C_{2h}	+49.91
$Zn_7Te_7^{GM}$	2.50-2.84	100.7-162.7	C_2	-
$Zn_7Te_7^{LM_1}$	2.51-2.90	101.0-177.7	C_s	+6.50
$Zn_7Te_7^{LM_2}$	2.51	173.6-178.2	D_{3d}	+50.76
$Zn_8Te_8^{GM}$	2.62-2.74	103.9-137.9	S_4	-
$Zn_8Te_8^{LM_1}$	2.63-2.77	105.6-147.6	C_{4v}	+83.84
$Zn_8Te_8^{LM_2}$	2.51	177.5	D_{4d}	+150.98
$Zn_9Te_9^{GM}$	2.61-2.71	103.7-128.9	C_{3h}	-
$Zn_9Te_9^{LM}$	2.60-2.83	100.8-151.6	D_{3d}	+199.15

minimum. $Zn_6X_6^{LM_1}$ is built from four linked Zn_3X_3 forming a ring, caped at the top and the bottom by two Zn_2X_2 rings. $Zn_6X_6^{LM_2}$ is a ring structure related to global minima of clusters of group 1.

$Zn_7Se_7^{GM}$ is a structure of C_s symmetry, and can be envisioned as two joined Zn_3Se_3 and one bent Zn_4Se_4 rings, related to $Zn_7S_7^{GM}$. $Zn_7Se_7^{LM_1}$ is built from four Zn_2Se_2 and four Zn_3Se_3 rings, yielding a final C_2 spheroid structure. These two structures are constructed from the smaller building blocks mentioned in smaller clusters. $Zn_7Se_7^{LM_2}$ is a ring structure which belongs to the C_s point group. In the case of Zn_7Te_7, the global minimum resembles the structure of $Zn_7Se_7^{LM_1}$. Conversely the $Zn_7Te_7^{LM_1}$ is related to $Zn_7Se_7^{GM}$.

Three structures have been characterized for Zn_8X_8, which are depicted in Figure 4.3 and 4.4. $Zn_8X_8^{GM}$ is a three dimensional structure built by six squares and four hexagons, similar to $Zn_8S_8^{GM}$ and $Zn_8O_8^{LM_1}$. The $Zn_8X_8^{LM_1}$ may be viewed as being built by two "parallel" Zn_4X_4 rings linked together by Zn_2X_2 rings. Rings are not entirely planar, thus, $Zn_8X_8^{LM_2}$ has all zincs on the same plane, but the X atoms alternate up and down with respect to the ring's plane.

Two structures have been characterized for Zn_9X_9. $Zn_9X_9^{GM}$ is a three dimensional spheroid composed by Zn_2X_2 and Zn_3X_3 rings, as in smaller clusters. In total, there are six squares and five hexagons, forming a structure resembling $Zn_9O_9^{GM}$ and $Zn_9S_9^{GM}$. $Zn_9X_9^{LM}$ is formed by three stacked Zn_3X_3 rings, linked together by Zn_2X_2 units, like $Zn_9O_9^{LM_1}$ and $Zn_9S_9^{LM_1}$. No ring structures have been characterized since they are expected to lie quite high in energy.

Geometrical parameters follow the trend of clusters of group 1. 3D structures have larger bond lengths than the ring structures, which are similar to the Zn_5X_5 rings. Besides, linear X-Zn-X angles are found in these rings, as was found in smaller cases.

For smaller clusters, rings have been found to be the global minima and 3D spheroids local minima. However, recall that as the cluster size increases, the relative energies between these rings and three dimensional local minima was found to decrease. Thus, for $i = 4$ the relative energies were 97.79 kJ/mol for Zn_iSe_i and 69.13 kJ/mol for Zn_iTe_i. This relative energy shrunk for $i = 5$ to 49.64 kJ/mol (Zn_iSe_i) and 24.09 kJ/mol (Zn_iTe_i). Finally, for $i = 6$ the three-dimensional structure became the global minima by 36.84 kJ/mol in the case of Zn_iSe_i and by 37.34 kJ/mol in the case of Zn_iTe_i.

Three-dimensional structures have been seen to be the global minima for the clusters of group 2. These structures are basically built from rombi and hexagon building blocks, as were the three-dimensional local minima in group 1. The relative energies between global minima and ring local minima increase as cluster size becomes larger. These relative energies are similar for Zn_iS_i, Zn_iSe_i and Zn_iTe_i, but are much smaller for Zn_iO_i. This means that ring structures are more favourable in Zn_iO_i, which may be explained by the preferrence of S, Se and Te to achieve coordination numbers higher than two.

Table 4.6: Natural Orbital charges (e) of the shown global minima.

	Zn_iSe_i		Zn_iTe_i	
i	Zn	Se	Zn	Te
1	0.864	-0.864	0.739	-0.739
2	1.099	-1.099	0.933	-0.933
3	1.124	-1.124	0.959	-0.959
4	1.139	-1.139	0.972	-0.972
5	1.140 - 1.152	-1.139 - -1.153	0.971 - 0.989	-0.971 - -0.987
6	1.192	-1.192	1.003	-1.003
7	1.139 - 1.193	-1.157 - -1.200	1.000 - 1.004	-0.976 - -1.027
8	1.197 - 1.214	-1.205 - -1.206	1.007 - 1.028	-1.010 - -1.025
9	-	-	-	-

4.3.2 Natural orbital charges

The Natural Bond Orbital analysis [178] was used to compute charges on the atoms of these clusters, which are given in Table 4.6.

Zn_9X_9 charges have not been calculated since the limit of 500 basis functions was exceeded.

The cationic nature of zinc and the anionic nature of selenium and telurium can be observed in all the structures. It has been seen in previous chapters that natural orbital charges were larger for Zn_iS_i and even larger for Zn_iO_i. This statement is in agreement with the bulk characteristics, where ZnO crystals are of highest ionic nature.

4.3.3 Cohesive energies

The cohesive energy per zinc selenide unit is calculated as $E_f = (iE_{Zn} + iE_X - E_{Zn_iX_i})/i$, where i is the number of ZnX units. When the cohesive energy is plotted versus the inverse of the cubic root of i, a straight line can be fitted to the obtained points. Extrapolating to $i^{-1/3}$=0, that is, to $i = \infty$, or the bulk, the theoretical value obtained for the cohesive energy can be compared to the experimental one.

Muilu et. al. used the same approach for large ZnS clusters [141]. The representative points were seen to be those corresponding to three dimensional structures. Four points are therefore available for both Zn_iSe_i and Zn_iTe_i. The cohesive energies of the Zn_iX_i predicted global minima are given in Table 4.7, and are ploted vs $i^{-1/3}$ in Figure 4.5.

Note that E_f decreases with i, smoothly for 3D structures and sharply for ring structures.

Figure 4.5 shows that $i = 7$ points lie below the fitted lines for both Zn_iSe_i and Zn_iTe_i. All attempts to locate global minima which fit the line eventually led to already characterized structures.

Table 4.7: Cohesive energy, E_f, (kJ/mol) of characterized global minima.

i	E_f (Zn_iSe_i)	E_f (Zn_iTe_i)
1	85.18	56.69
2	259.85	216.61
3	338.74	280.51
4	352.29	289.41
5	353.71	289.86
6	362.47	299.46
7	361.10	297.76
8	374.68	309.82
9	379.91	313.95

Hence, it is not clear if these four point are meaningful in each case, or only three of them, those corresponding to $i = 6, 8, 9$. Both cases have been studied and the obtained extrapolations are the following. If we take into account four poits, the predicted cohesive energies are 511.28 kJ/mol for Zn_iSe_i and 425.06 kJ/mol for Zn_iTe_i, and removing the points corresponding to $i = 7$, the predicted cohesive energies are 499.43 kJ/mol for Zn_iSe_i and 413.76 kJ/mol for Zn_iTe_i. The experimental values are calculated according to the CODATA data [191], by the next equation:

$$E_{f,exp} = \left|\Delta H_f^o(ZnX) - \Delta H_f^o(Zn) - \Delta H_f^o(X)\right| - RT$$

which are 518.0 kJ/mol and 487.6 kJ/mol for Zn_iSe_i and Zn_iTe_i, respectively. We observe that the cohesive energy is better predicted by taking into account all the points corresponding to 3D structures. Anyway, we believe that to obtain a more reliable extrapolation the cohesive energies of larger three-dimensional structures should be taken into account. Nevertheless, it is worth mentioning that no enthalpy of formation was found for Zn_iTe_i in the CODATA data, and this value was taken from [192]. The provided Zn_iTe_i enthalpy of formation is surprisingly similar to that of Zn_iSe_i as provided by CODATA. According to the trend provided by our calculations we believe that this experimental estimate requires further verification. This might account for the poorer prediction of the Zn_iTe_i cohesive energy.

The extrapolated E_f are smaller than the bulk values. This is due to some aspects. On one hand the fact that the coordination number in the clusters is three, whereas it is four in the bulk crystals. On the other hand, long-range effects of the electrostatic attractive forces of the crystals do a sizeable contribution to the total cohesive energy of bulk crystals.

Figure 4.5: Cohesive energy (kJ/mol) vs $i^{-1/3}$. Above dots represent Zn_iSe_i clusters, and below dots Zn_iTe_i ones.

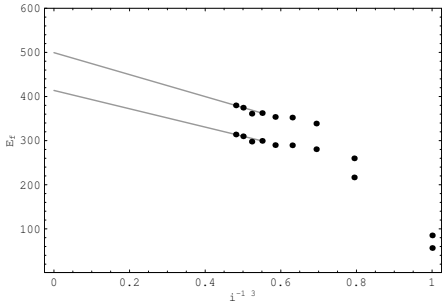

4.4 Conclusions

The lowest energy minima of the clusters Zn_iSe_i and Zn_iTe_i. studied in the present work, have been found to undergo a ring-to-three-dimensional structural transition. This behavior parallels that of the previously investigated Zn_iS_i clusters (chapter 2), but differs markly from that of Zn_iO_i clusters (chapter 3).

The structural transition allued to above, arises from a delicate balance between two opposite tendencies. On the one hand rings are favored by the tendency to linearity of the X-Zn-X bonds and, on the other hand, three-dimensional structures are favored by the tendency of achieving higher coordination. Our calculations indicate that the former dominates when the higher coordination does not carry to much of strain for the bond angles. This takes place at $i = 6$ for Zn_iX_i, with X=S,Se,Te and at $i = 6$ for X=O. Naturally, the smaller size of the oxygen valence orbitals accounts for its transition occurring at higher cluster sizes.

The predicted structures of the lowest energy three-dimensional spheroid structures of Zn_iX_i, X=Se,Te, can be envisioned as being built of smaller basic building units, namely, the Zn_2X_2 rombi and Zn_3X_3 hexagons. These structures appear to be the basic structural units for larger cluster in the same sense that C_5 pentagons and C_6 hexagons constitute the basic structural units of fullerenes.

Chapter 5

Large Spheroid Clusters of II-VI Materials: Zn_iX_i, X=O, S, Se, Te, $i = 12, 15$

Abstract

In this chapter Zn_iX_i, X=O, S, Se, Te, $i = 12, 15$ spheroid structures are characterized. These structures are built by smaller building blocks, namely squares and hexagons, as were smaller spheroid clusters characterized in previous chapters. The study of the cohesive energy of these species shows a trend towards bulk values. Moreover, since the cohesive energy may be taken as an indicator of the stability, our work shows that $Zn_{12}X_{12}$ spheroids are the most stable ones according to this criterium. The most spheric fullerene, C_{60}, is also the most stable one, and this is a behavior observed in II-VI clusters as well, since $Zn_{12}X_{12}$ structures are the most spheric ones. Therefore, one can picture a relationship between the sphericity and the stability, at least in a qualitatively way.

Table 5.1: Structural characteristics of spheroid carbon clusters and II-VI clusters

	C_{20}	C_{32}	C_{50}	C_{60}	C_{70}	C_{84}
Hexagons	0	6	15	20	25	32
Pentagons	12	12	12	12	12	12
	Zn_4X_4	Zn_6X_6	Zn_8X_8	Zn_9X_9		
Hexagons	0	2	4	5		
Rombi	6	6	6	6		

5.1 Introduction

Recent expectacular growth of nanotechnology agrees with the predictions of some of the pioneers in the field, such as Arthur von Hippel [28] and K. Eric Drexler [29, 30]. Revolutionary techniques such as the atomic force microscope (AFM), and the scanning tunneling microscope (STM) have been developed. These techniques allow the interaction with individual atoms, which is a remarkable step forward for the development of new materials and systems. Henceforth, new nanocompounds that could be useful in a more broad way than their bulk counterparts might be created. One of the best known 'new' clusters or nanostructures are the so called fullerenes, carbon spheroid structures discovered in 1985 [42].

Fullerenes are built by pentagons and hexagons. As the cluster size increases the number of hexagons also increases, one per two added carbon atoms, while the number of pentagons remains constant. Thus, the smallest spheroid C_{20} is formed by twelve pentagons. Adding more carbon atoms C_{22}, formed by 12 pentagons and 1 hexagon, C_{24}, 12 pentagons and two hexagons, and so on are obtained. The most spheric and most stable fullerene is C_{60}, which is formed by 12 pentagons and 20 hexagons, similar to a football ball, while larger fullerenes loose systematically the sphericity, and consequently stability. Related structures characterized for Zn_iX_i, $i = 1-9$, X=O, S, Se, Te, have been presented previously in this thesis. Spheroid structures were found to be the global minima for $i \geq 6$ in the case of X=S, Se, Te, and $i \geq 8$ for X=O. These spheroids are built by squares and hexagons. The number of squares remains constant, six, while the number of hexagons augments by one for every ZnX unit added, that is, two atoms. So, similar structural tendencies are observed in both carbon fullerenes and II-VI spheroids, as may be observed in Table 5.1.

According to the structural tendencies observed in Table 5.1, one could imagine larger structures that are built by hexagons and squares as well. Concretely, in [177], $Zn_{12}O_{12}$ and $Zn_{15}O_{15}$ structures built by 8 hexagons and 6 rombi and 11 hexagons and 6 rombi, respectively, were studied. In the present study two different aspects have been analyzed. On the one hand we have characterized these spheroid structures for Zn_iX_i, $i = 12, 15$, X=O,S,Se,Te, and then have studied their electronic properties. Additionally an extensive study of the stability of all clusters, $i = 1 - 9, 12, 15$ has been performed. All the calculations

have been performed at the B3LYP level of theory, combined with the SKBJ relativistic pseudopotentials.

5.2 Method

All geometries were fully optimized using the hybrid [109] Becke 3 Lee-Yang-Parr (B3LYP) gradient-corrected approximate density-functional procedure [99, 110, 111]. Harmonic vibrational frequencies were determined by analytical differentiation of gradients.

The relativistic compact effective core potentials and shared-exponent basis set [133] of Stevens, Krauss, Basch and Jasien (SKBJ) was used as the basic basis set in this study. The d electrons of Zn were included in the valence. An extra d function was added on Zn, O, and S, and two extra d and one f on both Se and Te, as described in Chapters 2,3 and 4, respectively, due to their importance for the proper description of the high coordination of the atoms in the three-dimensional cluster structures. The exponents of all of these added functions were energy optimized using the GAMESS US [165] package. Note that pure angular momentum functions were used throughout this study. We denote the final basis set used as SKBJ(d) for Zn_iX_i, X=O, S, and SKBJ(d/2df) for X=Se, Te.

All the geometry optimizations and frequency calculations were carried out with the GAUSSIAN98 [163] package.

5.3 Results

In this section the obtained results are presented and discussed. In section 5.3.1 the structures of Zn_iX_i, $i = 12, 15$, X=O, S, Se, Te, clusters are presented, along with several electronic and structural properties. Besides, an extensive discussion on the cohesive energy of these structures along with the cohesive energies of smaller clusters is performed.

5.3.1 Characterized structures of Zn_iX_i, $i = 12, 15$, X=O, S, Se, Te, clusters

The Zn_iX_i, $i = 1-9$, X=O, S, Se, Te, clusters have been presented in previous chapters. There we show that spheroid clusters were preferred for large systems, and henceforth only spheroid clusters have been considered for $i = 12, 15$. These spheroids are shown in Figure 5.1 for $i = 12$ and Figure 5.2 for $i = 15$. In Table 5.2 molecular geometries, energies and the symmetry of the structures are presented.

The four $Zn_{12}X_{12}$ structures belong to the D_{2h} symmetry point group, and are built by Zn_2X_2 and Zn_3X_3 units, as were smaller spheroids. Moreover, the number of squares is the same as smaller cases, being six, and the number of

Figure 5.1: characterized structures of $Zn_{12}X_{12}$, X=0,S,Se and Te respectively.

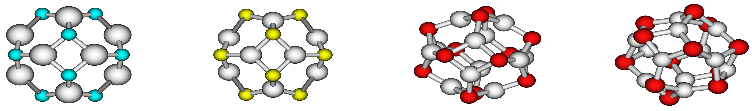

Figure 5.2: characterized structures of $Zn_{15}X_{15}$, X=0,S,Se and Te respectively.

hexagons is eight. The way these building blocks are linked is similar in the four cases. Rombi are positionated in the top, bottom, front, back, left and right, and are linked by the hexagons, four in the upper half and four in the lower half. The bond lengths and bond angles are similar to the smaller spheroids (see previous chapters).

The $Zn_{15}X_{15}$ structures belong to the C_{3h} symmetry point group. Again, these structures are built by hexagons and squares. One hexagon is located at the top of the structure and another one in the bottom, both being linked to three rombi. These two parts of the structure are bonded by the remaining nine hexagons. The bond lengths and bond angles are similar to the $Zn_{12}X_{12}$ structures and the smaller spheroids.

Table 5.2: Zn-X bond lengths (Å), X-Zn-X angles (degrees), symmetry groups, and cohesive energies (kJ/mol) of structures of Figure 1 and 2.

	R (Zn-X)	α (X-Zn-X)	Symmetry	Cohes. E.
$Zn_{12}O_{12}$	1.87-1.96	90.9-127.5	D_{2h}	512.65
$Zn_{12}S_{12}$	2.27-2.35	97.7-130.1	D_{2h}	438.16
$Zn_{12}Se_{12}$	2.39-2.48	98.9-130.6	D_{2h}	395.78
$Zn_{12}Te_{12}$	2.61-2.68	100.8-129.6	D_{2h}	322.82
$Zn_{15}O_{15}$	1.90-1.97	91.2-131.4	C_{3h}	519.65
$Zn_{15}S_{15}$	2.26-2.36	97.6-130.4	C_{3h}	440.91
$Zn_{15}Se_{15}$	2.38-2.48	98.9-131.9	C_{3h}	397.55
$Zn_{15}Te_{15}$	2.60-2.68	100.5-130.6	C_{3h}	324.17

Table 5.3: Experimental and theoretical cohesive energies of Zn_iX_i materials, in kJ/mol.

	Theoretical	Experimental
Zn_iO_i	718.7	727.6
Zn_iS_i	556.1	611.1
Zn_iSe_i	505.2	518.0
Zn_iTe_i	398.4	487.6

Figure 5.3: Cohesive energy (kJ/mol) vs the inverse of the cubic root of the ZnX units $\left(i^{1/3}\right)$.

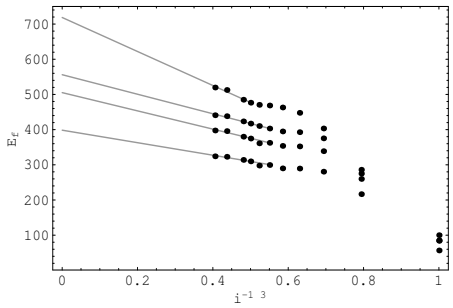

Cohesive energy

The cohesive energy per ZnX unit is calculated as $E_f = (iE_{Zn} + iE_X - E_{Zn_iX_i})/i$, where i is the number of ZnX units. When the cohesive energy is plotted versus the inverse of the cubic root of i, a straight line can be fitted to the obtained points. Extrapolating to $i^{-1/3}$=0, that is, to i =∞, or the bulk, the theoretical value obtained for the cohesive energy can be compared to the experimental one.

We have previously shown that the representative points are those corresponding to three dimensional structures. Four points are therefore available for Zn_iO_i, six for Zn_iS_i, and five for Zn_iSe_i and Zn_iTe_i.

The cohesive energies of the Zn_iX_i predicted global minima are plotted vs $i^{-1/3}$ in Figure 5.3. The extrapolated theoretical values are given in Table 5.3 along with the experimental data, which have been calculated according to the CODATA data [191], by the next equation:

$$E_{f,exp} = \left|\Delta H_f^o(ZnX) - \Delta H_f^o(Zn) - \Delta H_f^o(X)\right| - RT$$

Therefore, our predicted values represent the 98.8% for Zn_iO_i, the 91.0% for Zn_iS_i, the 97.5% for Zn_iSe_i and the 81.2% for Zn_iTe_i. Nevertheless, it is worth mentioning that no enthalpy of formation was found for Zn_iTe_i in the

CODATA data, and this value was taken from [192]. The provided Zn_iTe_i enthalpy of formation is surprisingly similar to that of Zn_iSe_i as provided by CODATA. According to the trend provided by our calculations we believe that this experimental estimate requires further verification. This might account for the poorer prediction of the Zn_iTe_i cohesive energy.

As expected, the extrapolated E_f are smaller than the bulk values. Recall that the coordination number in the clusters is three, whereas it is four in the bulk crystals. On the other hand, long-range effects of the electrostatic attractive forces of the crystals do a sizeable contribution to the total cohesive energy of bulk crystals.

The cohesive energy may be also interpreted as a measurement of the stability of a system. In Figure 5.3 it can be seen that in all cases $Zn_{12}X_{12}$ points lie above the line. Likewise, Zn_7X_7 points lie below. This situation might be interpreted in the following way: $Zn_{12}X_{12}$ are the most stable spheroids. Nevertheless, in order to asses this point further analysis are needed.

5.4 Conclusions

Zn_iX_i, X=O S, Se, Te, $i = 12 - 15$ spheroid structures have been found to be built by Zn_2X_2 and Zn_3X_3 rings, squares and hexagons, respectively. This structural characteristic was previously found for smaller spheroids. The number of squares remains constant in all structures, 6, while the number of hexagons increases by one as the number of ZnX unit increases by one as well. In this way Zn_4X_4 spheroids are the smallest ones, having 6 squares and 0 hexagons. Zn_6X_6 structures have 2 hexagons, Zn_8X_8 structures 4, Zn_9X_9 structures 5, $Zn_{12}X_{12}$ structures 8 and $Zn_{15}X_{15}$ structures 11. A related trend is found in carbon fullerenes as well. They are built by pentagons and hexagons. The number of pentagons remains constant (6), while the number of hexagons increases by one when two C atoms are added.

The analysis of the cohesive energies of these combinations show that even with such small clusters a very accurate prediction of the bulk values are achieved, 98.8%, 91.0%, 97.5% and 81.2% for Zn_iO_i, Zn_iS_i, Zn_iSe_i and Zn_iTe_i, respectively. The cohesive energy also gives a first insight into the relative stability of these clusters, and predict that $Zn_{12}X_{12}$ structures are the most stable ones. These $Zn_{12}X_{12}$ structures are the most spherical ones, similar to C_{60} in the case of fullerenes. This points forward to a relationship between the stability and the sphericity in cluster physics, which awaits theoretical rationalization.

Part II

Electronic excitation energies

Chapter 6

Electronic Excitation Energies of Small Zn_iS_i Clusters: Method comparison

Abstract

In Chapter 2 the global minima of small Zn_iS_i clusters, $i = 1 - 9$, were characterized. In order to calculate the excitation energies of these clusters basically two methods are available: Configuration Interaction Singles (CIS) and Time Dependent Density Functional Theory (TDDFT). Calculations of the excitation energies of small $Zn_iS_i^{GM}$ clusters, $i = 1 - 3$, have been performed with both methods, in an attempt to find the most appropriate one. The relativistic compact effective core potentials and shared-exponent basis set of Stevens, Krauss, Basch and Jasien (SKBJ), systematically enlarged with extra functions, was used along this work. These basis sets were combined with both methods. In this way the most appropriate method/basis set combination was chosen, for further excitation energy calculations on larger $Zn_iS_i^{GM}$ clusters. The chosen combination has been TDDFT/SKBJ(1sp2d2f). Due to the fact that no experimental data are available, some results confirming the TDDFT ones are necessary, ensuring in this way that our choice is the correct one. Multi Reference Configuration Interaction (MR-CI) calculations combined with a triple-ζ double polarization (TZ2P) basis set were carried out These results were clearly in agreement with the TDDFT results, and confirm our previous choice.

6.1 Introduction

Interest in II-VI compound semiconductors has grown spectacularly in recent years due to their paramount technological potential.

The band gaps of these compounds make them specially interesting for photovoltaic solar cells. The sun irradiates the most of the energy within the visible range. This region of the electromagnetic spectrum is very narrow, from 1.75 to 3 eV. Therefore, a good material for its use in photovoltaic solar cells must have band gaps close to the energies given above. In addition to this property, the solar cell must have an n-type semiconductor and a p-type semiconductor in order to obtain a potential difference between the two materials, which is necessary to produce electricity. The II-VI compound semiconductors have these properties. The band gaps go from 1.45 eV for CdTe to 3.66 eV for ZnS, and all these compounds present either p or n-type semiconduction [13]. Therefore these materials are ideal for solar cells.

Nowadays all the II-VI based solar cells are composed of bulk systems, which basically have one absorbing band gap. Nevertheless, the fact that cluster and nanoparticle characterization is becoming technologically possible opens new possibilities. Cluster properties change as size increases, and henceforth different-sized clusters should have different excitation energies. Combined together in an hypothetic cluster-based solar cell, the efficiency of it could increase considerably.

Theoretically the excitation energies may be accurately calculated at the Complete Active Space Second Order Perturbation [91, 92] (CASPT2) level of theory. However, the large amount of electrons of the systems under study makes impossible the use of it. Henceforth less sophisticate methods have to be considered. The Configuration Interaction Single (CIS) method and recently developed Time Dependent Density Functional Theory (TDDFT) method have been considered. The later one has been claimed to yield more accurate results [124, 193]. However, it has been seen that Rydberg states are not calculated accurately [130].

Our goal is to find the most proper method in order to calculate the excitation energies of $Zn_iS_i^{GM}$, $i = 1 - 9$, characterized previously in Chapter 2 ([185]). For that purpose CIS and TDDFT calculations have been performed for $i = 1 - 3$, using the SKBJ basis set, to which extra sp, d and f functions were systematically added in order to find the most proper basis. Unfortunately, in dealing with such compounds which have not been experimentally characterized has a clear drawback: the no availability of experimental data. Hence, it is difficult to perform a proper comparison between both methods. In order to dispel the uncertainties that may arise about this choice, Multi Reference Configuration Interaction (MR-CI) calculations have been performed. These results will be used as a confirmation of our previous choice.

Table 6.1: Extra functions added to the SKBJ basis.

	Zn			S		
	α	d	d	α	d	d
sp	0.017900	1.00	1.00	0.033139	0.21652	0.30748
sp	0.005967	1.00	1.00	0.01104	0.21652	0.30748
sp	0.001989	1.00	1.00	0.00368	0.21652	0.30748
d	0.3264	1.00		0.7	1.00	
d	0.1088	1.00		0.2333	1.00	
d	0.03627	1.00		0.07777	1.00	
d	0.01209	1.00		0.02592	1.00	
f	3.1109	1.00		0.55	1.00	
f	1.037	1.00		0.1833	1.00	
f	0.3457	1.00		0.0611	1.00	
f	0.1152	1.00		0.02037	1.00	

6.2 Methods

Two methods have been tested in order to find the most accurate one in order to calculate the excitation energies of small Zn_iS_i global minima, $i = 1-3$. On one hand the CIS [**?**] and on the other the TDDFT [131, 119, 132].

In order to perform the TDDFT calculations the hybrid Becke-style one parameter functional using modified Perdew-Wang exchange and Perdew-Wang 91 correlation (MPW1PW91) [195] was used. This combination was seen to provide the best results [124], along with the Becke3 [109] Perdew86 [196] functional B3P86. Both CIS and TDDFT calculations were performed with the relativistic compact effective core potentials and shared-exponent basis set [133] of Stevens, Krauss, Basch and Jasien (SKBJ). The Zn d electrons were treated as valence electrons. In order to analyze the influence of the basis set size on the calculated excitation energies, extra functions were systematically added to SKBJ to a maximum of extra 3sp4d4f functions. The exponents are given in Table 6.1. These larger basis sets are labeled according to the number of added functions. Thus, as an example, the largest one is denoted SKBJ(3sp4d4f).

CIS and TDDFT calculations were carried out with the GAUSSIAN94 [162] and GAUSSIAN98 [163] packages.

Previously, the fact that unfortunately no experimental data are available for these compounds has been mentioned. In order to obtain some "confirmation" values ensuring that our choice is correct, Multireference Configuration Interaction (MR-CI) calculations were carried out with the PSI [197] program package. The all electron triple-ζ double polarization (TZ2P) basis set (14s11p6d2f/10s8p3d2f) for Zn [166, 167, 168] and (13s10p2d1f/6s5p2d1f) for S [169, 170] was used, except for Zn_3S_3. In the case of Zn_3S_3 no polarization functions were used, due to the fact that the basis set limit in PSI, 255 functions, was exceeded.

Table 6.2: CIS results for $Zn_1S_1^{GM}$. ΔE: excitation energy (eV).

	$^1\Pi$	$^1\Sigma$	$^3\Pi$	$^3\Sigma$
SKBJ +	ΔE	ΔE	ΔE	ΔE
-	1.1361	3.8757	0.5344	1.3347
1d	1.1410	3.8914	0.4932	1.4064
1sp1d	1.1564	3.8821	0.5142	1.4207
2sp1d	1.1573	3.8834	0.5154	1.4211
2d	1.1260	3.8970	0.4818	1.4106
3d	1.1328	3.9022	0.4916	1.4119
1sp2d	1.1389	3.8906	0.5002	1.4244
1sp3d	1.1394	3.8903	0.5027	1.4234
2sp2d	1.1398	3.8915	0.5014	1.4246
2sp3d	1.1403	3.8906	0.5034	1.4240
1f	1.1942	3.8925	0.5401	1.4122
1sp1f	1.2090	3.8827	0.5603	1.4271
1sp2d1f	1.1966	3.8934	0.5493	1.4304
1sp3d1f	1.1974	3.8931	0.5516	1.4307
2sp1f	1.2099	3.8839	0.5614	1.4276
2sp2d1f	1.1975	3.8941	0.5504	1.4307
2sp3d1f	1.1982	3.8934	0.5512	1.4313
2sp3d2f	1.2397	3.8949	0.5991	1.4908
2sp3d3f	1.2557	3.8980	0.6165	1.5083
3sp4d4f	1.2576	3.8985	0.6186	1.5107

6.3 Results and discussion

The results of this study have been divided in three parts, hoping that in this way it will be more understandable for the reader. In section 5.3.1 the CIS results are analyzed and in section 5.3.2 the TDDFT results. In both sections the basis set size effect is analyzed. Finally, in section 5.3.3 the MR-CI values are shown and compared to the previously obtained CIS and TDDFT results. In this way, the best behaved method/basis set combination is chosen, which will be further used to calculate the excitation energies of larger Zn_iS_i clusters.

6.3.1 CIS results

In this section the CIS excitation energies for $Zn_iS_i^{GM}$, $i = 1 - 3$, are presented. This method is combined with the SKBJ effective core potential, and extra functions are systematically added to SKBJ in order to find the most appropriate combination. Only the results of $Zn_1S_1^{GM}$ are fully discussed, since the conclusions are similar for the rest.

In Table 6.2 the CIS excitation energies from the $^1\Sigma$ ground state of $Zn_1S_1^{GM}$ are shown. For the sake of brevity, we will focus the discussion into the calculated

Table 6.3: CIS results for $Zn_2S_2^{GM}$. ΔE : excitation energy (eV).

	$^1B_{2g}$	$^1B_{1u}$	^1A_u	$^3B_{2g}$	$^3B_{1u}$	^3A_u
SKBJ +	ΔE	ΔE	ΔE	ΔE	ΔE	ΔE
1d	3.3668	4.0397	4.1394	3.1271	3.2631	3.5060
1sp1d	3.3627	4.0299	4.1329	3.1262	3.2659	3.5084
1sp2d	3.3604	4.0823	4.1339	3.1059	3.3158	3.5098
1sp3d	3.3645	4.0843	4.1361	3.1072	3.3169	3.5091
2sp1d	3.3650	4.0240	4.1349	3.1276	3.2667	3.5088
2sp2d	3.3613	4.0825	4.1346	3.1061	3.3158	3.5101
2sp3d	3.3644	4.0842	4.1366	3.1062	3.3163	3.5084
1d1f	3.4117	4.0401	4.1816	3.1713	3.2613	3.5105
1d2f	3.4362	4.0701	4.2035	3.1942	3.2923	3.5325
1d3f	3.4495	4.0932	4.2145	3.2058	3.3101	3.5398
1sp1d1f	3.4064	4.0227	4.1742	3.1692	3.2643	3.5131
1sp1d2f	3.4299	4.0533	4.1971	3.1915	3.2964	3.5369
1sp1d3f	3.4443	4.0792	4.2061	3.2046	3.3145	3.5447
2sp1d1f	3.4086	4.0239	4.1762	3.1705	3.2652	3.5135
2sp1d2f	3.4320	4.0548	4.1988	3.1929	3.2976	3.5376
2sp1d3f	3.4461	4.0804	4.2072	3.2060	3.3157	3.5457
1sp2d2f	3.4383	4.0976	4.2081	3.1827	3.3294	3.5385
2d3f	3.4460	4.1101	4.2193	3.1875	3.3296	3.5359
1sp2d3f	3.4491	4.1070	4.2178	3.1929	3.3383	3.5440
1sp2d1f	3.4098	4.0770	4.1808	3.1544	3.3083	3.5164
3d3f	3.4605	4.1204	4.2233	3.2019	3.3427	3.5463
1sp3d3f	3.4540	4.1117	4.2212	3.1960	3.3421	3.5468
2sp3d3f	3.4541	4.1120	4.2216	3.1954	3.3419	3.5466

excitation energies with different basis sets for the $^1\Pi$ excitation. Observe that the basis set size effect is similar in all states. The influence of extra sp, extra d and extra f functions is analyzed separately, a procedure used along all this work.

In order to study the influence of extra sp functions, the results of SKBJ(1d), SKBJ(1sp1d) and SKBJ(2sp1d) are compared, which are 1.1410 eV, 1.1564 eV and 1.1573 eV, respectively. It is seen that while the addition of an extra s and an extra p function to SKBJ(1d) changes the resulting excitation energies significantly, more s and p additions do not. The same behaviour was observed comparing the SKBJ(1sp2d1f) and SKBJ(2sp2d1f) results, i.e. 1.1966 eV and 1.1975 eV.

Analyzing the influence of extra d functions, from the SKBJ(2sp1d), SKBJ(2sp 2d) and SKBJ(2sp3d) results, 1.1573 eV, 1.1398 eV and 1.1403 eV, respectively, the need of at least two extra d functions is concluded. Similar conclusion is obtained comparing the SKBJ(1sp1d1f), SKBJ(1sp2d1f) and SKBJ(1sp3d1f) results, 1.2090 eV, 1.1966 eV and 1.1974 eV, respectively. A third extra d function does not change significantly the final result.

Table 6.4: CIS results for $Zn_3S_3^{GM}$. ΔE: excitation energy (eV).

	$^1E^{'}$	$^1E^{''}$	$^3E^{'}$	$^3E^{''}$
SKBJ +	ΔE	ΔE	ΔE	ΔE
1d	2.8602	2.8676	2.4687	2.5739
2d	2.8689	2.8438	2.4559	2.5426
3d	2.8857	2.8674	2.4725	2.5643
1sp1d	2.8693	2.8816	2.4808	2.5877
2sp1d	2.8702	2.8834	2.4817	2.5892
1sp2d	2.8835	2.8625	2.4727	2.5601
2sp2d	2.8840	2.8633	2.4732	2.5607
1d1f	2.9132	2.9387	2.5206	2.6439
1d2f	2.9735	2.9988	2.4559	2.5426
1d3f	-	-	-	-

The largest jump in the ΔE is produced by the addition of extra f functions. Comparing the results of SKBJ(2sp3d), SKBJ(2sp3d1f), SKBJ(2sp3d2f), SKBJ (2sp3d3f) and SKBJ(3sp4d4f)), which are 1.1403 eV, 1.1982 eV, 1.2397 eV, 1.2557 eV and 1.2576 eV, respectively, we conclude that at least three extra f functions are needed. From these CIS results, for the $Zn_1S_1^{GM}$ structure the SKBJ(1sp2d3f) basis set appears to be the best choice.

Similar analysis may be performed for the excitation energies of $Zn_2S_2^{GM}$, of D_{2h} symmetry and ^1A_g ground state, given in Table 6.3.

It may be seen that again SKBJ(1sp2d3f) seems to be the smallest proper basis.

The CIS excitation energies for $Zn_3S_3^{GM}$, of D_{3h} symmetry and $^1A_1^{'}$ ground state, are given in Table 6.4.

There it can be viewed that the SKBJ basis only was enlarged by a maximum of two f functions. This was due to the fact that the addition of a third one required too large disc space. Hence, it was not possible to perform an analysis as in the previous cases.

These results show the importance of including polarization functions in the basis set. Although it is too large even for $Zn_3S_3^{GM}$, SKBJ(1sp2d3f) basis set has been seen to be the smallest proper basis to be combined to CIS in order to calculate reliable excitation energies. Nevertheless, this combination can not be used for larger clusters, and therefore does not seem to be a practical choice.

6.3.2 TDDFT results

In this section the calculated TDDFT excitation energies for $Zn_iS_i^{GM}$, $i = 1-3$, are shown. As in the CIS case, the SKBJ effective core potential systematically enlarged in order to find the most proper basis set. Similarly to the CIS case, only the $Zn_1S_1^{GM}$ case is fully discussed.

Table 6.5: TDDFT results for $Zn_1S_1^{GM}$. ΔE : excitation energy (eV).

	$^1\Pi$	$^1\Sigma$	$^3\Pi$	$^3\Sigma$
SKBJ +	ΔE	ΔE	ΔE	ΔE
1d	0.7633	3.9933	-0.3156	1.8412
1sp1d	0.7687	3.9782	-0.3068	1.8457
2sp1d	0.7685	3.9777	-0.3068	1.8448
1sp2d	0.7414	3.9808	-0.3244	1.8296
2sp2d	0.7416	3.9803	-0.3243	1.8292
1sp3d	0.7393	3.9775	-0.3247	1.8226
2sp3d	0.7394	3.9770	-0.3247	1.8226
1d1f	0.8051	3.9795	-0.3188	1.8204
1d2f	0.8203	3.9646	-0.3095	1.8438
1sp1d1f	0.8094	3.9649	-0.3098	1.8253
1sp2d1f	0.7844	3.9678	-0.3302	1.8092
1sp1d2f	0.8243	3.9506	-0.2997	1.8510
1sp2d2f	0.8061	3.9560	-0.3159	1.8384
2sp3d3f	0.8135	3.9537	-0.3130	1.8409
3sp4d4f	0.8135	3.9536	-0.3128	1.8400

In Table 6.5 the TDDFT excitation energies of $Zn_1S_1^{GM}$ are shown.

It may be observed that the addition of extra functions to the SKBJ basis changes significantly the final result. As in the CIS case, we follow a step by step method. First the influence of extra sp is studied, then the influence of extra d and finally the influence of extra f functions.

An extra sp function seems to be not very important for the $^1\Pi$ state, as SKBJ(1d) yields an excitation energy of 0.7633 eV and SKBJ(1sp1d) 0.7687 eV. Nevertheless, for the $^1\Sigma$ state it is, notice that the SKBJ(1d) energy is 3.9933 eV and the SKBJ(1sp1d) 3.9782 eV. The influence of a second extra sp function, on the other hand, is small in all the cases. For instance, for the $^1\Pi$ state, SKBJ(1sp1d) and SKBJ(2sp1d) almost yield the same ΔE: 0.7687 eV and 0.7685 eV, respectively. One extra sp function seems a good choice at this point. At least two extra d functions are needed, as follows from the results of SKBJ(1sp1d), SKBJ(1sp2d) and SKBJ(1sp3d), which are 0.7687 eV, 0.7414 eV and 0.7393 eV, respectively. The results obtained adding two and three extra d functions do not differ significantly. Two extra f functions have been seen to be necessary as well. For the $^1\Pi$ state we focus now on the SKBJ(1sp2d), SKBJ(1sp2d1f) and SKBJ(1sp2d2f) excitation energies, 0.7414 eV, 0.7844 eV and 0.8061 eV, respectively. This last value still diverges considerably from the one with only one extra f function. However, comparing it to the SKBJ(2sp3d3f), which is 0.8135 eV, it is seen that a third one is not necessary. This value is also found for a larger basis set. The difference between SKBJ(1sp2d2f) and SKBJ(2sp3d3f) is small enough that we can choose this first basis as a proper one to combine with TDDFT, saving in this way CPU usage. It should be also pointed out the negative excitation energy calculated

Table 6.6: TDDFT results for $Zn_2S_2^{GM}$. ΔE: excitation energy (eV).

	$^1B_{2g}$	$^1B_{1u}$	$^1B_{3u}$	$^3B_{2g}$	$^3B_{1u}$	^3A_u
SKBJ +	ΔE	ΔE	ΔE	ΔE	ΔE	ΔE
1d	2.0627	2.8697	2.9279	1.8958	2.2998	2.5978
1sp1d	2.0651	2.8654	2.9274	1.8997	2.3031	2.5992
2sp1d	2.0655	2.8654	2.9275	1.8999	2.3030	2.5997
1sp2d	2.0597	2.8898	2.9081	1.8863	2.3287	2.5863
2sp2d	2.0596	2.8891	2.9079	1.8863	2.3278	2.5867
1sp3d	2.0612	2.8877	2.9086	1.8878	2.3264	2.5887
2sp3d	2.0611	2.8876	2.9086	1.8873	2.3260	2.5889
1d1f	2.1036	2.8674	2.9662	1.9363	2.2936	2.6285
1d2f	2.1215	2.8845	2.9817	1.9540	2.3109	-
1sp1d1f	2.1048	2.8633	2.9647	1.9391	2.2973	2.6287
1sp1d2f	2.1225	2.8813	2.9801	1.9566	2.3159	2.6462
1sp2d1f	2.1035	2.8845	2.9482	1.9300	2.3182	2.6177
1sp2d2f	2.1251	2.8978	2.9669	1.9521	2.3295	2.6388
2sp3d3f	2.1296	2.8928	2.9691	1.9559	2.3226	2.6448
3sp4d4f	2.1332	2.8963	2.9723	1.9594	2.3259	2.6463

for the $^3\Pi$ state.

Of course, one should think that maybe the proper basis for $Zn_1S_1^{GM}$ is not for larger clusters. Following the results for $Zn_2S_2^{GM}$ are studied, which are given in Table 6.6.

Having a look to this table, one may observe that the smallest basis yielding good values is SKBJ(1sp2d2f).

The $Zn_3S_3^{GM}$ data, given in Table 6.7, also shows SKBJ(1sp2d2f) basis set as the smallest one yielding good results. These calculations were performed with C_{2v} symmetry, $^1A_1$ ground state, for better comparison with MR-CI results.

It seems logical then to choose this SKBJ(1sp2d2f) for further calculations. It is seen, as happened for CIS, that the inclusion of more than one polarization functions in the basis set is indispensable. For TDDFT, two polarization functions are enough, and three for CIS.

6.3.3 MR-CI results

Already we have obtained results with both CIS and TDDFT, and have found a proper basis to combine with each one. However, the no availability of experimental data makes one uncertain about the accuracy of these calculations. In order to check the suitability of CIS/SKBJ(1sp2d3f) or TDDFT/SKBJ(1sp2d2f), MR-CI/TZ2P calculations were performed, and the obtained results were used as reference values.

Table 6.7: TDDFT results for $Zn_3S_3^{GM}$. ΔE: excitation energy (eV).

	$^1B_1$	$^1A_2$	$^1B_1$	$^3B_1$	$^3A_2$	$^3B_1$
	ΔE	ΔE	ΔE	ΔE	ΔE	ΔE
1d	3.6054	3.6056	4.3346	3.4464	3.4467	4.0456
1sp1d	3.5996	3.5997	4.3279	3.4406	3.4408	4.0385
2sp1d	3.5995	3.5997	4.3277	3.4403	3.4406	4.0382
1sp2d	3.5502	3.5503	4.2747	3.3859	3.3861	3.9868
2sp2d	3.5503	3.5504	4.2748	3.3859	3.3861	3.9870
2sp3d	3.5535	3.5536	4.2774	3.3866	3.3868	3.9867
1d1f	3.6409	3.6410	4.3688	3.4813	3.4815	4.0792
1d2f	3.6423	3.6424	4.3705	3.4818	3.4820	4.0809
1sp1d1f	3.6338	3.6339	4.3610	3.4742	3.4744	4.0711
1sp1d2f	3.6343	3.6345	4.3618	3.4740	3.4742	4.0722
1sp2d1f	3.5873	3.5874	4.3099	3.4225	3.4227	4.0219
1sp2d2f	3.5969	3.5970	4.3205	3.4320	3.4022	4.0325
2sp3d3f	3.6017	3.6018	4.3273	3.4339	3.4341	4.03 54

The MR-CI calculations were carried out with the PSI program package, as mentioned earlier. This program makes use of the molecular point group and the corresponding irreducible representations. Nevertheless, one of the drawbacks is that the largest available symmetry is D_{2h}. Therefore, in the cases of $Zn_1S_1^{GM}$ and $Zn_3S_3^{GM}$, belonging to the $C_{\infty v}$ and D_{3h}, respectively, lower symmetries must be used. For $Zn_1S_1^{GM}$ $^1\Sigma$ states C_{2v} symmetry was used, and for the $^1\Pi$ state C_2, as will be explained further. $Zn_3S_3^{GM}$ calculations were carried out with the C_{2v} symmetry, as the TDDFT calculations. Two electron excitations were allowed in the MR part, and in the configuration interaction as well, resulting in final CISD(TQ) calculations.

In Table 6.8 MR-CI results are shown for $Zn_1S_1^{GM}$. The energy of the $^1\Sigma$ states, both the ground state and the excited state, were calculated with 461 determinants in the valence reference, and 217013 determinants in the CISD, with C_{2v} symmetry. The $^1\Pi$ excited state energy was calculated with 524 determinants as reference for the 221666 determinants of the CISD, with C_2 symmetry. The obtained MR-CI excitation energies for the $^1\Pi$ and the $^1\Sigma$ states are 0.7562 eV and 3.9221 eV, respectively. These results are in agreement with the TDDFT/SKBJ(1sp2d2f) energies, i. e. 0.8061 eV and 3.9560 eV.

The excitation energy of the $^1\Pi$ state was calculated with C_{2v} symmetry at the beginning. The obtained ΔE was close to that of CIS, 1.13 eV. With C_{2v} symmetry there were two degenerate states, a B_1 and a B_2 states, that due to the fact that they belong to different irreducible representations they do not mix. That is, this excitation is treated as a single excitation. If this is correct, calculations with C_2 symmetry should be similar. We have seen that they are not. If the calculation is performed with C_2 symmetry, both B_1 and B_2 states in C_{2v} belong to the B irreducible representation. In this way they mix and the excitation is correctly described as a double excitation. CIS method is

Table 6.8: MR-CI results for $Zn_1S_1^{GM}$ different electronic states. N_{MR} indicates the number of reference determinants and N_{CI} the number of determinants used in the CI part of the calculation. The obtained MR-CI energy in Hartrees, and the MR-CI, CIS and TDDFT excitation energies in eV.

	$^1\Sigma$ (g.s.)	$^1\Pi$ (e.s.)	$^1\Sigma$ (e.s.)
N_{MR}	461	524	461
N_{CI}	217013	221666	217013
E (MR-CI)	-2175.418042	-2175.390274	-2175.273990
ΔE (MR-CI)	-	0.7562	3.9221
ΔE (CIS/SKBJ(3sp4d4f))	-	1.2576	3.8985
ΔE (TDDFT/SKBJ(1sp2d2f))	-	0.8061	3.9560

Table 6.9: MR-CI results for $Zn_2S_2^{GM}$ different electronic states. N_{MR} indicates the number of reference determinants and N_{CI} the number of determinants used in the CI part of the calculation. The obtained MR-CI energy in Hartrees, and the MR-CI, CIS and TDDFT excitation energies in eV.

	^1A_g	$^1B_{2g}$	$^1B_{1u}$
N_{MR}	905	1598	1596
N_{CI}	281382	773112	772023
E (MR-CI)	-4350.814847	-4350.733628	-4350.692521
ΔE (MR-CI)	-	2.211	3.284
ΔE (CIS/SKBJ(1sp2d3f))	-	3.4491	4.1070
ΔE (TDDFT/SKBJ(1sp2d2f))	-	2.1251	2.8978

not able to describe these excitations, since only single excitations are taken into account. On the other hand TDDFT method describes these excitations correctly. At this point the use of TDDFT method seems logical in further calculations.

In Table 6.9 the obtained MR-CI results for $Zn_2S_2^{GM}$ are given, and are compared to the CIS and TDDFT results.

The ^1A_g state energy was calculated using 905 determinants as reference, and the CISD calculation made use of 281382 determinants. The energy of $^1B_{2g}$ was calculated with 1598 determinants in the reference and 773112 determinants in the CISD, similarly to $^1B_{1u}$ state, 1596 determinants in the reference and 772023 in the CISD level. The calculated excitation energies again are in more agreement with the TDDFT/SKBJ(1sp2d2f) method. The ΔE (MR-CI) $^1B_{2g}$ excitation energy, 2.211 eV, is very close to that obtained at the TDDFT/SKBJ(1sp2d2f) level, which is 2.1251 eV. However, the $^1B_{1u}$ excitation energy is not so accurately calculated, 3.284 eV at MR-CI level and 2.8978

Table 6.10: MR-CI results for $Zn_3S_3^{GM}$ different electronic states. N_{MR} indicates the number of reference determinants and N_{CI} the number of determinants used in the CI part of the calculation. The obtained MR-CI energy in Hartrees, and the MR-CI, CIS and TDDFT excitation energies in eV. In parenthesis the states corresponding to the CIS D_{3h} calculations.

	$^1A_1$	$^1B_1$ ($^1E'$)	$^1B_1$ ($^1E''$)
N_{MR}	121	115	115
N_{CI}	141337	191195	191195
E (MR-CI)	-6526.144962	-6525.983187	-6525.953076
ΔE (MR-CI)	-	4.4046	5.2245
ΔE (CIS/SKBJ(1d2f)	-	2.9735	2.9988
ΔE (TDDFT/SKBJ(1sp2d2f))	-	3.5969	4.3205

at the TDDFT level. Again CIS result is further, 4.1070 eV.

In Table 6.10 the $Zn_3S_3^{GM}$ MR-CI results may be seen.

The symmetry of $Zn_3S_3^{GM}$ was reduced from D_{3h} to C_{2v}, as explained before. The $^1E'$ state found in the CIS D_{3h} calculations splits into the near degenerate $^1B_1$ and $^1A_2$ states found in the C_{2v} calculations. The remaining $^1B_1$ state corresponds to the $^1E''$ state. No polarization functions were added to the TZ basis set. This was due to the fact that the limit of 255 functions was exceeded. One may think that the obtained results will not be very accurate, but nevertheless could be very useful to compare qualitatively to the CIS and TDDFT results. It may be seen that the MR results are a bit far from the TDDFT results, but are even further from the CIS results. In addition to this, the energy difference between the two $^1B_1$ excited states are very similar in both MR and TDDFT, 0.8199 eV and 0.7236 eV, respectively, which compare well and lends further support to the TDDFT calculations.

These results show that TDDFT is more appropriate than CIS in order to perform this type of calculations. It describes better both single and double excitations. Therefore, for further calculations of the excitation energies of $Zn_iS_i^{GM}$ clusters TDDFT/SKBJ(1sp2d2f) is chosen.

6.4 Conclusions

It has been seen that both CIS and TDDFT methods need basis sets with more than one polarization functions. SKBJ(1sp2d2f) was seen to be the smallest basis yielding converged results with TDDFT, and SKBJ(1sp2d3f) with CIS. Nevertheless, this basis was too large to be used even for $Zn_3S_3^{GM}$, so it appeared to be a bad choice for further calculations.

The MR-CI results used as reference show a clear advantage of TDDFT method. It describes sensible better than CIS the two-fold degenerate $^1\Pi$ excitation

in $Zn_1S_1^{GM}$ and also appears to be superior for the rest of the studied excitation in all the clusters investigated. Therefore, for further calculations TDDFT/SKBJ(1sp 2d2f) combination is recommended.

Chapter 7

Electronic Excitation Energies of $Zn_iS_i^{GM}$ Clusters

Abstract

Time Dependent Density Functional Theory (TDDFT) excitation energies are calculated for $Zn_iS_i^{GM}$ clusters, $i = 1-9$. The geometry of the global minima is ring like for $i = 1-5$ and three dimensional spheroids for $i = 6-9$. In general, the calculated excitations happen from non-bonding p orbitals of sulfur. These orbitals are perpendicular to the molecular plane in the case of the rings, and normal to the spheroid surface for 3D clusters. The calculated excitation energies are larger for ring like clusters as compared to 3D ones, with the excitation energies of the latter structures lying close to the visible spectrum. The difference between Kohn-Sham eigenvalues of the orbitals involved in the electronic excitations studied have also been compared with the TDDFT results for two approximate density functionals, *i.e.*: MPW1PW91 and B3LYP, being the latter more accurate. The B3LYP excitation energies calculated as the difference between Kohn-Sham eigenvalues of the orbitals involved in the excitation have been found to be only 0.30-0.40 eV too high for the smaller 3D like clusters and to decrease as the cluster size increases. Therefore, this might be a practical approach to estimate exctitation energies of large $Zn_iS_i^{GM}$ clusters.

7.1 Introduction

The end of the 20th century has seen an spectacular growth of the interest in II-VI compound allows. Semiconduction arises from the existence of no nule band gaps that may be gained getting energy from the environment. One manner of achieving this is absorbing the energy of the photons that come from the sun. This is basically the physical fenomenum occurring in solar cells. The II-VI compound semiconductors fullfil the necessary requirements in order to be used in solar cells.

Since the recent development of nanotechnology, clusters and nanostructures have become interesting in themselves. They might be experimentally characterized, hence, they are not longer only a theoretical tool to study infinite systems. A neat example of this are the fullerenes, carbon spheroids discovered by R.F. Curl, R.E. Smalley and H.W. Kroto, which have also photovoltaic applications [52, 53].

In this paper a full investigation of the electronic excitation energies of $Zn_iS_i^{GM}$, $i = 1 - 9$, clusters as characterized in Chapter 2 is presented. For that purpose the method/basis set combination chosen in Chapter 6 is used. The motivation of this study is to calculate the absorption properties of these small clusters, in order to see if they are suitable for constructing higher efficient solar cells.

7.2 Method

The electronic excitation energies have been calculated with the Time Dependent Density Functional Theory (TDDFT) [131, 119, 132], as recommended in our previous analysis [199] of the excitation energies of small clusters. For the TDDFT calculations the hybrid Becke-style one parameter functional using modified Perdew-Wang exchange and Perdew-Wang 91 correlation (MPW1PW91) [195] was used.

The relativistic compact effective core potentials with shared-exponent basis set [133] of Stevens, Krauss, Basch and Jasien (SKBJ) was used as the starting basis set. We demonstrated previously [199] that polarization and diffusion functions were needed in order to yield accurate results, and showed that the SKBJ(1sp2d2f) basis, where there were added one s and p, two d and two f functions, was the ideal one for an accurate though affordable calculation of the electronic excitation energies of small $Zn_iS_i^{GM}$ clusters. Nevertheless, the size of the basis set makes the calculation of the excitation energies of large clusters prohibitive. Henceforth, the smaller SKBJ(d) basis set was chosen for these larger clusters. All the exponents of the expanded SKBJ basis are the same as used in Chaper 5 ([199]).

All the calculations were carried out with the GAUSSIAN98 [163] package.

Table 7.1: Valence configuration of the clusters of Group 1, $Zn_iS_i^{GM}$, $i = 1-5$.

i	Val. Conf.	LUMO
1	$2\delta^2\,4\sigma^2\,5\sigma^2\,5\pi^4$	6σ
2	$5b_{2u}^2\,3b_{3g}^2\,3b_{3u}^2\,4b_{1u}^2\,2b_{2g}^2$	$7a_g$
3	$14a_1^2\,12b_2^2\,6b_1^2\,5a_2^2\,7b_1^2$	$15a_1$
4	$4b_{2g}^2\,3a_{2u}^2\,7e_g^2\,8e_g^2\,2b_{1u}^2$	$7a_{1g}$
5	$33a'^2\,29a''^2\,34a'^2\,35a'^2\,30a''^2$	$36a'$

7.3 Results and Discussion

In Chapter 2 ([185]) it was concluded that the global minima of small Zn_iS_i, $i = 1-5$, clusters were ring structures while the global minima for larger clusters, $i = 6-9$, were three dimensional spheroids. Ring like structures will constitute our Group 1 and the three dimensional structures Group 2, in an attempt to present the results in a more understandable way.

For clusters of Group 1 the previously mentioned SKBJ(1sp2d2f) basis was used. However, as mentioned in the previous section, for clusters of Group 2 this basis is too large. Henceforth, the smaller SKBJ(d) basis set was chosen for these larger clusters. However, for the clusters of Group 1 we have obtained the electronic excitation energies with both SKBJ(d) and SKBJ(1sp2d2f) basis sets. This allows us to asses the performance of the smaller basis set and consequently to highlight the limitations of the SKBJ(d) basis set with respect to SKBJ(1sp2d2f).

7.3.1 TD-DFT excitation energies of $Zn_iS_i^{GM}$, $i = 1-9$

Group 1

In Table 7.1 the valence configuration and LUMO orbital symmetry of the clusters of Group 1, namely Zn_iS_i, $i = 1-5$, depicted in Figure 2.1, are given. Table 7.2 collects the SKBJ(d) and SKBJ(1sp2d2f) excitation energies and oscillator strengths for the mentioned clusters.

The lowest excitation of $Zn_1S_1^{GM}$ occurs when an electron is excited from the HOMO to the LUMO, yielding a $^1\Pi$ excited state. This transition needs 0.81 eV to happen, and has a small oscillator strength, $f = 0.002$. The other calculated transition involves the $^1\Sigma$ ground state and an excited state of the same symmetry. Now the electron is excited from the inner 5σ orbital to the LUMO. The excitation energy is 3.96 eV, 3.15 eV larger than the $^1\Sigma \rightarrow ^1\Pi$ excitation, but the oscillator strength is one order of magnitude larger.

The excitation of an electron from the HOMO to the LUMO is dipole forbidden in $Zn_2S_2^{GM}$, as shown in Table 7.2. The lowest energy allowed excitation

Table 7.2: SKBJ(d) and SKBJ(1sp2d2f) excitation energies (eV) and oscillator strengths of small $Zn_iS_i^{GM}$, $i = 1-5$. $\Delta(\Delta E)$ is the difference between SKBJ(1sp2d2f) ΔE and SKBJ(d) ΔE. Similarly for Δf.

	Transition		SKBJ(1sp2d2f)		SKBJ(1d)			
i	orbitals	states	ΔE	f	ΔE	f	$\Delta(\Delta E)$	Δf
1	$5\pi \rightarrow 6\sigma$	$^1\Sigma \rightarrow^1 \Pi$	0.81	0.002	0.76	0.001	0.05	0.001
	$5\sigma \rightarrow 6\sigma$	$^1\Sigma \rightarrow^1 \Sigma$	3.96	0.062	3.99	0.060	0.03	0.002
2	$2b_{2g} \rightarrow 7a_g$	$^1A_g \rightarrow^1 B_{2g}$	2.13	forbidden	2.06	forbidden	0.07	-
	$4b_{1u} \rightarrow 7a_g$	$^1A_g \rightarrow^1 B_{1u}$	2.90	0.015	2.87	0.014	0.03	0.001
	$3b_{3u} \rightarrow 7a_g$	$^1A_g \rightarrow^1 B_{3u}$	2.97	0.020	2.93	0.015	0.04	0.005
3	$7b_1 \rightarrow 15a_1$	$^1A_1 \rightarrow^1 B_1$	3.60	forbidden	3.61	forbidden	0.01	-
	$5a_2 \rightarrow 15a_1$	$^1A_1 \rightarrow^1 A_2$	3.60	forbidden	3.61	forbidden	0.01	-
	$6b_1 \rightarrow 15a_1$	$^1A_1 \rightarrow^1 B_1$	4.32	0.038	4.33	0.042	0.01	0.004
4	$2b_{1u} \rightarrow 7a_{1g}$	$^1A_{1g} \rightarrow^1 B_{1u}$	3.74	forbidden	3.72	forbidden	0.02	-
	$3a_{2u} \rightarrow 7a_{1g}$	$^1A_{1g} \rightarrow^1 A_{2u}$	4.66	0.005	4.65	0.011	0.01	0.006
	$3a_{2u} \rightarrow 8a_{1g}$	$^1A_{1g} \rightarrow^1 A_{2u}$	4.92	0.088	4.95	0.096	0.03	0.008
5	$30a'' \rightarrow 36a'$	$^1A' \rightarrow^1 A''$	4.01	0.001	3.97	0.001	0.04	-
	$35a' \rightarrow 36a'$	$^1A' \rightarrow^1 A'$	4.21	0.001	4.18	0.001	0.03	-
	$30a'' \rightarrow 37a'$	$^1A' \rightarrow^1 A''$	4.39	0.001	4.39	0.007	0	0.006

happens when an electron is excited from the $4b_{1u}$ orbital to the LUMO, resulting in a $^1B_{1u}$ excited state. This transition absorbs 2.90 eV and the oscillator strength is $f = 0.015$. The second allowed excitation occurs exciting an electron from the $3b_{3u}$ orbital to the LUMO. This transition needs 2.97 eV, and $f = 0.020$, a bit larger than the previous one. These two excitation energies lie within the range of the visible spectrum.

Two dipole forbidden transitions have been reported for $Zn_3S_3^{GM}$. The only allowed transition calculated occurs exciting an electron from the $6b_1$ orbital to the LUMO, yielding a $^1B_1$ state. The excitation energy is 4.32 eV, and $f = 0.038$. This excitation energy is larger than the allowed excitation energies of $Zn_2S_2^{GM}$, and lies within the UV spectrum.

The two calculated $^1A_{1g} \rightarrow^1 A_{2u}$ transitions are allowed for $Zn_4S_4^{GM}$. The electron is excited from the $3a_{2u}$ orbital to the LUMO in one case, being the excitation energy 4.66 eV and the oscillator strength 0.005. The other transition is likely to be more intense, since the oscillator strength is much larger, 0.088, and the excitation energy is only 0.26 eV larger. In this last transition the electron is excited from the $3a_{2u}$ orbital to the second virtual orbital, $8a_{1g}$.

Finally, three dipole allowed transitions of $Zn_5S_5^{GM}$ are collected in Table 7.2. The first one occurs when an electron from the HOMO is excited to the LUMO. The resulting excited state has $^1A''$ electronic structure. The excitation energy is 4.01 eV, and the oscillator strength 0.001. Exciting an electron from the $35a'$

Table 7.3: Valence configuration of the clusters of Group 2, $Zn_iS_i^{GM}$, $i = 6-9$.

i	Val. Conf.	LUMO
6	$21a_g^2\,16b_g^2\,22b_u^2\,22a_g^2\,17b_g^2$	$33a_g$
7	$38a''^2\,39a''^2\,50a'^2\,51a'^2\,40a''^2$	$52a'$
8	$50b^2\,51a^2\,52a^2\,51b^2\,52b^2$	$53a$
9	$50a''^2\,51a''^2\,64a'^2\,65a'^2\,66a'^2$	$67a'$

orbital to the LUMO needs 4.21 eV, and the oscillator strength is 0.001. The resulting excited state has $^1A'$ electronic structure. Finally, the last calculated transition is $^1A' \rightarrow^1 A''$. Now, the electron is excited from the HOMO to the second virtual orbital, $37a'$. The oscillator strength of this excitation is similar to the previous ones, 0.001. The excitation energy is 4.39 eV, which lies in the ultraviolet but close to the visible spectrum.

SKBJ(d) vs. SKBJ(1sp2d2f)

In Table 7.2 both the SKBJ(d) and SKBJ(1sp2d2f) excitation energies and oscillator strengths are given. Besides, the differences between them may also be viewed there. Having a look to these differences, one may observe that they are not very large. The largest difference in the excitation energy is 0.07 eV for the $^1A_g \rightarrow^1 B_{2g}$ transition in $Zn_2S_2^{GM}$, which represents only 3% of the total excitation energy. Nevertheless, most of the differences are smaller than 0.04 eV, which are less than 1% of the total excitation energies. Therefore, the SKBJ(d) results for the clusters of Group 2 are expected to be reasonably accurate.

Group 2

In Table 7.3 the valence configuration and LUMO orbital symmetry of the clusters of Group 2, namely Zn_iS_i, $i = 6-9$, depicted in Figure 2.3, are given. Table 7.4 collects the SKBJ(d) and SKBJ(1sp2d2f) excitation energies and oscillator strengths for the mentioned clusters.

In Table 8.4 three excitations are shown for $Zn_6S_6^{GM}$. Two of them are dipole forbidden, and the only predicted to be dipole allowed occurs from the ground state to the ^1B_u excited state, where an electron from the inner $22b_u$ orbital is excited to the LUMO. The excitation energy of 3.60 eV lies nearby the visible spectrum, and the oscillator strength is 0.029.

For $Zn_7S_7^{GM}$, three transitions are given in Table 8.4. The two transitions with smallest excitation energies occur from the $^1A'$ ground state to $^1A''$ excited states. In one case an electron from the HOMO is excited to the LUMO, being the excitation energy 3.10 eV, and in the other case the electron is excited

Table 7.4: SKBJ(d) excitation energies (eV) and oscillator strengths of small $Zn_iS_i^{GM}$, $i = 6 - 9$.

	Transition		SKBJ(d)	
i	orbitals	states	ΔE	f
6	$17b_g \rightarrow 33a_g$	$^1A_g \rightarrow ^1B_g$	3.37	forbidden
	$22a_g \rightarrow 33a_g$	$^1A_g \rightarrow ^1A_g$	3.37	forbidden
	$22b_u \rightarrow 33a_g$	$^1A_g \rightarrow ^1B_u$	3.60	0.029
7	$40a'' \rightarrow 52a'$	$^1A' \rightarrow ^1A''$	3.10	0.000
	$40a'' \rightarrow 53a'$	$^1A' \rightarrow ^1A''$	3.27	0.000
	$51a' \rightarrow 52a'$	$^1A' \rightarrow ^1A'$	3.53	0.004
8	$52b \rightarrow 53a$	$^1A \rightarrow ^1B$	3.65	0.009
	$51b \rightarrow 53a$	$^1A \rightarrow ^1B$	3.65	0.009
	$51a \rightarrow 53a$	$^1A \rightarrow ^1A$	3.94	forbidden
9	$66a' \rightarrow 67a'$	$^1A' \rightarrow ^1A'$	3.77	forbidden
	$65a' \rightarrow 67a'$	$^1A' \rightarrow ^1A'$	4.05	0.023
	$64a' \rightarrow 67a'$	$^1A' \rightarrow ^1A'$	4.05	0.023
	$62a' \rightarrow 67a'$	$^1A' \rightarrow ^1A'$	4.40	0.034
	$61a' \rightarrow 67a'$	$^1A' \rightarrow ^1A'$	4.40	0.034

to the second virtual orbital, $53a'$. The excitation energy in this case is 3.27 eV. In both cases the oscillator strength is very small, 0.0001. The transition with larger oscillator strength, 0.004, occurs exciting an electron from the $51a'$ orbital to the LUMO. The excitation energy of this transition is 3.53 eV.

$Zn_8S_8^{GM}$ has two dipole allowed transitions and one dipole forbidden transition. The two allowed ones end up in ^1B excited states, and are near degenerate. The excitation, therefore, consists of promoting one electron from either of the near degenerate $52b$ or the $51b$ orbital into the LUMO. Its excitation energy is 3.65 eV and the oscillator strength is 0.009. Exciting an electron from the inner $51a$ orbital to the LUMO another excitation is obtained which ends up in the ^1A excited state. Its energy is 3.94 eV, but the transition is not dipole allowed.

Finally, for $Zn_9S_9^{GM}$, two groups of degenerate excitations with large oscillator strengths have been predicted. In one group the exctitation energies are 4.05 eV, and the oscillator strength 0.023. These transitions occur when an electron is excited from the $65a'$ orbital and from the $64a'$ orbital to the LUMO, respectively. In the other group the excitation energies are 4.40 eV, electrons being excited from the $62a'$ orbital and from the $61a'$ orbital to the LUMO, respectively. The oscillator strength of both transitions is 0.034. When the electron is excited from the HOMO to the LUMO the excitation energy is 3.77 eV, but the oscillator strength is zero. All these five excitations happen from the $^1A'$ ground state to various of the $^1A'$ excited states.

Group 1 vs. Group 2

The excitation energies of the clusters of Group 1 are larger than those of Group 2. The basic main structural difference between Groups 1 and 2 is that structures in Group 1 are rings, whereas the structures of Group 2 are three dimensional spheroids. However, in all cases the excitations happen from orbitals that are non-bonding p-type of the sulfur. This agrees with the bulk's behaviour, for its highest occupied band is the p band associated to sulfur atoms.

From the photovoltaic viewpoint the excitation energies of spheroid clusters are the most interesting ones, since they lie closer to the visible spectrum. The ring structures have excitation energies larger than 4 eV, except $i = 1, 2$, which make them not very promising for photovoltaic applications. The smallest excitation energies of the spheroid clusters are lower than 4 eV. This is an interesting feature since the use of these spheroidal clusters in some hypothetical cluster based solids might increase the efficiency of the cell. We call for additional experimental investigation of the optical absorption properties of these clusters.

7.3.2 Excitation energies calculated as Kohn-Sham eigenvalue differences

The problem of the reliability of virtual orbitals within DFT is a topic of great controversy [101, 103, 200]. Are the energies of these virtual orbitals reliable enough in order to calculate excitation energies via Koopman's theorem? It has been recently demonstrated that working with an exact exchange-correlation functional the calculated excitation energies using the Kohn-Sham orbital energies are very reliable [201]. Nevertheless, in real problems one does not use exact but approximate exchange-correlation functionals. In this section we estimate the excitation energies using the Kohn-Sham eigenvalues, with B3LYP and MPW1PW91 approximate exchange correlation functionals. Those functionals were chosen because of their great usability. In particular B3LYP is becoming a standard for geometry optimizations and MPW1PW91 is one of the most employed approximate exchange-correlation functionals for the calculation of electronic excitation energies. Results are shown in Table 7.5.

A quick glance to Table 7.5 reveals that B3LYP orbital energy differences (D2 column) performed remarkably better than MPW1PWP91 differences (D1 column), as compared to the TDDFT excitation energies. It is also observed that as the cluster size increases both orbital energy differences get closer to their corresponding TDDFT predicted excitation energy value. Notice that the B3LYP orbital energy differences do it faster.

Further inspection of Table 7.5 shows that the B3LYP orbital energy differences for ring like (Group 1) clusters are always greater that 1 eV. However, for the 3D spheroidal (Group 2) clusters these differences are always less than 1 eV. Notice that for the largest cluster studied, $Zn_9S_9^{GM}$ the deviation of the orbital energy differences with respect to the TDDFT excitation energy is less than 0.4 eV, which represents less than 10% of the total excitation energy. Hence,

Table 7.5: Excitation energies calculated with TDDFT ($\Delta E(1)$), MPW1PW91 Kohn-Sham HOMO LUMO differences ($\Delta E(2)$) and B3LYP Kohn-Sham HOMO LUMO differences ($\Delta E(3)$). D1 ($\Delta E(2) - \Delta E(1)$) and D2 ($\Delta E(3) - \Delta E(1)$) denote the differences between MPW1PW91 and B3LYP with respect to TDDFT, respectively. All energies are in eV.

i	Excitation	$\Delta E(1)$	$\Delta E(2)$	D1	$\Delta E(3)$	D2
1	$^1\Sigma \rightarrow ^1\Pi$	0.81	2.29	1.48	1.82	1.01
	$^1\Sigma \rightarrow ^1\Sigma$	3.96	4.75	0.79	4.36	0.40
2	$^1A_g \rightarrow ^1B_{2g}$	2.13	3.37	1.24	2.78	0.65
	$^1A_g \rightarrow ^1B_{1u}$	2.90	3.95	1.05	3.40	0.50
	$^1A_g \rightarrow ^1B_{3u}$	2.97	4.20	1.23	3.61	0.64
3	$^1A_1 \rightarrow ^1B_1$	3.60	4.75	1.15	4.21	0.61
	$^1A_1 \rightarrow ^1A_2$	3.60	4.75	1.15	4.21	0.61
	$^1A_1 \rightarrow ^1B_1$	4.32	5.49	1.17	4.94	0.62
4	$^1A_{1g} \rightarrow ^1B_1$	3.74	4.88	1.14	4.48	0.74
	$^1A_{1g} \rightarrow ^1A_{2u}$	4.66	5.83	1.17	5.42	0.76
	$^1A_{1g} \rightarrow ^1A_{2u}$	4.92	6.01	1.09	5.48	0.56
5	$^1A' \rightarrow ^1A''$	4.01	5.07	1.06	4.59	0.58
	$^1A' \rightarrow ^1A'$	4.21	5.26	1.05	4.78	0.57
	$^1A' \rightarrow ^1A''$	4.39	5.49	1.10	5.01	0.62
6	$^1A_g \rightarrow ^1B_g$	3.37	4.33	0.96	3.87	0.50
	$^1A_g \rightarrow ^1A_g$	3.37	4.34	0.97	3.87	0.50
	$^1A_g \rightarrow ^1B_u$	3.60	4.51	0.91	4.04	0.44
7	$^1A' \rightarrow ^1A''$	3.10	3.85	0.75	3.34	0.24
	$^1A' \rightarrow ^1A''$	3.27	4.29	1.02	3.96	0.69
	$^1A' \rightarrow ^1A'$	3.53	4.30	0.77	3.79	0.26
8	$^1A \rightarrow ^1B$	3.66	4.56	0.90	4.04	0.38
	$^1A \rightarrow ^1B$	3.65	4.56	0.91	4.04	0.39
	$^1A \rightarrow ^1A$	3.94	4.82	0.88	4.35	0.41
9	$^1A' \rightarrow ^1A'$	3.77	4.65	0.88	4.13	0.36
	$^1A' \rightarrow ^1A'$	4.05	4.90	0.85	4.38	0.33
	$^1A' \rightarrow ^1A'$	4.40	5.26	0.86	4.72	0.32

it is concluded that the B3LYP orbital energy differences perform reasonably well to estimate the excitation energies from the Koopman theorem.

According to this statement, the excitation energies of $Zn_{12}S_{12}$ and $Zn_{15}S_{15}$, characterized in Chapter 5, may be estimated. The HOMO-LUMO differences in both cases are 4.48 eV and 4.34 eV for $i = 12$ and $i = 15$, respectively. Nevertheless, in view of the error made in smaller cases, one may thing that the energy differences will be around 4 eV, similar to that of $Zn_9S_9^{GM}$. However, no oscillation strength may be stimated, and there is no way to state whether these transitions are dipole allowed or not. Therefore, some calculations that could confirm these estimations and could provide oscillator strengths are still to be done.

7.4 Conclusions

TDDFT calculations yield interesting results for the excitation energies of $Zn_iS_i^{GM}$ clusters. Ring like structure clusters, $i = 2 - 5$ have larger excitation energies than three dimensional spheroidal clusters, $i \geq 6$. However, for both type of clusters the excitation occur from non bonding p type orbitals of sulfur. Recall that for the two crystal structures of bulk ZnS, wurtzite and zincblende, the highest occupied band is also associated with the non bonding p type orbitals of the sulfur atoms.

The predicted electronic excitation energies of the spheroidal clusters lie near the range of the visible spectrum, and in some cases are smaller than the bulk one. Therefore, those clusters constitute promising materials for its use in photovoltaic solar cells.

The difference between the B3LYP Kohn-Sham energies of the orbitals involved in the sought electronic excitation appears to be a reliable practical approach to the calculation of the electronic excitation energies for larger clusters, where TDDFT calculations become prohibitive. This approach has been found to yield better results as the cluster size increases. Nevertheless, its most salient drawback is that no oscillator strengths are obtained.

Chapter 8

Electronic Excitation Energies of $Zn_iO_i^{GM}$ Clusters

Abstract

Time-dependent density-functional theory (TDDFT) is used to study the excitation energies of previously characterized global minima of small Zn_iO_i clusters, $i = 1 - 9$. The relativistic compact effective core potentials and shared-exponent basis set of Stevens, Krauss, Basch and Jasien (SKBJ), systematically enlarged with extra functions, was used along this work. In general, the calculated excitations happen from non-bonding p orbitals of oxygen. These orbitals are perpendicular to the molecular plane in the case of the rings, and normal to the spheroid surface for 3D clusters. The calculated excitation energies are larger for ring like clusters as compared to 3D ones, with the excitation energies of the latter structures lying close to the visible spectrum. The difference between Kohn-Sham eigenvalues of the orbitals involved in the electronic excitations studied have also been compared with the TDDFT results of the corresponding excitations for two approximate density functionals, *i.e.*: MPW1PW91 and B3LYP, being the later more accurate. Moreover, they approach to the TDDFT value as the cluster size increases. Therefore, this might be a practical approach to estimate excitation energies of large Zn_iO_i clusters.

8.1 Introduction

Computer revolution and other technological devices have been and are in rapid development basically due to improved semiconductor materials. Some of these materials are the II-VI compounds, which interest has increased notably due to their paramount technological potential.

Many theoretical studies have been reported concerning the bulk electronic structure of these compound semiconductors [141, 142, 143, 144, 145, 146, 147, 148]. However, for many practical applications these materials are ensemble as layered stacks of different chemical composition. Recently, it has been pointed out that the boundaries between layers are not as sharp as previously assumed. Chemical reactions at the interface can cause an ultrathin layer of a new material to form. The characterization of the structures formed at the interface has revealed to be critical to understand how these layered materials work at the microscopic level [202]. Clusters of elements coming from adjacent layers are likely structures to be found at the interfaces. Hence, learning more on the structures and properties of the clusters could yield important information to develop more efficient devices.

The fact that cluster and nanoparticle characterization is becoming technologically possible opens new possibilities in the development of materials which could improve the efficiency of the cells. One of the best known 'new' clusters or nanostructures are the so called fullerenes, carbon spheroid structures discovered in 1985 [42].

Our goal is to calculate the excitation energies of $Zn_iO_i^{GM}$, $i = 1 - 9$, characterized previously in Chapter 3 ([187]). As C_{60} has very different properties compared to diamond and graphite, Zn_iO_i clusters have very different properties compared to the bulk system. Therefore the study of the Zn_iO_i clusters can provide new insight in the physics of these materials, and can be compared to the Zn_iS_i cluster excitatin energies.

8.2 Methods

The relativistic compact effective core potentials with shared-exponent basis set [133] of Stevens, Krauss, Basch and Jasien (SKBJ) was used as the starting basis set. We demonstrated previously [199] that polarization and diffusion functions were needed in order to yield accurate results, and showed that the SKBJ(1sp2d2f) basis, where there were added one s and p, two d and two f functions, was the ideal one for an accurate though affordable calculation of the electronic excitation energies of $Zn_iS_i^{GM}$ clusters. Nevertheless, the size of the basis set makes the calculation of the excitation energies of large clusters prohibitive. Henceforth, the smaller SKBJ(d) basis set was chosen for these larger clusters.

All the calculations were carried out with the GAUSSIAN98 [163] package.

TDDFT [131, 119, 132] calculations have been performed to calculate the excitation energies of $Zn_iO_i^{GM}$, in which the hybrid Becke-style one parameter

Table 8.1: Extra functions added to the SKBJ basis.

	Zn			O		
	α	d	d	α	d	d
sp	0.017900	1.00	1.00	0.066667	0.28472	0.30727
sp	0.005967	1.00	1.00	0.022222	0.28472	0.30727
sp	0.001989	1.00	1.00	0.007407	0.28472	0.30727
d	0.3264	1.00		0.85	1.00	
d	0.1088	1.00		0.283333	1.00	
d	0.03627	1.00		0.094444	1.00	
d	0.01209	1.00		0.031481	1.00	
f	3.1109	1.00		0.6	1.00	
f	1.037	1.00		0.2	1.00	
f	0.3457	1.00		0.066667	1.00	
f	0.1152	1.00		0.022222	1.00	

functional using modified Perdew-Wang exchange and Perdew-Wang 91 correlation (MPW1PW91) [195] was used. This combination was seen to provide the best results [199], along with the Becke3 [109] Perdew86 [196] functional B3P86.

The relativistic compact effective core potentials and shared-exponent basis set [133] of Stevens, Krauss, Basch and Jasien (SKBJ) was used throughout this study, being the Zn d electrons treated as valence electrons. In order to analyze the influence of the basis set size on the calculated excitation energies, extra functions were systematically added to SKBJ to a maximum of extra 3sp4d4f functions. These functions were systematically generated dividing the exponent of the previous function by three. The final exponents are given in Table 8.1. These larger basis sets are labeled according to the number of added functions. Thus, as an example, the largest one is denoted SKBJ(3sp4d4f).

TDDFT calculations were carried out with the GAUSSIAN98 [163] package.

8.3 Results and discussion

In section 8.3.1 the basis set influence is discussed for small $Zn_iO_i^{GM}$ clusters, $i = 1-3$. In section 8.3.2 the obtained TDDFT excitation energies of $Zn_iO_i^{GM}$ clusters, $i = 1-9$ are fully discussed. Finally, in section 8.3.3, the reliability of the Kohn-Sham eigenvalues is discussed.

8.3.1 Basis set influence on the TDDFT excitation energies

In this section the calculated TDDFT excitation energies for $Zn_iO_i^{GM}$, $i = 1-3$, are shown. The SKBJ effective core potential systematically enlarged in order

Table 8.2: TDDFT results for $Zn_1O_1^{GM}$. ΔE : excitation energy (eV), and f the oscillator strength.

	$^1\Pi$		$^1\Sigma$	
SKBJ +	ΔE	f	ΔE	f
1d	0.7637	0.0020	3.8173	0.1007
2d	0.7592	0.0018	3.8227	0.1043
3d	0.7801	0.0017	3.8359	0.1130
1sp1d	0.7877	0.0019	3.8180	0.1129
2sp1d	0.7875	0.0019	3.8181	0.1135
1sp2d	0.7801	0.0018	3.8237	0.1126
2sp2d	0.7804	0.0018	3.8238	0.1128
1sp3d	0.7786	0.0018	3.8225	0.1128
2sp3d	0.7771	0.0018	3.8210	0.1128
1d1f	0.8181	0.0022	3.8000	0.0996
1sp1d1f	0.8396	0.0021	3.7999	0.1116
1sp2d1f	0.8351	0.0020	3.8033	0.1128
1sp3d1f	0.8339	0.0020	3.8025	0.1128
1sp2d2f	0.8629	0.0021	3.7928	0.1106
1sp2d3f	0.8719	0.0021	3.7972	0.1099
2sp1d1f	0.8394	0.0021	3.7999	0.1121
2sp1d2f	0.8671	0.0022	3.7887	0.1104
2sp1d3f	0.8805	0.0023	3.7957	0.1086
2sp2d1f	0.8352	0.0020	3.8033	0.1130
2sp2d2f	0.8630	0.0021	3.7926	0.1107
2sp2d3f	0.8718	0.0021	3.7963	0.1100
2sp3d1f	0.8328	0.0020	3.8011	0.1129
2sp3d2f	0.8618	0.0021	3.7924	0.1107
2sp3d3f	0.8726	0.0021	3.7954	0.1097
3sp4d4f	0.8743	0.0021	3.7951	0.1098

to find the most proper basis set. Only the $Zn_1O_1^{GM}$ case is fully discussed, since the conclusions are similar for the rest.

In Table 8.2 the TDDFT excitation energies of $Zn_1O_1^{GM}$ are shown. In a rapid glance it may be observed that the addition of extra functions to the SKBJ basis changes significantly the final result. For the sake of brevity, we will focus the discussion on the calculated excitation energies with different basis sets for the $^1\Pi$ state. Observe that the basis-set size effect is similar in the $^1\Sigma$ state, and therefore only the small differences will be pointed out. The influence of extra sp, d and f functions is analyzed separately.

In order to study the influence of extra sp functions, the results of SKBJ(1d), SKBJ(1sp1d) and SKBJ(2sp1d) are compared, which are 0.7637 eV, 0.7877 eV and 0.7875 eV, respectively. It is seen that while the addition of an extra s and p functions to SKBJ(1d) changes the resulting excitation energy significantly, more s and p additions do not. The same behavior is observed comparing

Table 8.3: TDDFT results for $Zn_2O_2^{GM}$. ΔE : excitation energy (eV). f: the oscillator strength.

	$^1B_{1g}$		$^1B_{2u}$		$^1B_{3u}$	
SKBJ +	ΔE	f	ΔE	f	ΔE	f
1d	1.6979	0.0000	1.9192	0.0088	2.7118	0.0238
2d	1.7575	0.0000	1.9933	0.0089	2.7322	0.0221
3d	1.8092	0.0000	2.0265	0.0101	2.7688	0.0220
1sp1d	1.7987	0.0000	1.9879	0.0102	2.7716	0.0237
2sp1d	1.7988	0.0000	1.9880	0.0102	2.7715	0.0236
1sp2d	1.8100	0.0000	2.0267	0.0102	2.7636	0.0224
2sp2d	1.8102	0.0000	2.0266	0.0102	2.7639	0.0223
1sp3d	1.8138	0.0000	2.0260	0.0103	2.7679	0.0221
2sp3d	1.8131	0.0000	2.0244	0.0103	2.7671	0.0221
1sp1d1f	1.8535	0.0000	2.0055	0.0102	2.8244	0.0241
1sp2d1f	1.8737	0.0000	2.0410	0.0103	2.8235	0.0229
1sp2d2f	1.9061	0.0000	2.0743	0.0105	2.8517	0.0231
1sp2d3f	1.9166	0.0000	2.0791	0.0103	2.8587	0.0228
2sp2d2f	1.9061	0.0000	2.0741	0.0105	2.8517	0.0231
2sp2d3f	1.9167	0.0000	2.0792	0.0103	2.8588	0.0228
2sp3d3f	1.9182	0.0000	2.0808	0.0104	2.8606	0.0228
3sp4d4f	1.9205	0.0000	2.0828	0.0104	2.8638	0.0227

the SKBJ(1d1f), SKBJ(1sp1d1f) and SKBJ(2sp1d1f) results, i.e. 0.8181 eV, 0.8396 eV and 0.8394 eV, respectively. We henceforth conclude that one extra sp function seems a good choice at this point.

Analyzing the influence of extra d functions, it is seen that the addition of three extra d functions is not necessary, as follows from the results of SKBJ(1sp1d), SKBJ(1sp2d) and SKBJ(1sp3d), which are 0.7877 eV, 0.7801 eV and 0.7786 eV, respectively. The results obtained adding two and three extra d functions do not differ significantly, but they do in a considerable manner adding only one. Therefore, two d functions were added.

Three extra f functions have been seen to be necessary as well. For the $^1\Pi$ state we focus now on the SKBJ(2sp2d), SKBJ(2sp2d1f), SKBJ(2sp2d2f) and SKBJ(2sp2d3f) excitation energies, 0.7804 eV, 0.8352 eV, 0.8630 and 0.8718 eV, respectively. This last value still diverges considerably from the one with only two extra f functions. However, comparing it to the SKBJ(2sp3d3f) ΔE, which is 0.8726 eV, and to the SKBJ(2sp3d3f) ΔE, which is 0.8743, a convergence is achieved. Therefore, the differences between SKBJ(1sp1d3f) ΔE and SKBJ(1sp2d3f) ΔE with SKBJ(3sp4d4f) ΔE are small enough that we can choose one of these basis as a proper one to combine with TDDFT, saving in this way CPU usage.

Following the results for $Zn_2O_2^{GM}$ and $Zn_3O_3^{GM}$ are given in Table 8.3 and 8.4, respectively.

Table 8.4: TDDFT results for $Zn_3O_3^{GM}$. ΔE : excitation energy (eV). f: the oscillator strength.

	$^1A_2$		$^1B_1$		$^1B_1$	
SKBJ +	ΔE	f	ΔE	f	ΔE	f
1d	3.5782	0.0000	3.5793	0.0000	4.5588	0.0668
2d	3.6006	0.0000	3.6015	0.0000	4.5606	0.0615
3d	3.6232	0.0000	3.6242	0.0000	4.5794	0.0628
1sp1d	3.6170	0.0000	3.6180	0.0000	4.5771	0.0686
1sp2d	3.6109	0.0000	3.6118	0.0000	4.5633	0.0639
1sp3d	3.6140	0.0000	3.6149	0.0000	4.5687	0.0634
1sp2d1f	3.6570	0.0000	3.6578	0.0000	4.6115	0.0645
1sp2d2f	3.6642	0.0000	3.6650	0.0000	4.6197	0.0645
1sp2d3f	3.6697	0.0000	3.6704	0.0000	4.6246	0.0636
1sp3d2f	3.6655	0.0000	3.6663	0.0000	4.6208	0.0637
1sp3d3f	3.6708	0.0000	3.6715	0.0000	4.6261	0.0634
2sp2d2f	3.6642	0.0000	3.6650	0.0000	4.6197	0.0644
2sp2d3f	3.6700	0.0000	3.6707	0.0000	4.6249	0.0637
2sp3d3f	3.6713	0.0000	3.6721	0.0000	4.6267	0.0634

These data also shows SKBJ(1sp2d3f) basis set as the smallest one yielding good results.

It seems logical then to choose this SKBJ(1sp2d3f) for further calculations. It is seen that the inclusion of more than one polarization functions in the basis set is indispensable.

8.3.2 TDDFT Excitation energies of small $Zn_iO_i^{GM}$ clusters, $i = 1 - 9$.

We have concluded above that the MPW1PW91/SKBJ(1sp2d3f) level of theory is the addecuate one for an accurate though affordable calculation of the electronic excitation energies of small $Zn_iO_i^{GM}$ clusters. However, for clusters as big as $i = 6$ the size of the basis set makes the calculations prohibitive. Henceforth, the smaller SKBJ(d) basis set was chosen for these larger clusters. According to this statement, we have divided the clusters in two groups. In group 1 the excitation energies of $Zn_iO_i^{GM}$, $i = 1 - 5$ are discussed, and in group 2 the excitation energies of $Zn_iO_i^{GM}$, $i = 6 - 9$.

The range of the excitations we are interested in are those close to the visible spectrum, smaller than 5 eV. Since in some cases there may be many excitations within this range we have basically calculated the lowest lying three excitations. Nevertheless, in some cases more have been calculated due to the fact that dipole allowed transitions did not lie within that range.

Table 8.5: Valence configuration of the clusters of Group 1, $Zn_iO_i^{GM}$, $i = 1-5$.

i	Val. Conf.	LUMO
1	$2\delta^2\,4\sigma^2\,5\sigma^2\,5\pi^4$	6σ
2	$5b_{1u}^2\,3b_{3g}^2\,3b_{3u}^2\,2b_{1g}^2\,4b_{2u}^2$	$7a_g$
3	$6b_1^2\,15a_1^2\,12b_2^2\,5a_2^2\,7b_1^2$	$16a_1$
4	$18e_u^2\,7e_g^2\,8e_g^2\,4b_{2g}^2\,2b_{1u}^2$	$7a_{1g}$
5	$28a''^2\,34a'^2\,29a''^2\,30a''^2\,35a'^2$	$36a'$

Group 1: $Zn_iO_i^{GM}$ clusters, $i = 1-5$

For the small clusters we have obtained the electronic excitation energies with both SKBJ(d) and SKBJ(1sp2d3f) basis sets. This allows us to asses the performance of the smaller basis set and consequently to highlight the limitations of the SKBJ(d) basis set with respect to SKBJ(1sp2d3f).

In Table 8.5 the valence configuration and LUMO orbital symmetry of the clusters of Group 1, namely Zn_iO_i, $i = 1-5$, depicted in Chapter 3, are given. Table 8.6 collects the SKBJ(d) and SKBJ(1sp2d2f) excitation energies and oscillator strengths for the mentioned clusters.

Two different possible excitations for $Zn_1O_1^{GM}$ are shown. The lowest excitation occurs from the $^1\Sigma$ ground state to a $^1\Pi$ excited state, exciting an electron to the LUMO vacant orbital from the HOMO. This transition needs 0.87 eV to happen, and has a small oscillator strength ($f = 0.002$). The other calculated transition involves the $^1\Sigma$ ground state and an excited state of the same symmetry. Now the electron is excited from the inner 5σ orbital to the LUMO. The excitation energy is 3.80 eV, 2.93 eV larger than the $^1\Sigma \rightarrow ^1\Pi$ excitation, but the oscillator strength is two orders of magnitude larger.

Three excitations of $Zn_2O_2^{GM}$ have been calculated. The lowest excited state is dipole forbidden. The lowest-energy allowed excitation happens when an electron is excited from the HOMO $4b_{2u}$ orbital to the LUMO, resulting in a $^1B_{2u}$ excited state. This transition absorbs 2.08 eV and the oscillator strength is $f = 0.010$. The second allowed excitation occurs exciting an electron from the $3b_{3u}$ orbital to the LUMO. This transition needs 2.86 eV, and $f = 0.023$, a bit larger than the previous one. These two excitation energies lie within the range of the visible spectrum.

Three excitations have been calculated for $Zn_3O_3^{GM}$. The lowest transition excites an electron from the $5a_2$ orbital to the LUMO, but this is dipole forbidden, i.e. $f = 0$. Similarly, the transition to the lowest $^1B_1$ state is not allowed either. The only allowed transition calculated occurs exciting an electron from the $6b_1$ orbital to the LUMO, yielding a $^1B_1$ state. The excitation energy is 4.62 eV, and $f = 0.064$. This excitation energy is larger than the allowed excitation energies of $Zn_2O_2^{GM}$.

Table 8.6: SKBJ(d) and SKBJ(1sp2d2f) excitation energies (eV) and oscillator strengths of small $Zn_iO_i^{GM}$, $i = 1-5$. $\Delta(\Delta E)$ is the difference between SKBJ(1sp2d3f) ΔE and SKBJ(d) ΔE. Similarly for Δf.

	Transition		SKBJ(d)		SKBJ(1sp2d3f)			
i	orbitals	states	ΔE	f	ΔE	f	$\Delta(\Delta E)$	Δf
1	$5\pi \rightarrow 6\sigma$	$^1\Sigma \rightarrow^1 \Pi$	0.76	0.002	0.87	0.002	0.11	0
	$5\sigma \rightarrow 6\sigma$	$^1\Sigma \rightarrow^1 \Sigma$	3.82	0.101	3.80	0.110	0.02	0.009
2	$2b_{1g} \rightarrow 7a_g$	$^1A_g \rightarrow^1 B_{1g}$	1.70	forbidden	1.92	forbidden	0.22	-
	$4b_{2u} \rightarrow 7a_g$	$^1A_g \rightarrow^1 B_{2u}$	1.92	0.009	2.08	0.010	0.16	0.001
	$3b_{3u} \rightarrow 7a_g$	$^1A_g \rightarrow^1 B_{3u}$	2.71	0.024	2.86	0.023	0.15	0.001
3	$5a_2 \rightarrow 16a_1$	$^1A_1 \rightarrow^1 A_2$	3.58	forbidden	3.67	forbidden	0.09	-
	$7b_1 \rightarrow 16a_1$	$^1A_1 \rightarrow^1 B_1$	3.58	forbidden	3.67	forbidden	0.09	-
	$6b_1 \rightarrow 16a_1$	$^1A_1 \rightarrow^1 B_1$	4.56	0.067	4.62	0.064	0.06	0.003
4	$2b_{1u} \rightarrow 7a_{1g}$	$^1A_{1g} \rightarrow^1 B_{1u}$	3.78	forbidden	3.83	forbidden	0.05	-
	$3a_{2u} \rightarrow 7a_{1g}$	$^1A_{1g} \rightarrow^1 A_{2u}$	5.17	0.095	5.19	0.084	0.02	0.011
	$18e_u \rightarrow 7a_{1g}$	$^1A_{1g} \rightarrow^1 E_u$	5.24	0.111	5.24	0.110	0	0.001
5	$35a' \rightarrow 36a'$	$^1A' \rightarrow^1 A'$	4.00	forbidden	4.02	forbidden	0.02	-
	$32a' \rightarrow 36a'$	$^1A' \rightarrow^1 A'$	5.27	0.106	5.28	0.091	0.01	0.015
	$31a' \rightarrow 36a'$	$^1A' \rightarrow^1 A'$	5.60	0.164	5.57	0.157	0.03	0.007

For $Zn_4O_4^{GM}$ three excitations are reported. The excitation to the $^1B_{1u}$ state is not dipole allowed. However, the other calculated $^1A_{1g} \rightarrow^1 A_{2u}$ and $^1A_{1g} \rightarrow^1 E_u$ transitions are allowed. The electron is excited from the $3a_{2u}$ orbital to the LUMO in the first case, being the excitation energy 5.19 eV and the oscillator strength 0.084. The other transition is likely to be more intense, since the oscillator strength is much larger, 0.110, and the excitation energy is only 0.06 eV larger. In this last transition the electron is excited from the $18e_u$ orbital to the LUMO $7a_{1g}$.

Three transitions, two of them dipole allowed, are collected for $Zn_5O_5^{GM}$. One of the allowed transition occurs exciting an electron from the $32a'$ orbital to the LUMO, resulting in a $^1A'$ state, which needs 5.28 eV, and the oscillator strength is 0.091. The other allowed transition is a $^1A' \rightarrow^1 A''$ transition, .where the electron is excited from the $31a'$ orbital to the LUMO. The oscillator strength of this excitation is the largest calculated one, 0.157. The excitation energy is 5.57 eV, which lies in the ultraviolet spectrum.

SKBJ(1sp2d2f) vs SKBJ(d)

In Table 7.5 the SKBJ(d) and SKBJ(1sp2d2f) excitation energies and oscillator strengths are given. Besides, the differences between them may also be viewed there. Having a look to these differences, one may observe that although important for smaller clusters ($i = 1-3$), they are not very large for the rest.

Table 8.7: Valence configuration of the clusters of Group 2, $Zn_iO_i^{GM}$, $i = 6-9$.

i	Val. Conf.	LUMO
6	$53a'^2\,54a'^2\,22a''^2\,23a''^2\,24a''^2$	$55a'$
7	$43b^2\,44b^2\,45a^2\,46a^2\,45b^2$	$47a$
8 (GM)	$18a_1^2\,13b_1^2\,13b_2^2\,51e^2\,52e^2$	$19a_1$
8 (LM)	$50a^2\,51a^2\,52a^2\,51b^2\,52b^2$	$53a$
9	$50a''^2\,51a''^2\,64a'^4\,65a'^2$	$66a'$

The largest difference in the excitation energy is 0.22 eV for the $^1A_g \rightarrow ^1 B_{1g}$ transition in $Zn_2O_2^{GM}$, which represents more than 10% of the total excitation energy. Nevertheless, in the case of $Zn_3O_3^{GM}$, the differences are reduced to 3-4% of the total energy. This percentage is reduced to less than 1% for $Zn_5O_5^{GM}$. Therefore, the SKBJ(d) results for the clusters of Group 2 are expected to be reasonably accurate. These conclusion was also obtained in the case of the excitation energies of $Zn_iS_i^{GM}$, as seen in Chapter 6.

Group 2: $Zn_iO_i^{GM}$ clusters, $i = 6 - 9$

In Table 8.7 the valence configuration and LUMO orbital symmetry of the clusters of Group 2, namely Zn_iO_i, $i = 6-9$, depicted in Chapter 3, are given. Table 8.8 collects the SKBJ(d) and SKBJ(1sp2d2f) excitation energies and oscillator strengths for the mentioned clusters.

Three calculated excitations of $Zn_6O_6^{GM}$ are shown, two of them being dipole forbidden. The only calculated dipole allowed transition occurs from the ground state to other $^1A''$ excited state, where an electron from the inner $19a''$ orbital is excited to the LUMO. The excitation energy is 5.34 eV, and the oscillator strength is 0.136.

Three transitions of $Zn_7O_7^{GM}$, one of them dipole forbidden, have been calculated. The first allowed excitation occurs when the electron is excited from the $42a$ orbital to the LUMO. The excitation energy in this case is 4.69 eV, but has a very small oscillator strength, 0.0004. The transition with larger oscillator strength, 0.004, occurs exciting an electron from the inner $42b$ orbital to the LUMO. The excitation energy of this transition is 5.18 eV.

In the case of Zn_8O_8, two structures very close in energy were found, as was explained in Chapter 3. Henceforth calculations of the excitation energies of both structures have been carried out. It has to be mentioned that these structures are three-dimensional spheroids, instead of ring-like structures as were for $i = 1-7$.

Three excitations have been calculated, two dipole forbidden and one allowed, for the $Zn_8O_8^{GM}$ structure. The two forbidden ones end up in ^1E excited states. The calculated allowed transition occurs when an electron from the $18a_1$ orbital

Table 8.8: SKBJ(d) excitation energies (eV) and oscillator strengths of $Zn_iO_i^{GM}$, $i = 6 - 9$, and $Zn_8O_8^{LM_1}$.

	Transition		SKBJ(d)	
i	orbitals	states	ΔE	f
6	$24a'' \rightarrow 55a'$	$^1A' \rightarrow ^1 A''$	3.96	forbidden
	$54a' \rightarrow 55a'$	$^1A' \rightarrow ^1 A'$	4.69	forbidden
	$19a'' \rightarrow 55a'$	$^1A' \rightarrow ^1 A''$	5.34	0.136
7	$45b \rightarrow 47a$	$^1A \rightarrow ^1 B$	4.11	forbidden
	$42a \rightarrow 47a$	$^1A \rightarrow ^1 A$	5.06	0.000
	$42b \rightarrow 47a$	$^1A \rightarrow ^1 B$	5.18	0.004
8 (GM)	$51e \rightarrow 19a_1$	$^1A_1 \rightarrow ^1 E$	3.50	forbidden
	$18a_1 \rightarrow 19a_1$	$^1A_1 \rightarrow ^1 A_1$	3.92	0.086
	$49e \rightarrow 19a_1$	$^1A_1 \rightarrow ^1 E$	4.39	forbidden
8 (LM)	$52b \rightarrow 53a$	$^1A \rightarrow ^1 B$	3.24	0.010
	$52a \rightarrow 53a$	$^1A \rightarrow ^1 A$	3.36	0.025
	$50b \rightarrow 53a$	$^1A \rightarrow ^1 B$	3.77	0.017
	$48b \rightarrow 53a$	$^1A \rightarrow ^1 B$	4.05	0.070
	$48a \rightarrow 53a$	$^1A \rightarrow ^1 A$	4.09	0.021
9	$65a' \rightarrow 66a'$	$^1A' \rightarrow ^1 A'$	3.20	forbidden
	$64a' \rightarrow 66a'$	$^1A' \rightarrow ^1 A'$	3.41	0.019
	$63a' \rightarrow 66a'$	$^1A' \rightarrow ^1 A'$	3.88	0.054

is excited to the LUMO, where 3.65 eV are needed, and the oscillator strength is 0.086.

Five allowed transitions have been seen to happen for the $Zn_8O_8^{LM_1}$ structure in a quite narrow energy range, in comparison to previous cases. Three excitations end up in a ^1B state, exciting an electron from the $52b$, $50b$ and $48b$ to the LUMO. The excitation energies are 3.24 eV, 3.77 eV and 4.05 eV, and the oscillator strengths 0.010, 0.017 and 0.070, respectively. The other two calculated transitions end up in a ^1A state. In the first case an electron is excited from the $52a$ orbital to the LUMO, absorbing 3.36 eV, and f =0.025. The second transition needs 4.09 eV to happen, being the oscillator strength 0.021.

Two dipole allowed excitations have been predicted for $Zn_9O_9^{GM}$. The first transition needs 3.41 eV to happen, and the second 3.88 eV. This last transition is predicted to be more intense since the oscillator strength is larger, 0.054 in opposite to 0.019. Both transitions are degenerate. The lowest one occurs when an electron is excited from the $65a'$ orbital or the $64a'$ orbital to the LUMO. The one with the largest oscillator may happen exciting an electron from the $62a'$ or the $63a'$ orbital to the LUMO.

The transition in the structure of the global minima, ring-like structures for $i \leq 7$ and 3D spheroids for $i \geq 8$, has dramatic consequences in the obtained

excitation energies. We observe that the lowest-energy transitions increases from $i = 3 - 6$ from 4.62 eV to 5.34 eV. Then, for $i = 7$ this value is decreases to 5.06 eV. And in 3D structures the obtained values are already smaller. 3.92 eV for $Zn_8O_8^{GM}$ and 3.24 eV for $Zn_8O_8^{LM_1}$, and 3,41 eV for $i = 9$. This difference in the values is explained as follows. The transitions in all cases occurs from non-bonding p orbitals of O to the LUMO. In the ring structures these orbitals lie perpendicular to the plane, while in the 3D case they lie perpendicular to the spheroid's surface. This situation was also found for $Zn_iS_i^{GM}$ clusters (Chapter 6), but the excitation energies were larger, around 3.6 eV. The excitation energies of the 3D clusters are very similar to the bulk one, which is 3.20 eV. This fact makes attractive the idea of calculating the excitation energies of larger clusters, and the study of the band gaps of cluster-based solids, as carbon fullerenes solids. Therefore, it seems that Zn_iO_i clusters are more appropriate as window materials for solar cells. Of course, further work are needed, but this is a promising beggining.

8.3.3 Excitation energies calculated as Kohn-Sham eigenvalue differences

The problem of the reliability of virtual orbitals within DFT is a topic of great controversy [101, 103, 200]. Are the energies of these virtual orbitals good in order to calculate excitation energies? It has been recently demonstrated that working with an exact exchange-correlation potential the calculated excitation energies using the Kohn-Sham orbital energies are very reliable [201]. Nevertheless, in real problems one does not use exact potentials, and deals with approximate exchange-correlation potentials. In this section we estimate the excitation energies using the Kohn-Sham eigenvalues, with B3LYP and MPW1PW91 approximate exchange correlation potentials. Those potentials were chosen because of their great usability. In particular B3LYP is becoming a standard for geometry optimizations and MPW1PW91 is one of the most employed approximate exchange-correlation functional for the calculation of electronic excitation energies. Results are shown in Table 8.9.

A quick glance to this table shows that B3LYP gives better results than MPW1PW91, as compared to the TDDFT excitation energies. The difference between B3LYP and TDDFT (D2 column) is much smaller than the difference between MPW1PW91 and TDDFT (D1 column).This is due to the fact that B3LYP HOMO lies higher and LUMO lower than the MPW1PW91 ones. Analyzing the results closer, it is observed that as the cluster size increases the D1 and D2 differences decrease. D1 and D2 are smaller for 3D structures rather than for ring structures. Let us see now more carefully the D1 and D2 results.

In the case of D1 it is seen that the values are always greater than 1 eV. but as the cluster size increases, the difference becomes smaller, and is smaller than 1 eV for $Zn_9O_9^{GM}$. Nevertheless, the descent is paulatine and does not have large oscillations.

The analysis is similar for D2. Ringlike clusters have values larger than 0.5 eV, being the values closer to 0.5 as cluster size increases. Then, for 3D clusters are smaller than 0.5 eV. It is observed that these values become smaller and

Table 8.9: Excitation energies calculated with TDDFT ($\Delta E(1)$), MPW1PW91 Kohn-Sham orbital differences ($\Delta E(2)$) and B3LYP Kohn-Sham orbital differences ($\Delta E(3)$). D1 ($\Delta E(2) - \Delta E(1)$) and D2 ($\Delta E(3) - \Delta E(1)$) denote the differences between MPW1PW91 and B3LYP with respect to TDDFT, respectively. All energies are in eV.

i	Excitation	$\Delta E(1)$	$\Delta E(2)$	D1	$\Delta E(3)$	D2
1	$^1\Sigma \rightarrow ^1\Pi$	0.87	2.97	2.10	2.49	1.62
	$^1\Sigma \rightarrow ^1\Sigma$	3.80	4.49	0.69	4.08	0.28
2	$^1A_g \rightarrow ^1B_{1g}$	1.92	3.42	1.50	2.67	0.75
	$^1A_g \rightarrow ^1B_{2u}$	2.08	3.29	1.21	2.59	0.51
	$^1A_g \rightarrow ^1B_{3u}$	2.86	4.29	1.43	3.58	0.72
3	$^1A_1 \rightarrow ^1A_2$	3.66	5.06	1.40	4.37	0.71
	$^1A_1 \rightarrow ^1B_1$	3.67	5.06	1.39	4.37	0.70
	$^1A_1 \rightarrow ^1B_1$	4.62	5.97	1.35	5.29	0.67
4	$^1A_{1g} \rightarrow ^1B_{1u}$	3.83	5.21	1.38	4.61	0.78
	$^1A_{1g} \rightarrow ^1A_{2u}$	5.19	6.51	1.32	5.93	0.74
	$^1A_{1g} \rightarrow ^1E_u$	5.24	6.39	1.15	5.82	0.58
5	$^1A' \rightarrow ^1A''$	4.02	5.31	1.29	4.76	0.74
	$^1A' \rightarrow ^1A'$	5.28	6.53	1.25	5.98	0.70
	$^1A' \rightarrow ^1A''$	5.57	6.69	1.12	6.15	0.58
6	$^1A' \rightarrow ^1A''$	3.96	5.19	1.23	4.63	0.67
	$^1A' \rightarrow ^1A'$	4.69	5.63	0.94	5.07	0.38
	$^1A' \rightarrow ^1A''$	5.34	6.54	1.20	5.99	0.65
7	$^1A \rightarrow ^1B$	4.11	5.30	1.19	4.74	0.63
	$^1A \rightarrow ^1A$	5.06	6.34	1.28	5.78	0.72
	$^1A \rightarrow ^1B$	5.18	6.21	1.03	5.65	0.47
8 (LM)	$^1A \rightarrow ^1B$	3.24	4.26	1.02	3.69	0.45
	$^1A \rightarrow ^1A$	3.36	4.38	1.02	3.81	0.45
	$^1A \rightarrow ^1B$	3.77	4.83	1.06	4.24	0.47
	$^1A \rightarrow ^1B$	4.05	5.07	1.02	4.49	0.44
	$^1A \rightarrow ^1A$	4.09	5.25	1.16	4.64	0.55
8 (GM)	$^1A \rightarrow ^1B$	3.50	4.56	1.06	3.99	0.49
	$^1A \rightarrow ^1B$	3.92	4.89	0.97	4.33	0.41
	$^1A \rightarrow ^1A$	4.39	5.48	1.09	4.88	0.49
9	$^1A' \rightarrow ^1A'$	3.20	4.19	0.99	3.31	0.11
	$^1A' \rightarrow ^1A'$	3.41	4.38	0.97	3.69	0.28
	$^1A' \rightarrow ^1A'$	3.88	4.87	0.99	4.29	0.41

smaller as cluster size increases, and in $Zn_9O_9^{GM}$, the values are smaller than 0.40 eV. This is an important point, since approximate excitation energies may be calculated for larger clusters where TDDFT calculations are prohibitively expensive. Henceforth, the excitation energies of $Zn_{12}O_{12}$ and $Zn_{15}O_{15}$, characterized in Chapter 5, may be estimated. The HOMO-LUMO differences in both cases are 4.12 eV and 3.90 eV for $i = 12$ and $i = 15$, respectively. Nevertheless, in view of the error made in smaller cases, one may thing that the energy differences will be around 3.6 eV, smaller than those for $Zn_{12}S_{12}$ and $Zn_{15}S_{15}$. However, no oscillation strength may be stimated, and there is no way to state wheter these transitions are dipole allowed or not. Therefore, some calculations that could confirm these estimations and could provide oscillator strengths are still to be done.

8.4 Conclusions

TDDFT calculations yield interesting results for the excitation energies of Zn_iO_i clusters. The calculated electronic excitation energies show a strong dependence on the geometry of the cluster. Our study reveals that ring like structure clusters, $i = 2 - 7$ have larger excitation energies than three dimensional spheroidal clusters, $i \geq 8$. However, for both type of clusters the excitation occurs from occupied non bonding p type orbitals of oxygen to the LUMO.

The predicted electronic excitation energies of the spheroidal clusters are close to the bulk minimum energy gap, and lie near the range of the visible spectrum. These energies are smaller than the energies of Zn_iS_i clusters, and therefore, the clusters considered in the present investigation constitute promising materials for its use in photovoltaic solar cells as window materials.

The difference between the B3LYP Kohn-Sham energies of the orbitals involved in the sought electronic excitation appears to be a reliable practical approach to the prediction of the electronic excitation energies for larger clusters, where TDDFT calculations become prohibitive. This approach has been found to yield better results as the cluster size increases. Nevertheless, its most salient drawback is that no oscillator strength are obtained.

Chapter 9

Electronic Excitation Energies of $Zn_iSe_i^{GM}$ and $Zn_iTe_i^{GM}$ Clusters

Abstract

Time-dependent density-functional theory (TDDFT) is used to study the excitation energies of previously characterized global minima of small $Zn_iSe_i^{GM}$ and $Zn_iTe_i^{GM}$ clusters, $i = 1 - 9$. The relativistic compact effective core potentials and shared-exponent basis set of Stevens, Krauss, Basch and Jasien (SKBJ), systematically enlarged with extra functions, was used along this work. In general, the calculated excitations happen from non-bonding p orbitals of oxygen. These orbitals are perpendicular to the molecular plane in the case of the rings, and normal to the spheroid surface for 3D clusters. The calculated excitation energies are larger for ring like clusters as compared to 3D ones, with the excitation energies of the latter structures lying close to the visible spectrum. The difference between Kohn-Sham eigenvalues of the orbitals involved in the electronic excitations studied have also been compared with the TDDFT results of the corresponding excitations for two approximate density functionals, *i.e.*: MPW1PW91 and B3LYP, being the later more accurate. Moreover, they approach to the TDDFT value as the cluster size increases. Therefore, this might be a practical approach to estimate excitation energies of large Zn_iSe_i and Zn_iTe_i clusters.

9.1 Introduction

Computer revolution and other technological devices have been and are in rapid development basically due to improved semiconductor materials. Some of these materials are the II-VI compounds, which interest has increased notably due to their paramount technological potential.

The fact that cluster and nanoparticle characterization is becoming technologically possible opens new possibilities in the development of materials which could improve the efficiency of the cells. One of the best known 'new' clusters or nanostructures are the so called fullerenes, carbon spheroid structures discovered in 1985 [42].

Our goal is to calculate the excitation energies of $Zn_iX_i^{GM}$, X=Se, Te, $i = 1-9$, characterized previously in Chapter 4 ([198]). Further studies of the excitation energies of other II-VI cluster materials are in mind. The study of the Zn_iX_i clusters can provide new insight in the physics of these materials, and can be compared to the Zn_iO_i and Zn_iS_i cluster excitation energies.

9.2 Methods

The relativistic compact effective core potentials with shared-exponent basis set [133] of Stevens, Krauss, Basch and Jasien (SKBJ) was used as the starting basis set. We demonstrated previously [199] that polarization and diffusion functions were needed in order to yield accurate results, and showed that the SKBJ(1sp2d2f) basis, where there were added one s and p, two d and two f functions, was the ideal one for an accurate though affordable calculation of the electronic excitation energies of small $Zn_iS_i^{GM}$ clusters. However, for $Zn_iO_i^{GM}$ an extra f function was needed compared to $Zn_iS_i^{GM}$ case. Nevertheless, the size of the basis set makes the calculation of the excitation energies of large clusters prohibitive. Henceforth, the smaller SKBJ(d) basis set was chosen for these larger clusters.

All the calculations were carried out with the GAUSSIAN98 [163] package.

TDDFT [131, 119, 132] calculations have been performed to calculate the excitation energies of $Zn_iX_i^{GM}$, in which the hybrid Becke-style one parameter functional using modified Perdew-Wang exchange and Perdew-Wang 91 correlation (MPW1PW91) [195] was used. This combination was seen to provide the best results [199], along with the Becke3 [109] Perdew86 [196] functional B3P86.

The relativistic compact effective core potentials and shared-exponent basis set [133] of Stevens, Krauss, Basch and Jasien (SKBJ) was used throughout this study, being the Zn d electrons treated as valence electrons. In order to analyze the influence of the basis set size on the calculated excitation energies, extra functions were systematically added to SKBJ to a maximum of extra 3sp4d4f functions. These functions were systematically generated dividing the exponent of the previous function by three. The final exponents are given in Table 9.1, being all the coefficients equalized to 1.00. These larger basis sets

Table 9.1: Extra functions added to the SKBJ basis. All the coefficients are 1.00

	Zn	Se	Te
	α	α	α
sp	0.017900	0.02607	0.022457
sp	0.005967	0.008690	0.007486
sp	0.001989	0.0029	0.002495
d	0.3264	0.53783	0.349496
d	0.1088	0.208111	0.155952
d	0.03627	0.06937	0.051984
d	0.01209	0.023123	0.017328
f	3.1109	0.396026	0.306353
f	1.037	0.132009	0.102118
f	0.3457	0.044003	0.03404
f	0.1152	0.014668	0.011347

are labeled according to the number of added functions. Thus, as an example, the largest one is denoted SKBJ(3sp4d4f).

TDDFT calculations were carried out with the GAUSSIAN98 [163] package.

9.3 Results and discussion

In section 9.3.1 the basis set influence is discussed for small $Zn_iX_i^{GM}$ clusters, X=Se,Te, $i = 1-3$. In section 9.3.2 the obtained TDDFT excitation energies of $Zn_iX_i^{GM}$ clusters, $i = 1-9$ are fully discussed. Finally, in section 9.3.3, the reliability of the Kohn-Sham eigenvalues is discussed.

9.3.1 Basis set influence on the TDDFT excitation energies

In this section the calculated TDDFT excitation energies for $Zn_iX_i^{GM}$, $i = 1-3$, are shown. The SKBJ effective core potential systematically enlarged in order to find the most proper basis set. Only the $Zn_1X_1^{GM}$ cases are fully discussed, since the conclusions are similar for the rest.

In Table 9.2 the TDDFT excitation energies of $Zn_1X_1^{GM}$ are shown. In the previous chapters we have shown the importance of polarization functions in obtaining accurate results, and therefore small basis have not been checked for $Zn_1X_1^{GM}$. It may be observed that in all cases the differences between SKBJ(1sp2d2f) ΔE and SKBJ(3sp4d4f) ΔE are small enough that we can choose the first as a proper one to combine with TDDFT, saving in this way CPU usage.

Table 9.2: TDDFT results for $Zn_1X_1^{GM}$. ΔE : excitation energy (eV), and f the oscillator strength.

	$Zn_1Se_1^{GM}$			
	$^1\Pi$		$^1\Sigma$	
SKBJ +	ΔE	f	ΔE	f
1d-2d1f	0.6987	0.0018	3.9739	0.0466
1sp2d2f	0.7257	0.0019	3.9401	0.0428
1sp2d3f	0.7305	0.0019	3.9378	0.0429
2sp3d3f	0.7294	0.0019	3.9356	0.0425
3sp4d4f	0.7303	0.0019	3.9378	0.0434

	$Zn_1Te_1^{GM}$			
	$^1\Pi$		$^1\Sigma$	
SKBJ +	ΔE	f	ΔE	f
1d/2d1f	0.5939	0.0013	3.8305	0.0165
1sp2d2f	0.6141	0.0014	3.7899	0.0131
1sp2d3f	0.6170	0.0014	3.7858	0.0133
2sp3d3f	0.6150	0.0014	3.7834	0.0131
3sp4d4f	0.6162	0.0014	3.7867	0.0136

Table 9.3: TDDFT results for $Zn_2X_2^{GM}$. ΔE : excitation energy (eV), and f the oscillator strength.

	$Zn_2Se_2^{GM}$					
	$^1B_{2g}$		$^1B_{3u}$		$^1B_{1u}$	
SKBJ +	ΔE	f	ΔE	f	ΔE	f
1d/2d1f	1.9887	0	2.7841	0.0204	2.8901	0.0166
1sp2d2f	2.0107	0	2.8046	0.0203	2.9157	0.0175
1sp2d3f	2.0110	0	2.8038	0.0202	2.9097	0.0175
2sp3d3f	2.0148	0	2.8059	0.0201	2.9111	0.0181
3sp4d4f	2.0106	0	2.8033	0.0201	2.9078	0.0181

	$Zn_2Te_2^{GM}$					
	$^1B_{2g}$		$^1B_{3u}$		$^1B_{1u}$	
SKBJ +	ΔE	f	ΔE	f	ΔE	f
1d/2d1f	1.9051	0	2.6109	0.0160	2.8843	0.0130
1sp2d2f	1.9126	0	2.6194	0.0167	2.8928	0.0140
1sp2d3f	1.9117	0	2.6182	0.0167	2.8866	0.0140
2sp3d3f	1.9104	0	2.6166	0.0165	2.8851	0.0142

Table 9.4: TDDFT results for $Zn_3X_3^{GM}$. ΔE : excitation energy (eV), and f the oscillator strength.

	$Zn_3Se_3^{GM}$					
	$^1A_2$ ($^1B_1$)		$^1B_1$		$^1A_2$ ($^1B_1$)	
SKBJ +	ΔE	f	ΔE	f	ΔE	f
1d/2d1f	3.3027	0	3.9716	0.0317	4.1811	0
1sp2d2f	3.2983	0	3.9667	0.0319	4.1440	0
1sp2d3f	3.3010	0	3.9719	0.0323	4.1481	0.
2sp3d3f	3.3018	0	3.9724	0.0331	4.1491	0

	$Zn_3Te_3^{GM}$					
	$^1A_2$ ($^1B_1$)		$^1B_1$		$^1A_2$ ($^1B_1$)	
SKBJ +	ΔE	f	ΔE	f	ΔE	f
1d/2d1f	2.8317	0	3.4088	0.0109	3.6453	0
1sp2d2f	2.8218	0	3.4006	0.0119	3.6101	0
1sp2d3f	2.8268	0	3.4078	0.0121	3.6128	0
2sp3d3f	2.8259	0	3.4069	0.0125	3.6113	0

Following the results for $Zn_2X_2^{GM}$ and $Zn_3X_3^{GM}$ are given in Table 9.3 and 9.4, respectively.

These data also shows SKBJ(1sp2d2f) basis set as the smallest one yielding good results.

It seems logical then to choose this SKBJ(1sp2d2f) for further calculations. It is seen that the inclusion of more than one polarization functions in the basis set is indispensable.

9.3.2 TDDFT Excitation energies of small $Zn_iX_i^{GM}$ clusters, $i = 1 - 9$.

We have concluded above that the MPW1PW91/SKBJ(1sp2d2f) level of theory is the addecuate one for an accurate though affordable calculation of the electronic excitation energies of small $Zn_iX_i^{GM}$ clusters. However, for clusters as big as $i = 6$ the size of the basis set makes the calculations prohibitive. Henceforth, the smaller SKBJ(d/2df) basis set was chosen for these larger clusters. According to this statement, we have divided the clusters in two groups. In group 1 the excitation energies of $Zn_iX_i^{GM}$, $i = 1 - 5$ are discussed, and in group 2 the excitation energies of $Zn_iX_i^{GM}$, $i = 6 - 9$.

The range of the excitations we are interested in are those close to the visible spectrum, smaller than 5 eV. Since in some cases there may be many excitations within this range we have basically calculated the lowest lying excitations. Nevertheless, in some cases more have been calculated due to the fact that dipole allowed transitions did not lie within that range.

Table 9.5: Valence configuration of the clusters of Group 1, $Zn_iX_i^{GM}$, $i = 1-5$.

	Zn_iSe_i		Zn_iTe_i	
i	Val. Conf.	LUMO	Val. Conf.	LUMO
1	$2\delta^2\,4\sigma^2\,5\sigma^2\,5\pi^4$	6σ	$2\delta^2\,4\sigma^2\,5\sigma^2\,5\pi^4$	6σ
2	$5b_{2u}^2\,3b_{3g}^2\,3b_{3u}^2\,4b_{1u}^2\,2b_{2g}^2$	$7a_g$	$5b_{2u}^2\,3b_{3g}^2\,4b_{1u}^2\,3b_{3u}^2\,2b_{2g}^2$	$7a_g$
3	$12b_2^2\,15a_1^2\,6b_1^2\,7b_1^2\,5a_2^2$	$16a_1$	$15a_1^2\,12b_2^2\,6b_1^2\,5a_2^2\,7b_1^2$	$16a_1$
4	$23b^2\,24b^2\,25b^2\,26a^2\,27a^2$	$28a$	$23b^2\,24b^2\,26a^2\,25b^2\,27a^2$	$28a$
5	$33a'^2\,34a'^2\,29a''^2\,35a'^2\,30a''^2$	$36a'$	$28a''^2\,34a'^2\,29a''^2\,30a''^2\,35a'^2$	$36a'$

Group 1: $Zn_iX_i^{GM}$ clusters, $i = 1-5$

For the small clusters we have obtained the electronic excitation energies with both SKBJ(d) and SKBJ(1sp2d2f) basis sets. This allows us to asses the performance of the smaller basis set and consequently to highlight the limitations of the SKBJ(d) basis set with respect to SKBJ(1sp2d2f).

In Table 9.5 the valence configuration and LUMO orbital symmetry of the clusters of Group 1, namely $Zn_iX_i^{GM}$, $i = 1-5$, described in Chapter 4, are given. Table 9.6 and 9.7 collects the SKBJ(d) and SKBJ(1sp2d2f) excitation energies and oscillator strengths for the mentioned clusters.

Two different possible excitations for $Zn_1X_1^{GM}$ are shown. The lowest excitation occurs from the $^1\Sigma$ ground state to a $^1\Pi$ excited state, exciting an electron to the LUMO vacant orbital from the HOMO. The other calculated transition involves the $^1\Sigma$ ground state and an excited state of the same symmetry. Now the electron is excited from the inner 5σ orbital to the LUMO. For X=Se the first transition needs 0.73 eV (0.61 eV for X=Te) to happen, and the second 3.94 eV (3.79 eV for X=Te). Nevertheless, the oscillator strength is in both cases an order of magnitude larger in the second transition.

Three excitations of $Zn_2X_2^{GM}$ have been calculated. The lowest excitation is dipole forbidden. The lowest-energy allowed excitation happens when an electron is excited from the $3b_{3u}$ orbital to the LUMO, resulting in a $^1B_{3u}$ excited state, and the second one exciting it from the $4b_{1u}$ orbital to the LUMO. For X=Se the excitation energies are 2.80 eV and 2.92 eV, respectively, both having similar f. In the X=Te case, ΔE's are smaller, 261 eV and 2.88 eV, respectively, being f similar. All these energies lie within the range of the visible spectrum.

Three excitations have been calculated for $Zn_3X_3^{GM}$. The lowest transition excites an electron from the $5a_2$ orbital to the LUMO, but this is dipole forbidden, i.e. $f = 0$. Similarly, the transition to the second $^1A_2$ state is not allowed either. The only allowed transition calculated occurs exciting an electron from the $6b_1$ orbital to the LUMO, yielding a $^1B_1$ state. The excitation energy is

Table 9.6: SKBJ(d) and SKBJ(1sp2d2f) excitation energies (eV) and oscillator strengths of small $Zn_iSe_i^{GM}$, $i = 1-5$. $\Delta(\Delta E)$ is the difference between SKBJ(1sp2d2f) ΔE and SKBJ(d) ΔE. Similarly for Δf.

	Transition		SKBJ(1d/2d1f)		SKBJ(1sp2d2f)			
i	orbitals	states	ΔE	f	ΔE	f	$\Delta(\Delta E)$	Δf
1	$5\pi \rightarrow 6\sigma$	$^1\Sigma \rightarrow ^1\Pi$	0.70	0.002	0.73	0.002	0.03	0
	$5\sigma \rightarrow 6\sigma$	$^1\Sigma \rightarrow ^1\Sigma$	3.97	0.047	3.94	0.043	0.03	0.004
2	$2b_{2g} \rightarrow 7a_g$	$^1A_g \rightarrow ^1B_{2g}$	1.99	forbidden	2,01	forbidden	0.02	-
	$3b_{3u} \rightarrow 7a_g$	$^1A_g \rightarrow ^1B_{3u}$	2.78	0.020	2.80	0.020	0.02	0
	$4b_{1u} \rightarrow 7a_g$	$^1A_g \rightarrow ^1B_{1u}$	2.89	0.017	2.92	0.018	0.03	0.001
3	$5a_2 \rightarrow 16a_1$	$^1A_1 \rightarrow ^1A_2$	3.30	forbidden	3.30	forbidden	0	-
	$6b_1 \rightarrow 16a_1$	$^1A_1 \rightarrow ^1B_1$	3.97	0.032	3.97	0.032	0	0
	$5a_2 \rightarrow 17a_1$	$^1A_1 \rightarrow ^1A_2$	4.18	forbidden	4.14	forbidden	0.04	-
4	$27a \rightarrow 28a$	$^1A \rightarrow ^1A$	3.55	forbidden	3.52	forbidden	0.03	-
	$25b \rightarrow 28a$	$^1A \rightarrow ^1B$	3.89	0.004	3.86	0.004	0.03	0
	$26a \rightarrow 29a$	$^1A \rightarrow ^1A$	4.09	0.001	4.06	0.001	0.03	0
5	$30a'' \rightarrow 36a'$	$^1A' \rightarrow ^1A''$	3.75	0.001	3.73	0.001	0.02	0
	$35a' \rightarrow 36a'$	$^1A' \rightarrow ^1A'$	3.99	0.001	3.97	0.001	0.02	0
	$29a'' \rightarrow 36a'$	$^1A' \rightarrow ^1A''$	4.11	0.007	4.09	0.008	0.02	0.001

Table 9.7: SKBJ(d) and SKBJ(1sp2d2f) excitation energies (eV) and oscillator strengths of small $Zn_iTe_i^{GM}$, $i = 1-5$. $\Delta(\Delta E)$ is the difference between SKBJ(1sp2d2f) ΔE and SKBJ(d) ΔE. Similarly for Δf.

	Transition		SKBJ(1d-2d1f)		SKBJ(1sp2d2f)			
i	orbitals	states	ΔE	f	ΔE	f	$\Delta(\Delta E)$	Δf
1	$5\pi \rightarrow 6\sigma$	$^1\Sigma \rightarrow ^1\Pi$	0.59	0.001	0.61	0.001	0.02	0
	$5\sigma \rightarrow 6\sigma$	$^1\Sigma \rightarrow ^1\Sigma$	3.83	0.017	3.79	0.013	0.04	0.004
2	$2b_{2g} \rightarrow 7a_g$	$^1A_g \rightarrow ^1B_{2g}$	1.91	forbidden	1.91	forbidden	0	-
	$3b_{3u} \rightarrow 7a_g$	$^1A_g \rightarrow ^1B_{3u}$	2.61	0.016	2.62	0.017	0.01	0.001
	$4b_{1u} \rightarrow 7a_g$	$^1A_g \rightarrow ^1B_{1u}$	2.88	0.013	2.89	0.014	0.01	0.001
3	$5a_2 \rightarrow 16a_1$	$^1A_1 \rightarrow ^1A_2$	2.83	forbidden	2.82	forbidden	0.01	-
	$6b_1 \rightarrow 16a_1$	$^1A_1 \rightarrow ^1B_1$	3.41	0.011	3.40	0.012	0.012	0.001
	$5a_2 \rightarrow 17a_1$	$^1A_1 \rightarrow ^1A_2$	3.65	forbidden	3.61	forbidden	0.04	-
4	$27a \rightarrow 28a$	$^1A \rightarrow ^1A$	3.16	forbidden	3.14	forbidden	0.02	-
	$25b \rightarrow 28a$	$^1A \rightarrow ^1B$	3.35	0.006	3.33	0.006	0.02	0
	$24b \rightarrow 28a$	$^1A \rightarrow ^1B$	3.66	0.002	3.64	0.002	0.02	0
	$26a \rightarrow 29a$	$^1A \rightarrow ^1A$	3.72	0.005	3.69	0.005	0.03	0
5	$30a'' \rightarrow 36a'$	$^1A' \rightarrow ^1A''$	3.36	0.000	3.34	0.000	0.02	0
	$35a' \rightarrow 36a'$	$^1A' \rightarrow ^1A'$	3.53	0.000	3.49	0.001	0.04	0.001
	$29a' \rightarrow 36a'$	$^1A' \rightarrow ^1A''$	3.69	0.004	3.67	0.004	0.02	0

3.97 eV, and $f = 0.032$ for X=Se. For X=Te ΔE is much smaller, 3.40 eV, but f as well, $f = 0.012$. These excitation energies are larger than the allowed excitation energies of $Zn_2X_2^{GM}$.

Three excitations are reported for $Zn_4Se_4^{GM}$ and four for $Zn_4Te_4^{GM}$. The excitation to the lowest lying ^1A state is not dipole allowed. However, the other calculated $^1A \rightarrow ^1 B$ and $^1A \rightarrow ^1 A$ transitions are allowed. The electron is excited from the $25b$ orbital to the LUMO in the first case, being the excitation energy 3.86 eV and the oscillator strength 0.004 in the case of X=Se, and 3.33 eV and $f = 0.006$ for X=Te. The last transition occurs when the electron is excited from the $26a$ orbital to the $29a$. For X=Se, this transition is likely to be less intense, since the oscillator strength is much smaller, 0.001, and the excitation energy is 0.20 eV larger. When X=Te, f is similar to the previous excitation, but the energy is 0.36 eV larger. For Zn_4Te_4 a forth transition is found when an electron is excited from the $24b$ orbital to the LUMO, having a small f.

Three transitions dipole allowed are collected for $Zn_5X_5^{GM}$. The lowest lying transition occurs exciting an electron from the HOMO to the LUMO, resulting in a $^1A''$ state, which needs 3.73 eV for X=Se and 3.34 eV for X=Te. In both cases f is very small. Exciting an electron from the $35a'$ orbital to the HOMO a $^1A'$ state is achieved. 3.97 eV are needed for that purpose when X=Se, and 3.49 eV when X=Te. The transition with the largest f is found when an electron is excited from the $29a''$ to the LUMO. This transition needs 4.09 eV and 3.67 eV, for X=Se and Te, respectively.

SKBJ(1sp2d2f) vs SKBJ(d)

In Table 9.6 and 9.7 the SKBJ(d) and SKBJ(1sp2d2f) excitation energies and oscillator strengths are given. Besides, the differences between them may also be viewed there. Having a look to these differences, one may observe that they are not very large, specially for the larger clusters. The percentage is less than 1% for $Zn_5Se_5^{GM}$ and $Zn_5Te_5^{GM}$. Therefore, the SKBJ(d/2df) results for the clusters of Group 2 are expected to be reasonably accurate. This conclusion was also obtained in the case of the excitation energies of $Zn_iS_i^{GM}$ and $Zn_iO_i^{GM}$.

Group 2: $Zn_iX_i^{GM}$ clusters, $i = 6 - 9$

In Table 9.8 the valence configuration and LUMO orbital symmetry of the clusters of Group 2, namely $Zn_iX_i^{GM}$, $i = 6 - 9$, depicted in Chapter 4, are given. The SKBJ(d/2df) excitation energies and oscillator strengths are shown in Tables 9.9 and 9.10.

Three calculated excitations of $Zn_6X_6^{GM}$ are shown, only two of them being dipole allowed. The lowest-energy dipole allowed transition occurs from the ground state to other $^1A''$ excited state, where an electron from the inner $22b_u$ orbital is excited to the LUMO. This transition needs 3.25 eV to occur, for

Table 9.8: Valence configuration of the clusters of Group 2, $Zn_iX_i^{GM}$, $i = 6-9$.

	Zn_iSe_i		Zn_iTe_i	
i	Val. Conf.	LUMO	Val. Conf.	LUMO
6	$17a_u^2\,21b_u^2\,22b_u^2\,22a_g^2\,17b_g^2$	$23a_g$	$17a_u^2\,16b_g^2\,22b_u^2\,22a_g^2\,17b_g^2$	$23a_g$
7	$38a''^2\,39a''^2\,50a'^2\,51a'^2\,40a''^2$	$52a'$	$44a^2\,45a^2\,46a^2\,44b^2\,45b^2$	$47a$
8	$50b^2\,51a^2\,52a^2\,51b^2\,52b^2$	$53a$	$50b^2\,51a^2\,52a^2\,51b^2\,52b^2$	$53a$
9	$64a'^2\,65a'^2\,50a''^2\,51a''^2\,66a'^2$	$67a'$	$64a'^2\,65a'^2\,50a''^2\,51a''^2\,66a'^2$	$67a'$

Table 9.9: SKBJ(d/2df) excitation energies (eV) and oscillator strengths of $Zn_iSe_i^{GM}$, $i = 6-9$.

	Transition		SKBJ(d/2df)	
i	orbitals	states	ΔE	f
6	$17b_g \to 23a_g$	$^1A_g \to ^1B_g$	2.99	forbidden
	$22b_u \to 23a_g$	$^1A_g \to ^1B_u$	3.25	0.023
	$21b_u \to 23a_g$	$^1A_g \to ^1B_u$	3.73	0.004
7	$40a'' \to 52a'$	$^1A' \to ^1A''$	2.78	forbidden
	$51a' \to 52a'$	$^1A' \to ^1A'$	3.17	0.002
	$51a' \to 53a'$	$^1A' \to ^1A'$	3.40	0.002
8	$52b \to 53a$	$^1A \to ^1B$	3.26	0.007
	$51a \to 53a$	$^1A \to ^1A$	3.61	0.026
	$50b \to 53a$	$^1A \to ^1B$	3.91	0.016
9	$66a' \to 67a'$	$^1A' \to ^1A'$	3.3566	forbidden
	$65a' \to 67a'$	$^1A' \to ^1A'$	3.6762	0.0201
	$62a' \to 67a'$	$^1A' \to ^1A'$	3.9808	0.0266

Table 9.10: SKBJ(d) excitation energies (eV) and oscillator strengths of $Zn_iTe_i^{GM}$, $i = 6 - 9$.

	Transition		SKBJ(d)	
i	orbitals	states	ΔE	f
6	$17b_g \rightarrow 23a_g$	$^1A_g \rightarrow^1 B_g$	2.51	forbidden
	$22b_u \rightarrow 23a_g$	$^1A_g \rightarrow^1 B_u$	2.79	0.006
	$17b_g \rightarrow 23b_u$	$^1A_g \rightarrow^1 A_u$	3.07	0.015
7	$45b \rightarrow 47a$	$^1A \rightarrow^1 B$	1.96	0.001
	$44b \rightarrow 47a$	$^1A \rightarrow^1 B$	2.84	0.001
	$46a \rightarrow 47a$	$^1A \rightarrow^1 A$	2.92	0.011
8	$52b \rightarrow 53a$	$^1A \rightarrow^1 B$	2.77	0.002
	$51a \rightarrow 53a$	$^1A \rightarrow^1 A$	3.15	0.014
	$50b \rightarrow 53a$	$^1A \rightarrow^1 B$	3.36	0.007
9	$66a' \rightarrow 67a'$	$^1A' \rightarrow^1 A'$	2.83	forbidden
	$65a' \rightarrow 67a'$	$^1A' \rightarrow^1 A'$	2.98	forbidden
	$62a' \rightarrow 67a'$	$^1A' \rightarrow^1 A'$	3.18	0.009

X=Se, and 2.79 eV for X=Te. Nevertheless, f is larger for X=Se. The second calculated excitation needs 3.73 eV when X=Se, and 3.07 eV when X=Te. In the first case it happens when an electron is excited from the $21b_u$ orbital to the LUMO, but in the second case the electron is excited from the $17b_g$ to the second virtual orbital $23b_u$.

Two dipole allowed transitions of $Zn_7Se_7^{GM}$, are reported in Table 9.9. The first allowed excitation occurs when the electron is excited from the $51a'$ orbital to the LUMO. The excitation energy in this case is 3.17 eV, but has a small f, 0.002. The second reported transition occurs exciting an electron from the inner $51a'$ orbital to the $53a'$ orbital, being the excitation energy 3.40 eV. For $Zn_7Te_7^{GM}$ three dipole allowed transitions are given in Table 9.10. The excitation with largest f occurs exciting an electron from the inner $46a$ orbital to the LUMO, which absorbs 2.92 eV.

In the case of $Zn_8X_8^{GM}$, three dipole allowed excitations have been calculated. The first one is a HOMO-LUMO transition. The second one occurs when an electron moves from the inner $51a$ orbital to the LUMO, and the last one from the $50b$ orbital to the LUMO, resulting in ^1A and ^1B states, respectively. The HOMO-LUMO transition absorbs 3.26 eV for X=Se, and 2.77 eV for X=Te. In the other two cases the excitation energies are smaller for X=Te as well, but the oscilator strength are larger.

Finally, three excitations are reported for $Zn_9X_9^{GM}$. The excitation of an electron from the HOMO to the LUMO is dipole forbidden in both cases. For X=Te, to excite an electron from the $65a'$ to the LUMO is not allowed, but it is for X=Se, absorbing 3.68 eV. The last transition, allowed for both cases, occurs when an electron moves from the $62a'$ to the LUMO. In the X=Se case

the absorbed photon is more energetic, as in previous cases, but the oscillator strength is three times larger.

The transition in the structure of the global minima, ring-like structures for $i \leq 5$ and 3D spheroids for $i \geq 6$, has dramatic consequences in the obtained excitation energies. We observe, for X=Se, that the lowest-energy transitions are bigger than 3.5 eV for the formers, but smaller for 3D structures. This value decreases to roughly 3 eV when X=Te.

This difference in the values is explained as follows. The transitions in all cases occurs from non-bonding p orbitals of X to the LUMO. In the ring structures these orbitals lie perpendicular to the plane, while in the 3D case they lie perpendicular to the spheroid's surface. This situation was also found for $Zn_iS_i^{GM}$ and $Zn_iO_i^{GM}$ clusters (Chapters 7 and 8). The excitation energies of the 3D clusters are somewhat larger than the bulk ones, which are 2.67 eV and 2.25 eV for ZnSe and ZnTe, respectively, but lie within the visible spectrum. This fact makes attractive the idea of calculating the excitation energies of larger clusters, and the study of the band gaps of cluster-based solids, as carbon fullerenes solids. Therefore, it seems that Zn_iTe_i clusters may be appropriate as both window or absorber materials in solar cells, while Zn_iSe_i may be more suitable as window materials, similarly to Zn_iS_i and Zn_iO_i. Of course, further studies are needed, but this constitutes a promising evidence.

9.3.3 Excitation energies calculated as Kohn-Sham eigenvalue differences

The problem of the reliability of virtual orbitals within DFT is a topic of great controversy [101, 103, 200]. Are the energies of these virtual orbitals good in order to calculate excitation energies? It has been recently demonstrated that working with an exact exchange-correlation potential the calculated excitation energies using the Kohn-Sham orbital energies are very reliable [201]. Nevertheless, in real problems one does not use exact potentials, and deals with approximate exchange-correlation potentials. In this section we estimate the excitation energies using the Kohn-Sham eigenvalues, with B3LYP and MPW1PW91 approximate exchange correlation potentials. Those potentials were chosen because of their great usability. In particular B3LYP is becoming a standard for geometry optimizations and MPW1PW91 is one of the most employed approximate exchange-correlation functional for the calculation of electronic excitation energies. Results are shown in Table 9.11 and 9.12.

A quick glance to these tables shows that B3LYP gives better results than MPW1PW91, as compared to the TDDFT excitation energies. The difference between B3LYP and TDDFT (D2 column) is much smaller than the difference between MPW1PW91 and TDDFT (D1 column).This is due to the fact that B3LYP HOMO lies higher and LUMO lower than the MPW1PW91 ones. Analyzing the results closer, it is observed that as the cluster size increases the D1 and D2 differences decrease. D1 and D2 are smaller for 3D structures rather than for ring structures. Let us see now more carefully the D1 and D2 results.

Table 9.11: Excitation energies of $Zn_iSe_i^{GM}$ calculated with TDDFT ($\Delta E(1)$), MPW1PW91 Kohn-Sham orbital differences ($\Delta E(2)$) and B3LYP Kohn-Sham orbital differences ($\Delta E(3)$). D1 ($\Delta E(2) - \Delta E(1)$) and D2 $\Delta E(3) - \Delta E(1)$) denote the differences between MPW1PW91 and B3LYP with respect to TDDFT, respectively. All energies are in eV.

i	Excitation	$\Delta E(1)$	$\Delta E(2)$	D1	$\Delta E(3)$	D2
1	$^1\Sigma \rightarrow ^1\Pi$	0.73	2.13	1.4	1.70	0.97
	$^1\Sigma \rightarrow ^1\Sigma$	3.94	4.78	0.84	4.39	0.45
2	$^1A_g \rightarrow ^1B_{2g}$	2.01	3.20	1.19	2.69	0.68
	$^1A_g \rightarrow ^1B_{3u}$	2.80	3.99	1.19	3.46	0.66
	$^1A_g \rightarrow ^1B_{1u}$	2.92	3.92	1.00	3.41	0.49
3	$^1A_1 \rightarrow ^1A_2$	3.30	4.40	1.10	3.92	0.62
	$^1A_1 \rightarrow ^1B_1$	3.97	5.08	1.11	4.60	0.63
	$^1A_1 \rightarrow ^1A_2$	4.14	5.35	1.21	5.03	0.89
4	$^1A \rightarrow ^1A$	3.52	4.58	1.06	4.22	0.70
	$^1A \rightarrow ^1B$	3.86	4.93	1.07	4.56	0.70
	$^1A \rightarrow ^1A$	4.06	5.10	1.04	4.69	0.63
5	$^1A' \rightarrow ^1A''$	3.73	4.74	1.01	4.33	0.60
	$^1A' \rightarrow ^1A'$	3.97	4.97	1.00	4.56	0.59
	$^1A' \rightarrow ^1A''$	4.09	5.10	1.01	4.69	0.60
6	$^1A_g \rightarrow ^1B_g$	2.99	3.97	0.98	3.52	0.53
	$^1A_g \rightarrow ^1A_u$	3.25	4.16	0.91	3.72	0.47
	$^1A_g \rightarrow ^1B_u$	3.73	4.72	0.99	4.25	0.52
7	$^1A' \rightarrow ^1A''$	2.78	3.53	0.75	3.09	0.31
	$^1A' \rightarrow ^1A'$	3.17	3.94	0.77	3.50	0.33
	$^1A' \rightarrow ^1A'$	3.40	4.35	0.95	3.98	0.58
8	$^1A \rightarrow ^1B$	3.26	4.14	0.88	3.68	0.42
	$^1A \rightarrow ^1A$	3.61	4.46	0.85	4.00	0.39
	$^1A \rightarrow ^1B$	3.91	4.78	0.87	4.31	0.40
9	$^1A' \rightarrow ^1A'$	3.36	4.21	0.85	3.76	0.40
	$^1A' \rightarrow ^1A'$	3.68	4.50	0.82	4.05	0.37
	$^1A' \rightarrow ^1A'$	3.98	4.81	0.83	4.34	0.36

For X=Se, D1 is seen to have values greater than 1 eV for ring-like structures, but as the cluster size increases, the difference becomes smaller, and is smaller than 1 eV for spheroid clusters. Nevertheless, the descent is paulatine and does not have large oscillations. For X=Te, similar behavior is observed, but the transition value is smaller, 0.9 eV. The analysis is similar for D2. Ring-like clusters have values larger than 0.6 eV, being the values closer to 0.6 as cluster size increases. Then, for 3D clusters are smaller than 0.6 eV. It is observed that these values become smaller and smaller as cluster size increases, and in $Zn_9X_9^{GM}$, the values are roughly 0.40 eV.

This is an important point, since approximate excitation energies may be calculated for larger clusters where TDDFT calculations are prohibitively expensive. Henceforth, the excitation energies of $Zn_{12}X_{12}$ and $Zn_{15}X_{15}$, characterized in Chapter 5, may be estimated. In the X=Se case, the HOMO-LUMO differences are 3.98 eV and 3.87 eV for $i = 12$ and $i = 15$, respectively. However, according to the errors given in Table 9.11, one may stimate that the energy differences will be around 3.5 eV, similar to $Zn_9Se_9^{GM}$. For X=Te we find the HOMO-LUMO differences to be smaller, 3.40 eV and 3.33 eV, respectively, for $i = 12$ and $i = 15$, and according to the errors of Table 9.12 we estimate values close to 3 eV. However, no oscillation strength may be stimated, and there is no way to state wheter these transitions are dipole allowed or not. Therefore, some calculations that could confirm these estimations and could provide oscillator strengths are still to be done.

9.4 Conclusions

TDDFT calculations yield interesting results for the excitation energies of $Zn_iX_i^{GM}$ clusters. The calculated electronic excitation energies show a strong dependence on the geometry of the cluster. Our study reveals that ring like structure clusters, $i = 2 - 5$ have larger excitation energies than three dimensional spheroidal clusters, $i \geq 6$. However, for both type of clusters the excitation occurs from occupied non bonding p type orbitals of selenium or tellurium to the LUMO.

The predicted electronic excitation energies of the spheroidal clusters are close to the bulk minimum energy gap, and lie near the range of the visible spectrum for X=Se case, and within it for X=Te. These energies are smaller than the energies of $Zn_iS_i^{GM}$ and $Zn_iO_i^{GM}$ clusters, and therefore, the clusters considered in the present investigation constitute promising materials for its use in photovoltaic solar cells as absorbers (X=Te) or both absorbers and window materials (X=Se).

The difference between the B3LYP Kohn-Sham energies of the orbitals involved in the sought electronic excitation appears to be a reliable practical approach to the prediction of the electronic excitation energies for larger clusters, where TDDFT calculations become prohibitive. This approach has been found to yield better results as the cluster size increases. Nevertheless, its most salient drawback is that no oscillator strength are obtained.

Table 9.12: Excitation energies of $Zn_iTe_i^{GM}$ calculated with TDDFT ($\Delta E(1)$), MPW1PW91 Kohn-Sham orbital differences ($\Delta E(2)$) and B3LYP Kohn-Sham orbital differences ($\Delta E(3)$). D1 ($\Delta E(2)-\Delta E(1)$) and D2 ($\Delta E(3)-\Delta E(1)$) denote the differences between MPW1PW91 and B3LYP with respect to TDDFT, respectively. All energies are in eV.

i	Excitation	$\Delta E(1)$	$\Delta E(2)$	D1	$\Delta E(3)$	D2
1	$^1\Sigma \rightarrow^1 \Pi$	0.61	1.90	1.29	1.51	0.90
	$^1\Sigma \rightarrow^1 \Sigma$	3.79	4.73	0.94	4.37	0.58
2	$^1A_g \rightarrow^1 B_{1g}$	1.91	3.01	1.10	2.56	0.65
	$^1A_g \rightarrow^1 B_{2u}$	2.62	3.73	1.11	3.25	0.63
	$^1A_g \rightarrow^1 B_{3u}$	2.89	3.86	0.97	3.39	0.50
3	$^1A_1 \rightarrow^1 A_2$	2.82	3.87	1.05	3.49	0.67
	$^1A_1 \rightarrow^1 B_1$	3.40	4.47	1.07	4.08	0.68
	$^1A_1 \rightarrow^1 B_1$	4.61	4.69	1.08	4.38	0.77
4	$^1A_{1g} \rightarrow^1 B_{1u}$	3.14	4.09	0.95	3.77	0.63
	$^1A_{1g} \rightarrow^1 A_{2u}$	3.33	4.29	0.96	3.97	0.64
	$^1A_{1g} \rightarrow^1 E_u$	3.64	4.62	0.98	4.30	0.66
5	$^1A' \rightarrow^1 A''$	3.34	4.30	0.96	3.96	0.62
	$^1A' \rightarrow^1 A'$	3.49	4.41	0.92	4.03	0.54
	$^1A' \rightarrow^1 A''$	3.67	4.59	0.92	4.24	0.57
6	$^1A' \rightarrow^1 A''$	2.51	3.44	0.93	3.10	0.59
	$^1A' \rightarrow^1 A'$	2.79	3.67	0.88	3.34	0.55
	$^1A' \rightarrow^1 A''$	3.07	3.89	0.82	3.49	0.42
7	$^1A \rightarrow^1 B$	1.96	2.69	0.73	2.34	0.38
	$^1A \rightarrow^1 A$	2.84	3.65	0.81	3.28	0.44
	$^1A \rightarrow^1 B$	2.92	3.74	0.82	3.38	0.46
8	$^1A \rightarrow^1 B$	2.77	3.61	0.84	3.26	0.49
	$^1A \rightarrow^1 B$	3.15	3.96	0.81	3.58	0.43
	$^1A \rightarrow^1 A$	3.36	4.20	0.84	3.83	0.47
9	$^1A' \rightarrow^1 A'$	2.83	3.65	0.82	3.29	0.46
	$^1A' \rightarrow^1 A'$	2.98	3.80	0.82	3.44	0.46
	$^1A' \rightarrow^1 A'$	3.18	3.97	0.79	3.61	0.43

Part III

Concluding Remarks

Chapter 10

Final Conclusions

10.1 Structures

Throughout this thesis we have observed that ring structures are the global minima for the small Zn_iX_i clusters and three-dimensional spheroids for the larger ones. The transition occurs at $i = 8$ for X=O, and at $i = 6$ for the remaining elements of group VIB. The evolution of the relative energies between the ring and spheroid structures is depicted in Figure 10.1. Notice that relative energies for $i = 9, 12, 15$ are not plotted, since no ring structures have been characterized. Points above the dashed line represent the situation where the ring structures are more stable than spheroids. It may be seen that as the cluster size increases the three dimensional structures are favoured, and all the lines tend to sunk into the spheroid stability region.

There are two main factors determining whether a ring or a three-dimensional structure will be the global minimum for the small Zn_iX_i clusters: the stability of very obtuse X-Zn-X bond angles, and the stability gained from higher coordination. For small clusters the first term outweighs the second and ring structures are predicted to be the global minima. For $i \geq 6$, ($i \geq 8$ for X=O) however, the size of the cluster allows for both obtuse X-Zn-X bond angles and higher coordination in the three dimensional spheroid structures, making these the most stable.

These three dimensional clusters can be envisioned as being built of smaller building blocks, basically Zn_2X_2 (squares) and Zn_3S_3 (hexagons) rings. These structures are also found in carbon fullerenes, where the most stable structures are formed by pentagons and hexagons. In binary clusters, however, structures based on pentagons are not so stable because of the formation of isoatomic bonds. The number of squares shared by the spheroid structures remains constant as the size increases, while the number of hexagons is augmented by one adding a ZnX unit. The number of hexagons and squares found in each spheroid is detailed in Table 10.1.

The representation of the cohesive energies versus the inverse cubic root of the ZnX units shows a trend towards bulk cohesive energies. The predicted cohesive

Figure 10.1: Evolution of the relative energies calculated as $\Delta E = E_{ring} - E_{spheroid}$ (kJ/mol) as the cluster size increases.

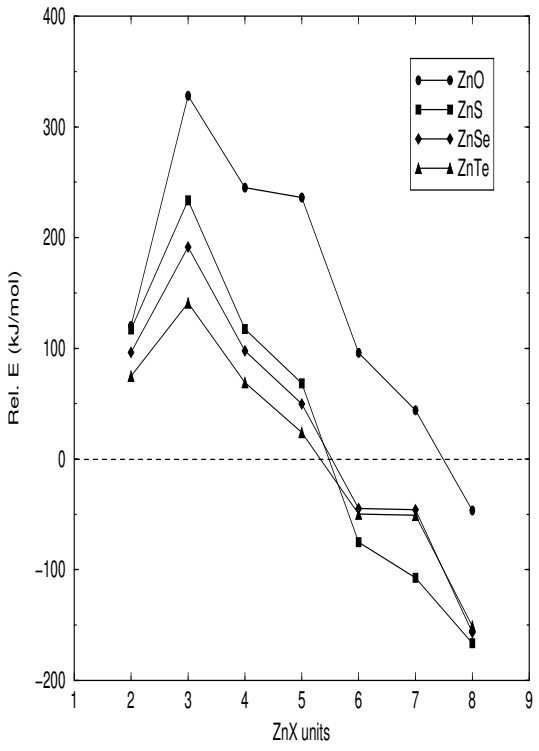

Table 10.1: Structural characteristics of spheroid carbon clusters and II-VI clusters

	Zn_4X_4	Zn_6X_6	Zn_8X_8	Zn_9X_9	$Zn_{12}X_{12}$	$Zn_{15}X_{15}$
Hexagons	0	2	4	5	8	11
Rombi	6	6	6	6	6	6

energies are more than 90% the experimental values, although these clusters are too small to represent the bulk. Moreover, the fact that the cohesive energies of these clusters fit a line indicates that we are dealing with the real global minima. The cohesive energy also gives a first insight into the relative stability of these clusters, and predict that $Zn_{12}X_{12}$ structures are the most stable ones, as was seen in Chapter 5.

10.2 Excitation energies

The MR-CI results used as reference show a clear advantage of the TDDFT method vs the CIS method. It describes sensibly better than CIS the two-fold degenerate $^1\Pi$ excitation in $Zn_1S_1^{GM}$ and also appears to be superior for the rest of the studied excitations in all the investigated clusters. It has been seen that both CIS and TDDFT methods need basis sets with more than one polarization functions. SKBJ(1sp2d2f) is the smallest basis yielding converged results for X=S, Se and Te, and SKBJ(1sp2d3f) for X=O. Nevertheless, this basis is too large for larger clusters.

The calculated electronic excitation energies show a strong dependence on the geometry of the cluster. Our study reveals that the ring like structure clusters, $i = 2 - 5$ have larger excitation energies than three dimensional spheroidal clusters, $i \geq 6$. However, for both type of clusters the excitation occurs from occupied non bonding p type orbitals of X to the LUMO. The predicted electronic excitation energies of the spheroidal clusters lie near the range of the visible spectrum for X=O,S,Se case, and within it for X=Te. When one goes down in the periodic table from O to Te the excitation energies are smaller, as may be appreciated in Figure 10.2, where the lowest allowed transitions are depicted. Four regions may be seen in Figure 10.2, the ultraviolet, which is entirely absorbed by the ozone shell in the atmosphere, the close ultraviolet, visible and the part corresponding to less energetic regions of the electromagnetic spectrum, i.e. infrared and so on. Only the radiation belonging to these last three regions reach the earth surface.

There are few clusters whose excitation energies lie within the visible region, which are $Zn_iX_i^{GM}$, $i = 2$, and $Zn_iTe_i^{GM}$ spheroids. Most of the clusters are in the close ultraviolet region, which are $Zn_iS_i^{GM}$ and $Zn_iSe_i^{GM}$ rings and spheroids and $Zn_iO_i^{GM}$ spheroids. Finally, in the ultraviolet region we find $Zn_iO_i^{GM}$ ring structures, which might be good protectors from the dangerous

Figure 10.2: Lowest allowed excitation energies of $Zn_iX_i^{GM}$ clusters.

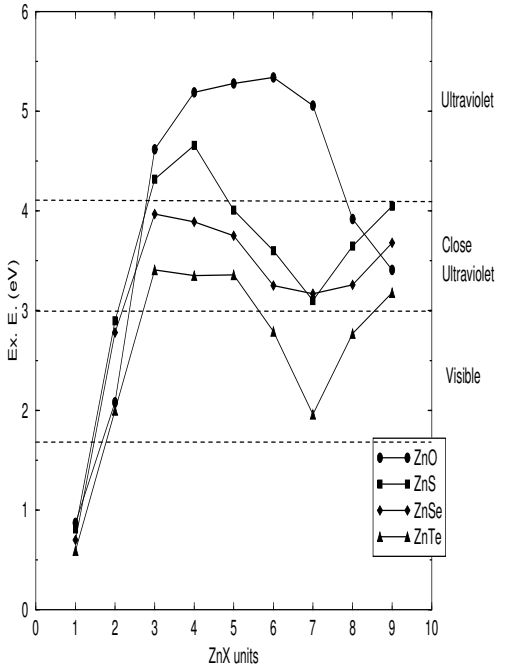

ultraviolet radiation. For $Zn_iX_i^{GM}$ X=S,Se,Te cases it is interesting to point out that the lowest lying excitation energy correspond to the $i = 7$ case.

Therefore, the clusters considered in the present investigation constitute promising materials for its use in photovoltaic solar cells as absorbers (X=Te) or both absorbers and window materials (X=Se) or only window materials (X=O and S).

The difference between the B3LYP Kohn-Sham energies of the orbitals involved in the sought electronic excitation appears to be a reliable practical approach to the stimation of the electronic excitation energies for larger clusters, where TDDFT calculations become prohibitive. This approach has been found to yield better results as the cluster size increases. Nevertheless, its most salient drawback is that no oscillator strengths are obtained.

10.3 Further work

Nowadays parallel machines allows one to perform calculations that few years ago were too expensive. Therefore, spheroids as large as $i = 12, 15$ have been characterized, and the characterization of the remaining large spheroids, i.e. Zn_iX_i, $i = 10, 11, 13, 14$, is still in process. In addition to this, the excitation

energies of these large spheroids could be performed. Once this is done a thermodynamical study of the stability of these clusters may be performed, in order to find which one is the most chemically stable one. Remember that according to the cohesive energies the $i = 12$ were the most stable ones.

Similar study is being performed for Cd_iX_i clusters. Besides, it is known that most of the absorption occurred in a solar cell happens in the junction of the two semiconductors. Therefore, ternary clusters such as $Cd_iS_1Te_{x-1}$ may be characterized and their excitation energies calculated.

Fullerene-based solids have many different applications as we have mentioned throughout this thesis. The interaction between the fullerenes in these solids is of Van der Waals type. Studies of the interactions between these clusters would be interesting in order to study the possibility of stable or metastable cluster-based solids, which could have very interesting properties.

Quantum Monte Carlo calculations have become a very powerfull tool in recent years. Diffusion Monte Carlo calculations may be performed for these solids, in order to calculate their band gaps.

Bibliography

[1] G.Wang, T. Ogawa, M. Umeno, T. Soga and T. Jimbo, Appl. Phys. Lett. **76**, 730 (2000).

[2] G.P. Summers, S.R. Messenger and E.A. Burke, Appl. Phys. Lett. **71**, 832 (1997).

[3] T. Soga, T. Jimbo, G. Wang, K. Ohtsuka and M. Umeno, J. Appl. Phys. **87**, 2285 (2000).

[4] A. Kampmann, D. Lincot, J. Electroanalitical Chem. **418,** 73 (1996).

[5] Y. Y. Loginov, K. Durose, H.M. Al-Allak, S.A. Galloway, S. Oktik, A. W. Brinkman, H. Richter, D. Bonnet, J. Crys. Wrowth **161,** 159 (1996).

[6] A. Niemegeers, M. Burgelman, J. Appl. Phys. **81**, 2881 (1997).

[7] K. Li, A.T.S. Wee, J. Lin, K. L. Tan, L. Zhou, S.F.Y. Li, Z.C. Feng, H.C. Chou, S. Kamra, A. Rohatgi, J. Mat. Sci: Mat. in Elec. **8,** 125 (1997).

[8] K. Omura, A. Hanahusa, T. Arita, H. Higuchi, T. Aramoto, T. Nishio, S. Sibutani, S. Kumazawa, M. Murozono, Y. Yabuuchi, H. Takakura, unpublished.

[9] C. Ferekides and J. Britt, Solar Energy Materials and Solar Cells **35,** 255 (1994).

[10] H.C. Chou, A. Rohatgi, N.M. Jokerst, S. Kamra, S.R. Stock, S.L. Lowrie, R.K. Ahrenkiel and D.H. Levi, Materials Chemistry and Physics **43,** 178 (1996).

[11] S. Naseem, D. Nazir, R. Mumtaz and K. Hussain, J. Mater. Sci. Technol. **12,** 89 (1996).

[12] T. Toukova, D. Kindl and J. Tousek, Thin Solid Films **293**, 272 (1997).

[13] T.L. Chu, S.S. Chu, Solid State Electronics **38**, 533 (1995).

[14] D.P. Halliday, J.M. Eggleston, and K. Durose, Thin Solid Films **322**, 314 (1998).

[15] T. Yamamoto, T. Toyama and H. Okamoto, Jpn. J. Appl. Phys. **37**, L916 (1998).

[16] J.H. Lee, H.Y. Lee, Y.K. Park, S.H. Shin and K.J. Park, Jpn. J. Appl. Phys. **37**, 3357 (1998).

[17] V.P. Singh, J.C. McClure, G.B. Lush, W. Wang, X. Wang, G.W. Thompson and E. Clark, Sol. Energy Mat. Sol. Cells **59**, 145 (1999).

[18] M. Burgelman, P. Nollet and S. Degrave, Appl. Phys. A **69**, 149 (1999).

[19] K. Durose, P.R. Edwards and D.P. Halliday, J. Crys. Growth **197**, 733 (1999).

[20] G. Contreras-Puente, O. Vigil, M. Ortega, A. Morales, J. Vidal, M.L. Albor Thin Solid Films **361-362**, 378 (2000).

[21] R. Chakrabarti, J. Dutta, S. Bandyopadhyay, D. Bhattacharyya, S. Chaudhuri and A.K. Pal, Sol. Ener. Mat. Sol. Cells **61**, 113 (2000).

[22] P.R. Edwards, S.A. Galloway and K. Durose, Thin Solid Films **361-362**, 364 (2000).

[23] `http://www.kyocera.co.jp/frame/product/applied/solar/light1.html`

[24] E. Schrodinger, Science and humanism: physics in our time, pp 27 and 58. Cambridge: CUP (1951).

[25] W. Heisenberg, Physics and philosophy, p 186. New York: Harper and Row (1958).

[26] H. C. von Baeyer, Taming the atom: The emergence of the visible microworld. New York: Random House (1992).

[27] R.P. Feynmann, Engineering and science, 1960, 23, 22. Reprinted in Miniaturization, H. D. Gilbert (ed), p 282. New York: Reinhold (1961).

[28] A.R. von Hippel, Science, **138**, 91, (1962)

[29] K.E. Drexler, Proc. Nat. Acad. Sci. USA, **78**, 5275 (1981).

[30] K.E. Drexler, Engines of creation. New York: Doubleday (1986).

[31] M.P. Zach, K.H. Ng, R.M. Penner, Science **290**, 2120 (2000).

[32] C. Joachim, J.K. Gimzewski and A. Aviram, Nature **408**, 541 (2000).

[33] A.V. Chadwick, Nature **408**, 925 (2000).

[34] N. Sata, K. Eberman, K. Eberl and J. Maier, Nature **408**, 946 (2000)

[35] `http://www.newscientist.com/dailynews/news.jsp?id=ns9999252`

[36] `http://www.nanosites.com/14transistor01.html`

[37] H.G. Craighead, Science **290**, 1532 (2000).

[38] S.R. Quake and A. Schrerer, Science **290**, 1536 (2000).

[39] E.W.H. Jager, E. Smela and O. Inganäs, Science **290**, 1540 (2000).

[40] R. Paiella, F. Capasso, C. Gmachi, D.L. Sivco, J.N. Baillargeon, A.L. Hutchinson, A.Y. Cho and H.C. Liu, Science **290**, 1739 (2000).

[41] K. Suenaga, M. Tencé, C. Mory, C. Colliex, H. Kato, T. Okazaki, H. Shinohara, K. Hirahara, S. Bandow and S. Lijima, Science **290**, 2280 (2000).

[42] H.W. Kroto, J.R. Head, S.C. O'Brien, R.F. Curl and R.E. Smalley, Nature **318**, 162 (1985).

[43] P.R.C. Kent, M.D. Towler, R.J. Needs and G.Rajagopal, Phys. Rev. B **62** (23), 15394 (2000).

[44] R.S. Ruoff and A.P. Hickman, J. Phys. Chem. **97**, 2494 (1993).

[45] X. Wang, C.Z. Wang, B.L. Zhang and K.M. Ho, Phys. Rev. Lett. **69**, 69 (1992).

[46] R.O. Jones, J. Chem. Phys. **110**, 5189 (1999).

[47] S.C. Erwin and M.R. Pederson, Phys, Rev. Lett. **67**, 1610 (1991)

[48] B.L. Zhang, C.Z. Wang, K.M. Ho and C.T. Chan, Europhys. Lett. **28**, 219 (1994).

[49] S. Chakravarty and S. Kivelson, Europhys. Lett. **16**, 751 (1991).

[50] J.L. Martins, Europhys. News **23**, 31 (1992).

[51] J.H. Schön, Ch. Kloc and B. Batlogg, Nature **408**, 549 (2000).

[52] P.V. Kamat, I. Bedja and S. Hotchandani, J. Phys. Chem. **98**, 9137 (1994).

[53] M. Freemantle, Chem. Eng. News **77**, 15 (1999).

[54] W. Andreoni, Phys. Rev. B **45**, 4203 (1992).

[55] A. Costales, A.K. Kandalam, R. Franco and R. Pandey, J. Phys. Chem B, jp013906f (2001).

[56] A.K. Kandalam, M.A. Blanco, R. Pandey, J. Phys. Chem. B. jp0140062 (2001).

[57] J.B. BelBruno, Chem. Phys. Lett. **313**, 795 (1999).

[58] V. Tozzini, F. Buda and A. Fasolino, Phys. Rev. Lett. **85**, 4554 (2000).

[59] J. Pattanayak, T. Kar and S. Scheiner, J. Phys. Chem. A, jp013904v (2002).

[60] T.R. Taylor, K.R. Asmis, C. Xu and D.M. Neumark, Chem. Phys. Lett. **297**, 133 (1998).

[61] R.R. Li, P.D. Dapkus, M.E. Thompson, W.G. Jeong, C. Harrison, P.M. Chaikin, R.A. Register and D.H. Adamson, Appl. Phys. Lett. **76**, 1689 (2000).

[62] J.H. Chung, C.S. Ah and D. Jang, J. Phys. Chem. B, jp002692j (2001).

[63] P. Yang, M. Lü, D. Xü, D. Yuan ang G. Zhou, Chem. Phys. Lett. **336**, 76 (2001).

[64] P.J. Sebastian and J. Narvaez, Thin. Sol. Films, **130** (1996).

[65] D.J. Norris, N. Yao, F.T. Charnock and T.A. Kennedy, Nanolett. **1**, 3 (2001).

[66] L. Svob, C. Thiandoume, A. Lusson, M. Bouanani, Y. Marfaing and O. Gorochov, Appl. Phys. Lett. **76**, 1695 (2000).

[67] I. Suemune, J. Hirose and A. Ueta, Appl. Phys. Lett. **76**, 1701 (2000).

[68] J. Xue-yin, J. Yan, Z. Zhi-lin and X. Shao-hong, J. Crys. Grow. **191**, 692 (1998).

[69] Z. Peng and X. Peng, J. Am. Chem. Soc., ja0027766 (2000).

[70] E, Schrödinger, Ann. Physik **79**, 361 (1926).

[71] W. Heisenberg, Z. Physik **33**, 879 (1925).

[72] P.A.M. Dirac, Proc. R. Soc. Lond. A **113**, 621 (1926).

[73] E, Schrödinger, Ann. Physik **79**, 734 (1926).

[74] M Born and J.R. Oppenheimer, Ann. Physik **44**, 455 (1927).

[75] N.I. Levine, Quantum Chemistry; Prentince-Hall Inc., (1991).

[76] A. Szabo, N.S. Ostlund, Modern Quantum Chemistry; McGraw-Hill, (1992).

[77] R.G. Parr, W. Yang, Density-Functional Theory of Atoms and Molecules; Oxford University Press, New York (1989).

[78] E.S. Kryachko, E.V.L. Na, Energy Density Functional Theory of Many-Electron Systems, Kluwer Academic Publishers: London (1990).

[79] W.M.C. Foulkes, L. Mitas, R.J. Needs and G. Rajagopal, Rev. Mod. Phys. **73**, 33 (2001).

[80] W. Heitler and F. London, Z. Physik **44**, 455 (1927).

[81] F. Hund, Z. Physik **73**, 1 (1931).

[82] R.S. Mulliken, Phys. Rev. **40**, 55 (1932).

[83] D.R. Hartree, Proc. Cambridge Philos. Soc. **24**, 89 (1928).

[84] V. Fock, Z. Phys. **61**, 126 (1930).

[85] C. Moller and M.S. Plesset, Phys. Rev. **46**, 618 (1934).

[86] I. Shavitt, Mol. Phys. **94**, 3 (1998).

[87] C.D. Sherrill and H.F. Schaefer, Adv. Quantum Chem. **34**, 143 (1999).

[88] J.A. Pople, R. Krishnan, H.B. Schlegel and J.S. Binkley, Int. J. Quant. Chem. **14**, 545 (1978).

[89] R.J. Bartlett and G.D. Purvis, Int. J. Quant. Chem. **14**, 516 (1978).

[90] R.J. Bartlett, 'Modern electronic structure theory' (World Scientific, London, 1995).

[91] K. Andersson, P.-Å. Malmqvist, B.O. Roos, A, J. Sadlej and K. Wolinski, J. Phys. Chem. **94**., 5483 (1990).

[92] K. Andersson, P.-Å. Malmqvist and B.O. Roos, J. Phys. Chem. **96**, 1218 (1992).

[93] J.C. Grossman and L. Mitas, Phys. Rev. Lett. **74**, 1323 (1995).

[94] J.C. Grossman and L. Mitas, Phys. Rev. Lett. **79**, 4353 (1997).

[95] J.C. Grossman, L. Mitas and K. Raghavachari, Phys. Rev. Lett. **75**, 3870 (1995).

[96] W.M.C. Foulkes, R.Q. Hood and R.J. Needs, Phys. Rev. B **60**, 4558 (1999).

[97] A.R. Porter, M.D. Towler and R.J. Needs, Phys. Rev. B **64**, 035320 (2001)

[98] A. Lüchow, J.B. Anderson, Annu. Rev. Phys. Chem. **51**, 501 (2000).

[99] P. Hohenberg and W. Kohn, Phys. Rev. **136**, B864 (1964).

[100] W. Kohn and L.J. Sham, Phys. Rev. A **140**, 1133 (1965).

[101] R. Stowaser, R. Hoffmann, J. Am. Chem. Soc. **121**, 3414 (1999).

[102] O. Gunnarsson, B.I. Lundqvist, J.W. Wilkens, Phys. Rev. Lett. **10**, 1319 (1974).

[103] T. Kar, J.G. Angyan, A.B. Shannigrahi, J. Phys. Chem. A **104**, 9953 (2000).

[104] S.H. Vosko, L. Wilk, M. Nusair, Can. J. Phys. **58**, 1299 (1980).

[105] J.C. Slater, Quantum Theory of Molecules and Solids. Vol. 4. The Self-Consistent Field for Molecules and Solids; McGraw-Hill: New York (1974).

[106] J. Labanowski, J. Andelzelm, Density Functional Methods in Chemistry; Springer-Verlag: New York (1991).

[107] V. Tschinke, T. Ziegler, Theor. Chim. Acta **81**, 651 (1991).

[108] B.G. Johnson, P.M.W. Gill, J.A. Pople, J. Chem. Phys. **98**, 5612 (1993).

[109] A.D. Becke, J. Chem. Phys. **98**, 5648 (1993).

[110] C. Lee, W. Yang and R.G. Parr, Phys. Rev. B **37**, 785 (1988).

[111] A.D. Becke, Phys. Rev. A **38**, 3098 (1988).

[112] T. Ziegler, Chem. Rev. **91**, 651 (1991), and references therein.

[113] E.K.U. Gross and W. Kohn, Ad. Quant. Chem. **21**, 255 (1990).

[114] M.E. Casida, Recent Advances in Density Functional Methods, Vol. 1, edited by D.P. Chong (World Scientific, Singapore, 1995).

[115] M.E. Casida, Recent Developments and Applications of Modern Density Functional Theory, Theoretical and Computational Chemistry, Vol 4, edited by J.M. Seminario (Elsevier, Amsterdam, 1996).

[116] C. Jamorski, M.E. Casida and D.R. Salahub, J. Chem. Phys. **104**, 5134 (1996).

[117] M. Petersilka, U.J. Gossmann and E.K.U. Gross, Phys. Rev. Lett. **76**, 1212 (1996).

[118] M. Petersilka and E.K.U. Gross, Int. J. Quant. Chem., Symp. **30**, 181 (1996).

[119] R. Bauernschmitt and R. Ahlrichs, Chem. Phys. Lett. **256**, 454 (1996).

[120] P. Boulet, H. Chermette, C. Daul, F. Gilardoni, F. Rogemond, J. Weber and G. Zuber, J. Phys. Chem. A **105**, 885 (2001).

[121] S.J.A. van Gisbergen, J.A. Groeneveld, A. Rosa, J.G. Snijders and E.J. Baerends, J. Phys. Chem. A **103**, 6835 (1999).

[122] A. Rosa, E.J. Baerends, S.J.A. van Gisbergen, E. van Lenthe, J.A. Groeneveld and J.G. Snijders, J. Am. Chem. Soc. **121**, 10356 (1999).

[123] S. Hirata, T.J. Lee and M. Head-Gordon, J. Chem. Phys. **111**, 8904 (1999).

[124] S. Hirata, and M. Head-Gordon, Chem. Phys. Lett. **302**, 375 (1999).

[125] N.N. Matsuzawa, A. Ishitani, D.A. Dixon and T. Uda, J. Phys. Chem. A **105**, 4953 (2001).

[126] Z. Cai and J.R. Reimers, J. Chem. Phys. **112**, 527 (2000).

[127] R. Bauernschmitt, R. Ahlrichs, F.H. Hennrich and M.M. Kappes, J. Am. Chem. Soc. **120**, 5052 (1998).

[128] S. Hirata, M. Head-Gordon and R.J. Bartlett, J. Chem. Phys **111**, 10774 (1999).

[129] D.J. Tozer and N.C. Handy, Phys. Chem. Chem. Phys. **2**, 2117 (2000).

[130] J. C. Shieh, J. L. Chang, J. C. Wu, R. Li, A. M. Mebel, N. C. Handy and Y. T. Chen, J. Chem. Phys. **112**, 7384 (2000).

[131] R. E. Stratmann, G.E. Scuseria and M.J. Frisch, J. Chem. Phys. **109**, 8218 (1998).

[132] M.E. Casida, J. Jamorski, K.C. Casida and D.R. Salahub, J. Chem. Phys. **108**, 4439 (1998).

[133] W.J. Stevens, M. Krauss, H. Basch and P.G. Jasien, Can. J. Chem. **70**, 612 (1992).

[134] J.P. Dexclaus, Comput. Phys. Commun. **9**, 31 (1975).

[135] P. J. Sebastian, M Ocampo, Sol. Energy Mater. Sol. Cells **44**, 1 (1996).

[136] A.J. Hoffman, G. Mills, H. Yee and M.R. Hoffmann, J. Phys. Chem. **96**, 5546 (1992).

[137] S. Kuwabata, K. Nishida, R. Tsuda, H. Inoue and H. Yoneyama, J. Electrochem. Soc. **141**, 1498 (1994).

[138] E. Corcoran, Sci. Am. **263** (11), 74 (1990).

[139] J. L. Martins, N. Troullier, Phys. Rev. B **43**, 2213 (1991).

[140] Y.N. Xu, W. Y. Ching, Phys. Rev. B **48**, 4335 (1993).

[141] J. Muilu, T.A. Pakkanen, Surf. Sci. **364**, 439 (1996).

[142] J. Muilu and T.A. Pakkanen, Phys. Rev. B **49**, 11185 (1994).

[143] P. Schroer, P. Kruger, and J. Pollmann, Phys. Rev. B **47**, 6971 (1993).

[144] P. Schroer, P. Kruger, and J. Pollmann, Phys. Rev. B **48**, 18264 (1993).

[145] P. Schroer, P. Kruger, and J. Pollmann, Phys. Rev. B **49**, 17092 (1994).

[146] D. Vogel, P. Kruger and J. Pollmann, Phys. Rev. B **52**, 14316 (1995).

[147] J. Pollmann, P. Kruger, M. Rohlfing, M. Sabisch and D. Vogel, App. Surf. Sci. **104/105**, 1 (1996).

[148] D. Vogel, P. Kruger and J. Pollmann, Phys. Rev. B **54**, 5495 (1996).

[149] A. Ecker, E. Weckert, and H. Schnockel, Nature (London) **387**, 379 (1997).

[150] R. Rousseau, G. Dietrich, S, Kruckeberg, K. Lutzenkirchen, D. Marx, L. Schweikhard, C. Walther, Chem. Phys. Lett. **295**, 41 (1998).

[151] J. Cizeron, M.P. Pileni, J. Phys. Chem. B **101**, 8887 (1997).

[152] V. S. Gurin, J. Phys. Chem **100**, 869 (1996).

[153] B. Guo, K. Kerns, A. Castleman, Science **255**, 1411 (1992).

[154] B. Guo, S. Wei, J. Purnell, S. Buzza, A. Castleman, Science **256**, 515 (1992).

[155] J.E. Fowler and J.M. Ugalde, Phys. Rev. A **58**, 383 (1998).

[156] T. Qureshi, V. Kumar, e-print `http://www.lanl.gob.abs/cond-mat/9806167`

[157] A. Tomasulo, M. V. Ramakrishna, Chem. Phys. **210**, 55 (1996).

[158] P. Fuentealba, O. Reyes, J. Phys. Chem. A **103**, 1376 (1999).

[159] M. Haser, U. Schneider, R. Ahlrichs, J. Am. Chem. Soc. **114**, 9551 (1992).

[160] L. Lou, T. Guo, P. Nordlander, R. E. Smalley, J. Chem. Phys. **99**, 5301 (1993).

[161] J. J. P. Stewart, J. Comp. Chem.**12**, 320 (1991).

[162] M. J. Frisch, G. W. Trucks, H. B. Schlegel, `P.M.W. Gill, B.G. Johnson, M. A. Robb, J. R. Cheeseman, T. Keith, G.A. Peterson, J. A. Montgomery, K. Raghavachari, M.A. Allaham, V.G. Zakrzewski, J. V. Ortiz, J.B. Foresman, C. Y. Peng, P.Y. Ayala, W. Chen, M. W. Wong, J. L. Andres, E. S. Replogle, R. Gomperts, R. L. Martins, D. J. Fox, J.S. Binkley, D.J. Defrees, J. Baker, J.P. Stewart, M. Head-Gordon, C. Gonzalez and J. A. Pople, GAUSSIAN 94 B.2, Gaussian Inc., Pittsburgh PA, 1995.

[163] M. J. Frisch, G. W. Trucks, H. B. Schlegel, G. E. Scuseria, M. A. Robb, J. R. Cheeseman, V. G. Zakrzewski, J. A. Montgomery, R. E. Stratmann, B. J. Burant, S. Dapprich, J. M. Millam, A. D. Daniels, K. N. Kudin, M. C. Strain, O. Farkas, J. Tomasi, V. Barone, M. Cossi, R. Cammi, B. Mennucci, C. Pomelli, C. Adamo, S. Clifford, J. Ciolowski, J. V. Ortiz, B.B. Stefanov, G. Liu, A. Liashenko, P. Piskorz, I. Komaromi, R. Gomperts, R. L. Martins, D. J. Fox, T. Keith, M. A. Al-Laham, C. Y. Peng, A. Nanayakkara, C. Gonzalez, M. Challacombe, P. M. W. Gill, B. G. Johnson, W. Chen, M. W. Wong, J. L. Andres, M. Head-Gordon, E. S. Replogle and J. A. Pople, GAUSSIAN 98, (Revision A5), Gaussian, Inc., Pittsburgh PA, 1998.

[164] HyperChem^{TM}, Release 4.5 for Windows, Molecular Modeling System, Copyright 1994, 1995 Hypercube, Inc..

[165] GAMESS, M. W. Schmidt, K. K. Baldridge, J. A. Boatz, S. T. Elbert, M. S. Gordon, J. H. Jensen, S. Koseki, N. Matsunaga, K. A. Nguyen, S. J. Su, T. L. Windus, M. Dupuis, J. A. Montgomery, J. Comput. Chem. **14**, 1347 (1993).

[166] A. J. H. Wachters, J. Chem. Phys. **52**, 1033 (1970).

[167] P. J. Hay, J. Chem. Phys. **66**, 4377 (1977).

[168] D.M. Hood, R.M. Pitzer and H.F. Schaefer, J. Chem. Phys. **71**, 705 (1979).

[169] A D. McLean and G. S. Chandler, J. Chem. Phys. **72**, 5639 (1980).

[170] R. Krishnan, J. S. Binkley, R. Seeger and J. A. Pople, J. Chem. Phys. **72**, 650 (1980).

[171] R.W.F. Bader, Atoms in Molecules: A Quantum Theory, Vol. Chapter 7, Clarendon Press, Science Publications, Oxford, 1990.

[172] R. Ditchfield, W. J. Hehre and J. A. Pople, J. Chem. Phys. **54** (1971) 724.

[173] W. J. Hehre, R. Ditchfield and J. A. Pople, J. Chem. Phys. **56** (1972) 2257.

[174] P. C. Hariharan and J. A. Pople, Mol. Phys. **27**, 209 (1974).

[175] M. S. Gordon, Chem. Phys. Lett. **76**, 163 (1980).

[176] P. C. Hariharan and J. A. Pople, Theo. Chim. Acta **28**, 213 (1973).

[177] E.C. Behrman, R.K. Foehrweiser, J. R. Myers, B.R. French, M. E. Zandler, Phys. Rev. A **49**, 1543 (1994).

[178] A.E. Reed, L.A. Curtiss and F. Weinhold, Chem. Rev. **88**, 899 (1988).

[179] J. Cizek, Adv. Chem. Phys. **14**, 35 (1969).

[180] G.D. Purvis and R.J. Bartlett, J. Chem. Phys. **76**, 1910 (1982).

[181] G. E. Scuseria, C.L. Janssen and H.F. Schaefer, III, J. Chem. Phys. **89**, 7382 (1988),

[182] G.E. Scuseria and H.F. Schaefer, III, J. Chem. Phys. **90**, 3700 (1989).

[183] J.A. Pople, M. Head-Gordon, K. Raghavachari and G.W. Trucks, Chem. Phys. Lett. **164**, 185 (1989).

[184] P.E.M. Siegbahn, Adv. Chem. Phys. **43**, 333 (1996)..

[185] J. M. Matxain, J. E. Fowler and J. M. Ugalde, Phys. Rev. A **61**, 053201 (2000).

[186] C. Walther, G. Dietrich, W. Dostal, K. Hansen, S. Krückeberg, K. Lützenkirchen and L. Schweikhard, Phys. Rev. Lett. **83**, 3816 (1999).

[187] J. M. Matxain, J. E. Fowler and J. M. Ugalde, Phys. Rev. A **62**, 553 (2000).

[188] R.C. Binning Jr. and L.A. Curtiss, J. Comp. Chem. **11**, 1206 (1990).

[189] L.A. Curtiss, M.P. McGrath, J. P. Blaudeau, N.E. Davis, R.C. Binning Jr. and L. Radom, J. Chem. Phys. **103**, 6104 (1995).

[190] M.P.McGrath and L. Radom, J. Chem. Phys. **94**, 511 (1991).

[191] David R. Lide (chief editor) Handbook of Chem. and Phys. 79th ed., 5-24 (1998-1999).

[192] David R. Lide (chief editor) Handbook of Chem. and Phys. 79th ed., 12-98 (1998-1999).T.L. Chu and S.S. Chu, Solid-State Elec. **38**, 533 (1995).

[193] K. B. Wiberg, R. E. Stratmann, and M. J. Frisch, Chem. Phys. Lett. **297**, 60 (1998).

[194] J.B. Foresman, M. Head-Gordon, J.A. Pople and M.J. Frisch, J. Phys. Chem. **96**, 135 (1992).

[195] C. Adamo and V. Barone, Chem. Phys. Lett. **274**, 242 (1997).

[196] J. P. Perdew, Phys. Rev. B **33**, 8822 (1986).

[197] J.C. Stephens, G. Vacek, C.D. Sherrill, J.T. Fermann, T.J. Van Huis and T.D. Crawford, Center for Computational Quantum Chemistry, University of Georgia, Athens, GA, 1997, PSI 2.0.8. program package.

[198] J.M. Matxain, J.M. Mercero, J.E. Fowler and J.M. Ugalde, Phys. Rev. A **64**, 053201 (2001).

[199] J. M. Matxain, A. Irigoras, J. E. Fowler and J. M. Ugalde, Phys. Rev. A **63**, 013202 (2001).

[200] D.J. Tozer and N.C. Handy, J. Chem. Phys. **200**, 10180 (1998).

[201] A. Savin, C.J. Umrigar and X. Gonze, Chem. Phys. Lett. **288**, 391 (1998).

[202] H. Ohldag, T. J. Regan, J. Stöhr, A. Scholl, F. Nolting, J. Lüning, C. Stamm, S. Anders, R. L. White, Phys. Rev. Lett. **87**, 247201 (2001)

[203] J. M. Matxain, A. Irigoras, J. E. Fowler and J. M. Ugalde, Phys. Rev. A, **64**, 013201 (2001).

List of publications

1. 'Combined ab initio computational and statistical investigation of a model C-H...O Hydrogen bonded dimer as occurring in 1,4-Benzoquinone'
   J. Van de Bovenkamp, J. M. Matxain, F. B. Van Duijneveldt (Theoretical Chemistry Group, Utrecht University, Utrecht, The Netherlands) and T. Steiner (Institut für Kristallographie, Freie Universitat Berlin, Berlin, Germany.
   J. Phys. Chem. A **103**, 2784 (1999).

---

2. 'Small Clusters of II-VI Materials: Zn_iS_i, $i = 1 - 9$'
   Jon M. Matxain, Joseph E. Fowler and Jesus M. Ugalde
   Phys. Rev. A **61**, 512 (2000).

---

3. 'Small Clusters of II-VI Materials: Zn_iO_i, $i = 1 - 9$'
   Jon M. Matxain, Joseph E. Fowler and Jesus M. Ugalde
   Phys. Rev. A **62**, 553 (2000).

---

4. 'Electronic Excitation Energies of Small Zn_iS_i Clusters'
   Jon M. Matxain, Arantxa Irigoras, Joseph E. Fowler and Jesus M. Ugalde
   Phys. Rev. A **63,** 013202 (2001).

---

5. 'Electronic Excitation Energies of Zn_iS_i Clusters'
   Jon M. Matxain, Arantxa Irigoras, Joseph E. Fowler and Jesus M. Ugalde
   Phys. Rev. A **64**, 013201 (2001)

---

6. 'Small Clusters of Group (II-VI) Materials: Zn_iX_i, X=Se,Te, $i = 1 - 9$'
   Jon M. Matxain, Jose M. Mercero, Joseph E. Fowler and Jesus M. Ugalde
   Phys. Rev. A **64**, 053201 (2001)

---

7. 'Electronic Excitation Energies of Zn_iO_i Clusters, $i = 1 - 9$
   Jon M. Matxain, Joseph E. Fowler and Jesus M. Ugalde
   submitted to J. Am. Chem. Soc.

---

8. 'Small Clusters of Group (II-VI) Materials: Cd_iO_i, $i = 1 - 9, 12, 15$"
   Jon M. Matxain, Jose M. Mercero, Joseph E. Fowler and Jesus M. Ugalde
   submitted to Phys. Rev. A

---

9. 'Electronic Excitation Energies of Zn_iX_i Clusters, X=Se,Te, $i = 1 - 9$
   Jon M. Matxain, Jose M. Mercero, Joseph E. Fowler and Jesus M. Ugalde
   submitted to J. Am. Chem. Soc.

---

10. 'Small Clusters of Group (II-VI) Materials: Cd_iS_i, $i = 1 - 9, 12, 15$"
    Jon M. Matxain, Jose M. Mercero, Joseph E. Fowler and Jesus M. Ugalde
    submitted to Phys. Rev. A

---

11. 'Aluminum(III) interactions with aromatic aminoacid chains'
    Jose M. Mercero, Jon M. Matxain, Joseph E. Fowler and Jesus M. Ugalde
    accepted Int. J. Quantum Chem.